

THESIS

WIND TUNNEL INVESTIGATION OF WIND LOAD ON A GROUND MOUNTED
PHOTOVOLTAIC TRACKER

Submitted by

Swagat Mohapatra

Department of Civil and Environmental Engineering

In partial fulfillment of the requirements

For the Degree of Master of Science

Colorado State University

Fort Collins, Colorado

Spring 2011

Master's Committee:

Advisor: Bogusz Bienkiewicz

Karan Venayagamoorthy
Hiroshi Sakurai

ABSTRACT

WIND TUNNEL INVESTIGATION OF WIND LOAD ON A GROUND MOUNTED PHOTOVOLTAIC TRACKER

Wind loading is an important environmental factor to be considered in design of components and support structures of ground mounted photovoltaic tracker systems (PVT). Current understanding of action of wind on such systems is incomplete. Over the past decade, a number of investigations devoted to this topic have been carried out. However, majority of these efforts have been of proprietary nature. As a result, limited amount of data on wind loading on PV systems can be found in open literature. This study describes a wind tunnel study of wind effects on a generic ground mounted photovoltaic tracker system. The study was carried out at the Wind Engineering and Fluids Laboratory, Colorado State University. During the wind tunnel testing, the dynamic wind loading exerted on an isolated PVT system was measured and the effects of various parameters of the system on the wind loading were investigated. The investigated parameters included: the system porosity, inclination angle, wind direction and arrangement of the PV panels. A scaled model of the system was mounted on a High Frequency Force Balance (HFFB) and wind induced forces and moments were measured in a simulated atmospheric boundary layer flow. The work described herein presents an overview of the study and discusses the obtained main findings. It is concluded that

certain combinations of the system parameters led to a significant reduction in the exerted wind loads. A comparison of wind tunnel based design wind loads with those obtained from American Society of Civil Engineers Standard (ASCE 7-05) demonstrated reasonable agreement between the measured peak wind loads and design loads recommended by the standard.

ACKNOWLEDGEMENTS

I would like to express sincere gratitude to my advisor Dr. Bogusz Bienkiewicz, for his supervision, advice and guidance from the very early stage of this research and for introducing me to the unique field of Wind Engineering. I would also like to thank Dr. Karan Venayagamoorthy and Dr. Hiroshi Sakurai for their support and valuable advice provided as members of the graduate committee. I acknowledge the financial support provided by Clean Energy Supercluster at Colorado State University.

I am thankful to the Wind Engineering and Fluids Laboratory (WEFL) whose resources and facilities I used in my work and for the friendly atmosphere it provided. My sincere appreciation goes to Munehito Endo and Sung Su Bae, of WEFL who helped me set up the experimental configurations employed in the wind tunnel testing. I gratefully thank Eric Richards and Aparna Arunachalam for their constructive comments on initial versions of this thesis.

Lastly and most importantly, I wish to thank my family and friends for their support and encouragement throughout the course of this work.

TABLE OF CONTENTS

<i>Abstract</i>	ii
<i>Acknowledgements</i>	iv
<i>List of Figures</i>	vii
<i>List of Tables</i>	xi
<i>List of Symbols</i>	xii
1. Introduction.....	1
2. Literature Review.....	3
2.1 Investigations of Wind Load on Ground Mounted Photovoltaic Trackers	3
2.2 Wind Tunnel Testing.....	4
2.3 Wind Loads specified in Building Standards.....	6
3. Experimental Configuration.....	7
3.1 Test Setup.....	7
3.1.1 Wind Tunnel Modeling of Atmospheric Boundary Layer.....	7
3.1.2 High Frequency Force Balance.....	8
3.1.3 Design and Fabrication of Models of PVT.....	9
3.1.4 PVT Test Configurations.....	9
3.1.5 Data Acquisition.....	11
3.2 Analytical Background.....	11
4. Results and Discussion.....	14
4.1 Comparison of Representative Results with Data Reported in Open Literature.....	14

4.2 Effects of Porosity on Wind Loads.....	15
4.2.1 Drag Force.....	16
4.2.2 Lift Force.....	17
4.2.3 Normal Force.....	18
4.2.4 Pitching Moment.....	19
4.3 Normal Force Comparison with ASCE 7-05 Wind Loading Provisions....	20
5. Conclusions and Recommendations.....	23
5.1 Conclusions.....	22
5.2 Recommendations.....	23
<i>Figures</i>	25
<i>References</i>	65
<i>Appendix A</i>	67
<i>Appendix B</i>	95

LIST OF FIGURES

Figure 1.1	Examples of installations of ground mounted photovoltaic trackers (PVT), [1,3,11 and 15]	25
Figure 3.1	Layout of Meteorological Wind Tunnel at Wind Engineering and Fluids Laboratory (WEFL) at Colorado State University (CSU)	25
Figure 3.2	Experimental configuration developed for wind tunnel testing	26
Figure 3.3	(a) Wind velocity and (b) Turbulence intensity profiles	27
Figure 3.4	High frequency force balance	27
Figure 3.5	Structural components of PVT model	27
Figure 3.6	Overall view of PVT model with PV panel assembly	28
Figure 3.7	PVT configurations and porosities of PV panel assembly	28
Figure 3.8	Definition of PVT position angles and wind loading components	29
Figure 4.1	Heliostat model used by Peterka et al. [9]	29
Figure 4.2	Comparison of mean (a) force along x-axis, (b) force along z-axis and (c) pitching moment coefficients, Arrangement A2 and CSU-85, Pitch Angle 45°	30
Figure 4.3	Comparison of mean (a) force along x-axis, (b) force along z-axis and (c) pitching moment coefficients, Arrangement A3 and CSU-85, Pitch Angle 45°	31
Figure 4.4	Effects of porosity on (a) mean, (b) standard deviation and (c) peak drag force coefficients, Arrangement A2, Pitch Angle 30°	32
Figure 4.5	Effects of porosity on (a) mean, (b) standard deviation and (c) peak drag force coefficients, Arrangement A3, Pitch Angle 30°	33

Figure 4.6	Effects of porosity on (a) mean, (b) standard deviation and (c) peak drag force coefficients, Arrangement A2, Wind Direction 0°	34
Figure 4.7	Effects of porosity on (a) mean, (b) standard deviation and (c) peak drag force coefficients, Arrangement A3, Wind Direction 0°	35
Figure 4.8	Drag force reduction factor: (a) mean, (b) standard deviation and (c) peak, Arrangement A2, Wind Direction 0°	36
Figure 4.9	Drag force reduction factor: (a) mean, (b) standard deviation and (c) peak, Arrangement A2, Wind Direction 180°	37
Figure 4.10	Drag force reduction factor: (a) mean, (b) standard deviation and (c) peak, Arrangement A3, Wind Direction 0°	38
Figure 4.11	Drag force reduction factor: (a) mean, (b) standard deviation and (c) peak, Arrangement A3, Wind Direction 180°	39
Figure 4.12	Effects of porosity on (a) mean, (b) standard deviation and (c) peak lift force coefficients, Arrangement A2, Pitch Angle 30°	40
Figure 4.13	Effects of porosity on (a) mean, (b) standard deviation and (c) peak lift force coefficients, Arrangement A3, Pitch Angle 30°	41
Figure 4.14	Effects of porosity on (a) mean, (b) standard deviation and (c) peak lift force coefficients, Arrangement A2, Wind Direction 0°	42
Figure 4.15	Effects of porosity on (a) mean, (b) standard deviation and (c) peak lift force coefficients, Arrangement A3, Wind Direction 0°	43
Figure 4.16	Lift force reduction factor: (a) mean, (b) standard deviation and (c) peak, Arrangement A2, Wind Direction 0°	44
Figure 4.17	Lift force reduction factor: (a) mean, (b) standard deviation and (c) peak, Arrangement A2, Wind Direction 180°	45
Figure 4.18	Lift force reduction factor: (a) mean, (b) standard deviation and (c) peak, Arrangement A3, Wind Direction 0°	46
Figure 4.19	Lift force reduction factor: (a) mean, (b) standard deviation and (c) peak, Arrangement A3, Wind Direction 180°	47
Figure 4.20	Effects of porosity on (a) mean, (b) standard deviation and (c) peak normal force coefficients, Arrangement A2, Pitch	48

	Angle 30°	
Figure 4.21	Effects of porosity on (a) mean, (b) standard deviation ,and (c) peak normal force coefficients, Arrangement A3, Pitch Angle 30°	49
Figure 4.22	Effects of porosity on (a) mean, (b) standard deviation and (c) peak normal force coefficients, Arrangement A2, Wind Direction 0°	50
Figure 4.23	Effects of porosity on (a) mean, (b) standard deviation and (c) peak normal force coefficients, Arrangement A3, Wind Direction 0°	51
Figure 4.24	Normal force reduction factor: (a) mean, (b) standard deviation and (c) peak, Arrangement A2, Wind Direction 0°	52
Figure 4.25	Normal force reduction factor: (a) mean, (b) standard deviation and (c) peak, Arrangement A2, Wind Direction 180°	53
Figure 4.26	Normal force reduction factor: (a) mean, (b) standard deviation and (c) peak, Arrangement A3, Wind Direction 0°	54
Figure 4.27	Normal force reduction factor: (a) mean, (b) standard deviation and (c) peak, Arrangement A3, Wind Direction 180°	55
Figure 4.28	Effects of porosity on (a) mean, (b) standard deviation and (c) peak pitching moment coefficients, Arrangement A2, Pitch Angle 30°	56
Figure 4.29	Effects of porosity on (a) mean, (b) standard deviation and (c) peak pitching moment coefficients, Arrangement A3, Pitch Angle 30°	57
Figure 4.30	Effects of porosity on (a) mean, (b) standard deviation and (c) peak pitching moment coefficients, Arrangement A2, Wind Direction 0°	58
Figure 4.31	Effects of porosity on (a) mean, (b) standard deviation and (c) peak pitching moment coefficients, Arrangement A3, Wind Direction 0°	59
Figure 4.32	Pitching moment reduction factor: (a) mean, (b) standard deviation and (c) peak, Arrangement A2, Wind Direction 0°	60
Figure 4.33	Pitching moment reduction factor: (a) mean, (b) standard deviation and (c) peak, Arrangement A2, Wind Direction	61

180°

Figure 4.34	Pitching moment reduction factor: (a) mean, (b) standard deviation and (c) peak, Arrangement A3, Wind Direction 0°	62
Figure 4.35	Pitching moment reduction factor: (a) mean, (b) standard deviation and (c) peak, Arrangement A3, Wind Direction 180°	63
Figure 4.36	Comparison of prototype design wind loads on PVT	64

LIST OF TABLES

Table 3.1	Definition of model configurations	10
-----------	------------------------------------	----

LIST OF SYMBOLS

A1	Single PV panel arrangement
A2	Twin PV panel arrangement
A3	Quadruple PV panel arrangement
A_{ref}	Reference area of PV panel (actual area enclosed by PV panels)
B	Reference length for ground mounted photovoltaic tracker as shown in Figure 3.7
$\bar{C}_D, \tilde{C}_D, \hat{C}_D$	Mean, standard deviation and peak drag force coefficients
$\bar{C}_L, \tilde{C}_L, \hat{C}_L$	Mean, standard deviation and peak lift force coefficients
$\bar{C}_{FN}, \tilde{C}_{FN}, \hat{C}_{FN}$	Mean, standard deviation and peak normal force coefficients
$\bar{C}_{My}, \tilde{C}_{My}, \hat{C}_{My}$	Mean, standard deviation and peak pitching moment coefficients about y-axis
\bar{C}_{Fx}	Mean force coefficients measured along x-axis
\bar{C}_{Fz}	Mean force coefficients measured along z-axis
F_D	Drag force (force along the wind direction)
F_L, F_z	Lift force; force along the z-axis
F_x	Force along the x-axis
F_y	Force along the y-axis
F_N	Normal force (force perpendicular to the top PV panel surface)
H	Height of pivot axis of PVT model
L	Side dimension of PV panel assembly as shown in Figure 3.7
M_y	Pitching moment (moment about the pivot axis)

M_{yb}	Base pitching moment (moment about the y-axis measured from force balance)
p	Photovoltaic panel porosity: 0%, 5%, 10% and 15%
q	Velocity pressure
V_{33}	Basic wind speed obtained from ASCE 7-05.
\bar{V}_{33}	Hourly mean wind speed at 33 ft above ground
\bar{V}_H	Hourly mean wind speed at pivot height
\bar{V}_{ref}	Reference wind speed measured at reference height of 1 meter above the wind tunnel floor
Z_{ref}	Reference height above the wind tunnel floor
α	Power law exponent of the modeled wind profile
β	Pitch angle of PV panel of tracker
$\bar{\gamma}_D, \tilde{\gamma}_D, \hat{\gamma}_D$	Mean, standard deviation and peak drag force reduction factors
$\bar{\gamma}_L, \tilde{\gamma}_L, \hat{\gamma}_L$	Mean, standard deviation and peak lift force reduction factors
$\bar{\gamma}_{FN}, \tilde{\gamma}_{FN}, \hat{\gamma}_{FN}$	Mean, standard deviation and peak normal force reduction factors
$\bar{\gamma}_{My}, \tilde{\gamma}_{My}, \hat{\gamma}_{My}$	Mean, standard deviation and peak pitching moment reduction factors
θ	Wind direction
ρ	Mass density of air

1. INTRODUCTION

Recent years have seen a rising use of renewable energy all around the world. Various innovative systems have been introduced to harness such energy. Globally, solar energy is one of the fastest growing and the most popular renewable energy source. Solar energy has several uses such as heating, cooking, power generation, etc. Solar power generation, which is defined as harnessing of electric power from solar energy, is considered as the most widespread form of solar energy used around the world. Electric power generated from solar energy is not only considered to be renewable, but also clean, as it prevents generation of pollution associated with operation of coal and nuclear power plants. Despite the recent global financial crisis, in the area of solar power significant advances have been achieved in the conversion of photovoltaic (PV) energy, using fixed and sun-tracking systems. Worldwide, the installed solar photovoltaic capacity has grown by 44%, in the past year [18]. Representative examples of typical installations of PVT are displayed in Figure 1.1.

The dominant factor affecting the performance and design of PVT is wind action. In general, when wind flows past an object with sharp edges, flow separations occur at the windward edges and corners. High negative pressures (suctions) are generated in such areas and this leads to unfavorable aerodynamic loading – significant wind uplift, the drag force and the overturning moment. Due to the complicated nature of flow patterns and distribution of wind loading, these effects are typically evaluated during wind tunnel

tests carried out for generic configurations of PVT placed in representative wind exposures. Recent advances in laboratory instrumentation have allowed precise measurement of dynamic wind loading exerted on PVTs. These data were used in dynamic analyses of the PVT's wind induced structural responses. In the majority investigations of wind loading on PVTs, the primary objective has been to determine wind loads on trackers that could be utilized in development of design guidelines for specific PVTs and their configurations. With the increasing demand for the ground mounted photovoltaic trackers (PVT), there has been a surge in efforts focused on optimizing configurations of such trackers. The study of wind effects on individual solar tracker allows better understanding and optimized design of the tracker arrays, typically comprising of a large number of trackers in various spatial arrangements. Information on wind loading on PVTs, available in open literature, is limited. Furthermore, there exists the need for an efficient, non-conservative and thereby economical, structural design for PVT systems. In addition, it has been recognized that there is a potential for development of PVT configurations that would minimize the effect of wind load during various operation stages.

The work reported herein explores the potential for reduction in wind loading on an isolated generic ground mounted photovoltaic tracker (PVT), using aerodynamic optimization achieved via geometrical modifications of the PVT geometry. This study is focused on the experimental investigation of the effects of the porosity of the PV panel assembly, carried out in a boundary-layer wind tunnel at the Wind Engineering and Fluids Laboratory, Colorado State University.

2. LITERATURE REVIEW

2.1 INVESTIGATIONS OF WIND LOAD ON GROUND MOUNTED PHOTOVOLTAIC TRACKERS

For a ground mounted photovoltaic tracker (PVT), whether erected in an open field or in sub-urban area, wind loading is the primary load acting on the whole structure. Due to the complexity of flow patterns of wind past PVTs, most of the studies of the wind effects on trackers have been based on experimental studies. The majority of these investigations were carried out in boundary layer wind tunnels, with approach flow being a turbulent boundary-layer flow scaled for model conditions. In most cases, the primary objective of such studies has been to determine wind loads on PVT, for inclusion in guidelines for wind-resistant design [12, 16], or to investigate other important aspects of PVT design, such as the variation of the convective heat transfer from PV assemblies as functions of wind direction [8], and the effects of the wind velocity on settlement of dust on solar collectors [4]. Aside from wind tunnel experiments, investigations of wind loads acting on PVT systems have been carried out utilizing numerical simulations resulting from tools such as Computational Fluid Dynamics (CFD) [13] and Computational Structural Analysis (CSA) [17]. The CFD study carried out for isolated and array of solar trackers reported by Shademan et al. [13] discusses the effect of wind direction and tracker inclination angle on the load on an individual photovoltaic panel in a PVT system. Unlike the turbulent boundary layer flow used in most of the wind tunnel experiments,

uniform flow was considered in this study. Lately, studies have been carried out to optimize not only the wind load behavior but also to improve the reliability and performance of the whole PVT system [7, 14]. Innovative methods, such as use of motors and fluid filled dampers to adjust the orientation and tilt angle of the PV panels [5], have been implemented to reduce wind effects on PVT.

2.2 WIND TUNNEL TESTING

The wind loads of interest in the wind tunnel based experiments typically include: the overall along wind force (drag), vertical force (lift), pitching moment about the PVT pivot axis, and pressure distributions over the PV panel surface. Various shapes, sizes of trackers and spacings between trackers within an array of trackers have been considered in the past studies. The most recent experimental study relevant to the work described herein is a wind tunnel testing of parabolic trough solar collectors [6]. Wind loads were obtained for a collector placed within an array field and they were compared with the results obtained for an isolated collector. Two instrumentation set-ups were employed: a model installed on a high frequency force balance to measure the overall fluctuating loads, and a pressure-tapped model designed to map the distribution of the pressure loads across the faces of the collector. The pitching moment at the pivot center of the collector was measured using a torque transducer mounted at one end of the collector. For the pressure measurements, a 1:45 scale rigid plastic model with 60 pressure taps was used. A large number of the pressure taps were distributed near the PV panel edges and corners to accurately capture the wind induced pressures in these regions. Wind loads on the

models were obtained for different wind directions and inclination angles of the collector. Considerable reductions in wind loads were found for the collectors placed within an array, due to the shielding effects.

A study of wind loading on heliostats and wind loading reduction was reported by Peterka et al. [10]. The mean wind loads on solar collectors were obtained through tests carried out in a boundary layer wind tunnel. The wind loads were measured using a six component (force and moment) balance. They were acquired for an isolated heliostat and for heliostats in array configurations. The effects of the proximity of the heliostats in array arrangement, and the effects of the array perimeter fences and spoiler devices attached to the heliostats were investigated. Overall, the localized effects of the heliostat geometry on the wind loads were found to be limited. The effects of the heliostat proximity (within the heliostat array) were investigated in more detail. Based on the obtained results a concept of a generalized blockage area (GBA) defined on the basis of the parameters of the perimeter and in-field fences were developed. The report also provided the force and moment coefficients induced by wind, for the studied heliostats, for varying pitch (inclination) angles and wind directions. In a similar study of three panel heliostats with 8.7% porosity [9], the effects of internal fences and nearby heliostats on the wind loads were investigated in detail. The effects of the varying geometry of the PVT system on wind loads were not evaluated in these studies.

2.3 WIND LOADS SPECIFIED IN BUILDING STANDARDS

Typically, the design of PVT systems is carried out using forces or pressures for freestanding monoslope roofs, specified in various building standards. Scaletchi et al. [12] have reported a comparative analysis of design guidelines incorporated in various building standards around the world. As a part of this study the force and pressure coefficients for monoslope roof were compared for various inclination angles of the roof. It should be noted that although the definition of basic wind speed in all the considered standards was different (e.g. 3-sec average gust in ASCE7-05, 10-min averages for EN 1991-1-4: Eurocode 1), the force coefficients discussed in this study were not converted to a common reference (average) wind speed. Hosoya et al. [6] discuss this aspect – a conversion of the basic wind speed specified in the ASCE 7-05 standard to mean hourly speed - in a comparative discussion of the wind tunnel based design wind loads and the loads specified in the building standards.

3. EXPERIMENTAL CONFIGURATION

3.1 TEST SETUP

3.1.1 WIND TUNNEL MODELING OF ATMOSPHERIC BOUNDARY LAYER

The experimental tests reported in this thesis were carried out in the Meteorological Wind tunnel (MWT), located at the Wind Engineering and Fluids Laboratory (WEFL), Colorado State University (CSU), Figure 3.1. The atmospheric boundary layer (ABL) flow at a geometrical scale of 1:24 was developed. The target prototype flow was the turbulent ABL in open wind exposure – Exposure C. To model this flow, passive devices such as spires and barriers, and floor roughness (bricks and chains) were used. The configuration and arrangements of these devices and floor roughness were altered until the modeled ABL matched the target ABL. The generated flow was measured using hot-wire anemometry. A pitot-static probe placed at a reference height of 1 m above the wind tunnel floor was employed to monitor the reference wind speed. Figure 3.2 shows the wind tunnel setup developed to model the ABL.

The mean velocity and turbulence intensity profiles were acquired for this flow at the center of the turntable (with the PVT model removed) and they were compared with the corresponding profiles specified in the ASCE7-05 standard [2]. Several configurations of the passive devices employed were tested until the acquired wind profiles were in a good agreement with the ASCE standard. Figure 3.3 compares the measured values (denoted

CSU) with the target quantities (denoted ASCE). The mean velocity profile closely matched the ASCE model, with a power coefficient of 0.18, Figure 3.3(a). The turbulent intensity postulated by the ASCE standard was in agreement with the modeled turbulence intensity up to approximately 1.5 times the height of PVT, Figure 3.3(b). As can be seen, at larger heights the experimental values were smaller than those of ASCE. However, these deviations (in the turbulence intensity) were considered acceptable in view of approximations incorporated in turbulence intensity calculations using ASCE standard.

3.1.2 HIGH FREQUENCY FORCE BALANCE

To investigate wind forces on a single PVT, a High Frequency Force Balance (HFFB) was used, to measure the drag and lift forces, and the pitching moment. The HFFB system consisted of a high-frequency six-component force sensor (force balance), data acquisition board, cables, connections, and software and drivers interfaced with the data acquisition software developed at WEFL. A number of modifications were implemented in the wind tunnel turn table to accommodate the force balance support and its isolation from wind tunnel vibrations.

The force balance used was a Gamma US-15-50, fabricated by ATI Inc. A non-magnetic aluminum breadboard was used to support the balance to ensure the support rigidity and to minimize the relative motion of the whole system with respect to the wind tunnel floor. The PVT model was firmly connected to the force balance by a series of aluminum base plates and screws shown in Figure 3.4. The force balance electronics was connected with a computer-mounted data acquisition board, using a shielded co-axial cable. The HFFB data was acquired and processed using the data acquisition software developed at WEFL

using the LabView programming environment. This software provided an interface with the support drivers and software supplied by ATI, Inc.

3.1.3 DESIGN AND FABRICATION OF MODELS OF PVT

Prior to the development of geometry of a generic large PVT, configurations, dimensions and details of various trackers available in US market were examined [1, 3, 11, and 15]. Taking into account the flow blockage limitations of the available wind tunnel (MWT), a 1:24 geometrical scale was adopted to model a generic prototype PVT. The major components of the developed model were: frame, pivot tube, supporting tube, base plates, and plastic sheets. A square frame, 7.625 in. x 7.625 in., of the modeled PVT was fabricated out of aluminum bars and pipes to reduce the model weight and to ensure rigidity of the model assembly, see Figure 3.5. The center of the PVT (pivot axis) was 5.5 in. above the wind tunnel turn table. The pitch angle (inclination) of the panel of the tracker was adjustable over approximately 180-degree range. An overall view of the PVT model is shown in Figure 3.6. The displayed PV panels were modeled using 1/16-in. thick plastic sheets, fastened to the frame using flat socket cap screws.

3.1.4 PVT TEST CONFIGURATIONS

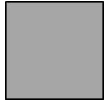
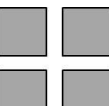
Wind tunnel tests were carried out for three arrangements and four porosities of the tested PVT. The arrangements of the PV panels are specified as follows:

- Single arrangement (A1): PV panels configured as one unit comprising of 32 PVs (8 rows x 4 columns);
- Twin arrangement (A2): PV panels configured as two similar units comprising of 16 PVs (8 rows x 2 columns); and

- Quadruple arrangement (A3): PV panels configured as four similar units comprising of 8 PVs (4 rows x 2 columns).

Arrangements A2 and A3 were employed in modeling three values of the PV panel porosity: 5%, 10% and 15%. The porosity is defined herein as the ratio of the void area to the overall area encompassing the PV panels. The resulting model configurations are listed in Table 3.1, and shown in Figure 3.7.

Table 3.1 Definition of Model Configurations

Model	Arrangement	Porosity (%)	L (in)	B (in)	A_{ref} (in ²)	
1	A1	0	8	8	64.0	
2	A2	5	8.43	8	67.5	
3	A2	10	8.93	8	71.5	
4	A2	15	9.43	8	75.5	
5	A3	5	8.25	8.25	68.0	
6	A3	10	8.43	8.43	71.2	
7	A3	15	8.68	8.68	75.5	

The wind-induced forces on the modeled PVT were acquired for the pitch angles (β) ranging from 0° through 90° , and for the wind directions (θ) in the range of 0° through 180° . The pitch angle and the wind direction are defined in Figure 3.8.

3.1.5 DATA ACQUISITION

For each tested case, the force measurement was carried out over a period of 120 seconds and the data was acquired at a sampling rate of 1000 samples per second. Thus, the obtained data records comprised of 120,000 data points, for each data channel. These data were subsequently used to calculate the mean and the standard deviation, and to extract the maximum and minimum values of the coefficients of the wind induced drag and lift forces, and the pitching moment exerted on the tested PVT. Two repetitions of the measurements were carried out for each test configuration. The obtained experimental results were used in a comparative analysis described in Chapter 4.

3.2 ANALYTICAL BACKGROUND

Figure 3.8 shows the Cartesian coordinate system and the force components considered in this study. The drag and lift forces, and the pitching moment were obtained from the force balance measurements and they were used to calculate the drag, lift, normal force, and pitching moment coefficients, defined below

$$C_D = \frac{F_D}{\frac{1}{2} \rho \bar{V}_H^2 A_{ref}} \quad [3.1]$$

$$C_L = \frac{F_L}{\frac{1}{2} \rho \bar{V}_H^2 A_{ref}} \quad [3.2]$$

$$C_{FN} = \frac{F_N}{\frac{1}{2} \rho \bar{V}_H^2 A_{ref}} \quad [3.3]$$

$$C_{My} = \frac{M_y}{\frac{1}{2} \rho \bar{V}_H^2 A_{ref} B} \quad [3.4]$$

where,

F_x = force measured along the x – axis

F_z = F_L = force measure along the z – axis; lift force

$$F_D = F_x \times \cos(\theta) - F_y \times \sin(\theta) \quad [3.5]$$

= drag force (force along the wind direction)

F_y = force measured along the y – axis

$$F_N = F_x \times \sin(\beta) - F_z \times \cos(\beta) \quad [3.6]$$

= normal force (force perpendicular to the PV surface, positive towards the exposed PV surface, see Figure 3.8(b))

$$M_y = M_{yb} - F_x \times H \quad [3.7]$$

= pitching moment (moment about the pivot axis, see Figure 3.8(a))

M_{yb} = base pitching moment (moment about the y-axis as obtained from HFFB);

ρ = mass density of air;

\bar{V}_H = hourly mean wind speed at model pivot height;

A_{ref} = reference area of PV panel surface (actual area enclosed by PV panel, see Table 3.1); and,

B = reference length (side dimension ‘B’ of PVT, see Figure 3.7).

H = Height of pivot axis of PVT model = 5.5in.

The wind speed \bar{V}_H at the height of the pivot axis was calculated using the power law

$$\bar{V}_H = \bar{V}_{ref} \left(\frac{H}{Z_{ref}} \right)^\alpha \quad [3.8]$$

where,

\bar{V}_{ref} = reference wind speed measured at reference height of 1 meter above the wind tunnel floor;

Z_{ref} = reference height = 1m; and

α = power law exponent of the modeled mean wind profile.

The force and moment coefficients in Eqs. [3.1] through [3.4], are discussed in the next chapter. They are used as the basis for discussion of the effects of the wind direction, pitch angle and porosity of PV panels on the wind induced forces.

4. RESULTS AND DISCUSSION

4.1 COMPARISON OF REPRESENTATIVE RESULTS WITH DATA REPORTED IN OPEN LITERATURE

Representative results obtained during the present study – the mean force coefficients along x-axis (\bar{C}_{Fx}) and z-axis (\bar{C}_{Fz}), and the mean pitching moment coefficients (\bar{C}_{My}) acquired for pitch angle of 45° and two porosities (5% and 10%) – are compared with the results reported by Peterka et al. [9] for a three-panel heliostat of 8.7% porosity, shown in Figure 4.1. For each value of the porosity, the data is displayed for two arrangements of the PV panels: twin arrangement (A2) comprising of two rectangular vertical panels and quadruple arrangement (A3) comprising of four square panels of the same overall area as that of arrangement A2. Figures 4.2 and 4.3 compare the data obtained from the present study (of the twin and quadruple arrangements) with the results reported in [9] and denoted as CSU-85, for pitch angle of 45° . It can be seen that \bar{C}_{Fx} , \bar{C}_{Fz} and \bar{C}_{My} obtained during the present and past studies [9], vary with the wind direction in a similar manner. \bar{C}_{Fx} (for both the arrangements) are found to be close to those reported in [9]. \bar{C}_{Fz} obtained in the present study for 5% porosity are similar to those of CSU-85, whereas they are larger for the 10% porosity. Similar trends are observed for the \bar{C}_{My} . Though the CSU-85 coefficients are close to those of the present 5% porosity results, lower values of the CSU-85 data exhibited at some wind directions are attributed to the uniform spatial distribution of openings in the CSU-85 PV panel assembly.

4.2 EFFECTS OF POROSITY ON WIND LOADS

After validation of the obtained results with data from past tests has been completed, the drag (C_D), lift (C_L), normal force (C_{FN}), and the pitching moment (C_{My}) coefficients were analyzed, to assess the effects of the porosity and the PVT configurations i.e. the PV panel arrangement, wind direction and pitch angle. The effect of the wind direction for the 30° inclined solid (Model 1, 0% porosity) and porous models (Models 3 & 6, 10% porosity) are discussed first. Subsequently, the effects of the pitch angle, for the same representative models (0% and 10% porosity), are analyzed for 0° wind direction. In the above comparisons, the twin and quadruple arrangements of PV panels are considered for the porous models. To evaluate the relative effects of the PV panel porosity (p), the mean, standard deviation and peak force, and the moment coefficients obtained for the porous PVT models were normalized using results obtained for the solid PVT (Model 1, 0% porosity).

The obtained mean, standard deviation and peak (non-dimensional) reduction factors, $\gamma_F = C_F(p)/C_F(p=0)$, are plotted for two representative wind directions (0° and 180°), four pitch angles (15°, 30°, 45° and 60°) and the two PV panel arrangements: arrangement A2 (twin PV modules) and arrangement A3 (quadruple PV modules). For each case an average fit (over the considered pitch angles) of the load reduction factor γ_F is included in the plots. A full listing of the statistical properties of wind load coefficients obtained for all the test configurations is presented in Appendix A.

4.2.1 DRAG FORCE

Drag force coefficients (C_D) calculated for porous models: Model 3 and Model 6 (10% porosity) are compared with the solid model (Model 1, 0% porosity). Representative comparisons of these coefficients are presented in Figures 4.4 and 4.5. It can be seen that for all the wind directions the mean (\bar{C}_D), standard deviation (\tilde{C}_D) and peak (\hat{C}_D) coefficients for the porous models are lower than those for the solid model. Similar effects of the model porosity were found for the remaining configurations. Representative comparisons for wind direction of 0° and varying pitch angles are presented in Figures 4.6 and 4.7, respectively, for the twin and quadruple arrangements of PV panels. It can be seen that for higher values of pitch angles the differences in the drag force coefficients, obtained for the porous and the solid models, are bigger.

The drag force reduction factors (γ_D) obtained for the twin and quadruple PV panel arrangements are presented in Figures 4.8 through 4.11, for wind directions 0° and 180° . Plots pertaining to the twin arrangement show that with an increasing porosity the average fits of the mean drag force reduction factor are found to have decreased by 10% (Figure 4.8). Similar effects of porosity are exhibited by the standard deviation and the peak reduction factors, with decrements of about 15~20%. Comparisons of the average fits of the drag force reduction factors obtained for the quadruple PV panel configuration, show 10~15% reductions for the same porosity range.

4.2.2 LIFT FORCE

The effects of the PV panel porosity and wind direction on the lift force coefficient (C_L) are depicted in Figures 4.12 and 4.13, for a pitch angle of 30° . The lift force coefficient is largest for the wind direction normal to the y-axis of the tracker, i.e. wind directions of 0° and 180° , and the lowest for the 90° wind direction, as expected. The mean, standard deviation and peak values obtained for both the twin and quadruple arrangements are found to be lower for the porous models. The lift force coefficient dependence on the pitch angle, for wind direction of 0° , is shown in Figures 4.14 and 4.15, respectively for PV panel arrangements A2 and A3. It is observed that for either of the arrangements, the mean, standard deviation and the peak coefficients attain the highest value at a pitch angle of 30° . Reduction in the lift force coefficient is exhibited by porous models for all the considered pitch angles. The degree of this reduction is quantified next by examining the lift force reduction factor.

Plots of lift force reduction factor (γ_L), for three porosity levels and PV panel arrangement A2, are shown in Figures 4.16 and 4.17. It can be seen that a reduction up to 25% can be achieved, for the average fits (over the considered pitch angles) when porosity is introduced. The effects of porosity, for arrangement A3 are displayed in Figures 4.18 and 4.19. It can be seen that in this case, introduction of porosity leads to smaller reductions in the lift force up to 15%. For wind direction of 180° the displayed results, obtained for arrangements A2 and A3, indicate that the porosity effects are highly dependent on the pitch angle and they range from beneficial through adverse. A comparison of the lift force reduction factors obtained for both the arrangements indicates

that the porous twin arrangements are more beneficial than the quadruple arrangements with similar porosity levels.

4.2.3 NORMAL FORCE

To have a better understanding of the net force (F_N) acting perpendicular to the PV surface, the normal force coefficient (C_{FN}) was calculated using Eq. 3.3. In the following discussion, the normal force is considered to be positive when acting towards the exposed PV surface, see Figure 3.8 (b).

Figures 4.20 and 4.21 illustrate the effects of porosity and wind direction on the normal force coefficient, for PVT models with pitch angle of 30° . It is observed that regardless of the arrangement of the PV panels, the porous models exhibit lower values of C_{FN} than the solid model. The results obtained for the wind direction of 0° , presented in Figures 4.22 and 4.23, reveal the reduction in C_{FN} as a function of the pitch angles as the porosity is introduced. It is observed that as the pitch angle is increased, C_{FN} increases gradually up to the pitch angle of 45° and then it remains approximately constant. The effects of porosity on C_{FN} are more significant for higher pitch angles. These effects are exhibited more clearly by the normal force reduction factors showed for representative pitch angles (15° , 30° , 45° and 60°) in Figures 4.24 through 4.27.

It can be seen that for wind direction of 0° introduction of porosity leads to a reduction of 20% in mean normal force coefficient (\bar{C}_{FN}), for both the considered PV panel arrangements (A2 and A3). The standard deviation and the peak values of the normal force reduction factors are found to be reduced by $15 \sim 20\%$ for the twin arrangement

(A2) and by 10% for the quadruple arrangement (A3). As it was in case of the lift force reduction factors, for wind direction of 180° , the effects of porosity on normal force reduction factors are found to be strongly dependent on the pitch angle.

4.2.4 PITCHING MOMENT

The absolute values of the obtained pitching moment coefficient, C_{M_y} , calculated using Eq. 3.4 is discussed herein. As expected, the maximum pitching moment coefficient is attained at wind flowing perpendicular to the y-axis, i.e. wind direction of 0° and 180° , Figure 4.28. Reductions in the mean and fluctuating values of C_{M_y} are observed as the porosity is increased, for all of the monitored wind directions with the exception of 90° . Similar dependencies were observed for the quadruple PV panel arrangement (A3), see Figure 4.29. In Figures 4.30 and 4.31 the effects of the porosity and the pitch angle on C_{M_y} , for wind direction 0° are respectively shown for arrangements A2 and A3. It is seen that the largest value of the pitching moment is attained at the pitch angle of 30° . It should be noted that the largest value of the lift force coefficient was also obtained at this pitch angle, as discussed in Section 4.2.2.

The average fit of the pitching moment reduction factors (γ_{M_y}) presented in Figures 4.32 through 4.35 indicated that with the PV panel arrangement A2, for wind direction of 0° , the pitching moment was significantly reduced up to 35%. When moderate levels of porosity were introduced, the reduction factors obtained for PV panel arrangement A3, did not indicate benefits of the increasing panel porosity.

4.3 NORMAL FORCE COMPARISON WITH ASCE 7-05 WIND LOADING PROVISION

Approximate loading on a PVT system can be determined using the building standards, such as ASCE 7-05, [2]. When ASCE 7-05 is used, a PVT system is typically idealized as a monoslope free roof. For a generic tracker (approximated as a monoslope roof), of prototype dimensions of 16 ft x 16 ft (with 0% porosity) and 11 ft elevation (height of pivot axis above ground), the net pressure coefficients can be obtained from Figure 6-18A of ASCE 7-05. Subsequently, these values can be used to calculate the normal force on the PVT system, associated with a specific basic (design) wind speed, V_{33} . ASCE 7-05 defines the basic wind speed as a 3-sec gust, at 33 ft height (above ground) in wind exposure category C. Thus the ASCE basic wind speed cannot be directly used to calculate the wind forces using the force coefficients based on the reference average wind speed. It needs to be converted to hourly mean wind speed, at the pivot height of the PVT. For comparison purpose, design wind speed of 90 mph is assumed hereafter

$$V_{33} = 90 \text{ mph} \quad [4.1]$$

The corresponding hourly mean wind speed at the 33-ft elevation above the ground is

$$\bar{V}_{33} = \frac{V_{33}}{1.53} = \frac{90}{1.53} = 58.82 \text{ mph} \quad [4.2]$$

Using the terrain exposure constants from Table 6-2 of ASCE 7-05, the hourly mean wind speed at the pivot height of PVT, $H = 11$ ft, is obtained from power law

$$\bar{V}_H = \bar{V}_{33} \left(\frac{H}{33} \right)^{\frac{1}{9.5}} = 58.82 \left(\frac{11}{33} \right)^{\frac{1}{9.5}} = 52.34 \text{ mph} \quad [4.3]$$

This design wind speed is used along with the normal force coefficients to obtain the design wind loads

$$F_N = q A_{ref} C_{FN} \quad [4.4]$$

where,

$q = (0.00256) \bar{V}_H^2$ = the design pressure corresponding to mean hourly wind speed at PVT pivot height

A_{ref} = prototype reference area of solid PVT = 16ft x 16ft = 256 ft²

The results of the above calculations along with the design loads obtained from ASCE 7-05 for open wind exposure (C) and wind directions: 0° and 180° are shown in Figure 4.36. The details of the above calculations are presented in Appendix B. Prototype design loads calculated from the standard are obtained for load cases A and B, and for clear wind flow referred in ASCE 7-05. While there is no discussion describing the two load cases, load cases A and B in ASCE 7-05 pertain to fluctuating loads and represent the upper and lower limits of the instantaneous wind load. It can be seen that the normal force calculated using the ASCE7-05 wind loading provision, and the peak normal loadings obtained from wind tunnel tests, are of comparable magnitudes and exhibit similar dependences on the pitch angle.

5. CONCLUSIONS AND RECOMMENDATIONS

5.1 CONCLUSIONS

The key outcomes of the experimental study are:

1. The mean force (along x and z axes) and pitching moment coefficients obtained during the wind tunnel study for twin arrangement (A2) of PV panels were in a good agreement with the results of a prior related investigation.
2. The drag force coefficient was reduced when PV panel porosity was introduced. The peak and standard deviation values exhibited higher levels of the reduction than the mean values.
3. The lift force coefficient was the largest at 30° pitch angle for 0° and 180° wind directions. Relatively weak impact of the PV panel porosity, for wind direction of 180°, was found on the mean, standard deviation and peak lift force coefficients. Lift force on the porous models at wind direction of 0° was lower than that on the non-porous model.
4. Normal force coefficients for the porous models decreased with an increasing porosity. These reductions for the mean and fluctuating components were more pronounced for wind direction of 0° than for 180°. The porosity effects were small for the quadruple arrangement of PV panels.
5. The pitching moment coefficient exhibited a maximum reduction of 35%, for the twin arrangement of PV panels. Minimal reduction in pitching moments was

observed for PV panels with quadruple arrangement. The pitching moment was found to be highest for the PVT pitch angle of 30° , for wind flowing normal to the pivot axis.

6. Introduction of porosity was not effective in reduction of wind forces on the tracker with quadruple arranged PV panels.
7. Design wind loads were calculated for the prototype scale of PVT using the normal force coefficients obtained from the wind tunnel tests and compared with ASCE 7-05 standard results for 0° and 180° wind directions. The peak design forces from wind tunnel results were found to be in good agreement with the ASCE 7-05 based design loads.

5.2 RECOMMENDATIONS

In view of the above findings, the following recommendations for further work are proposed:

1. The effects of higher porosities on PVT system should be explored in order to further investigate the reduction in wind loads. New PV panel arrangements, such as arranging the PV panels in three and more columns, to accommodate higher porosity levels are recommended. Inclusion of aerodynamic fairings to break the flow of wind over the PV panel edges should be investigated.
2. In future studies, torque transducers should be employed to directly measure the pitching moment at the tracker pivot height.
3. Studies of wind loading on trackers could be aided by using differential pressure measurements, to map the localized wind loads.

4. It is recommended that wind tunnel tests be carried out for a broad range of wind speeds to evaluate the Reynolds number effects on the loading measured on small porous models.
5. Future tests should incorporate field studies for isolated trackers, and trackers surrounding the instrumented tracker model in array arrangements.
6. Experimental investigations could be supplemented by parametric simulations carried out using numerical (CFD) calculation.

FIGURES



Figure 1.1 Examples of installations of ground mounted photovoltaic trackers (PVT),
[1, 3, 11 and 15]

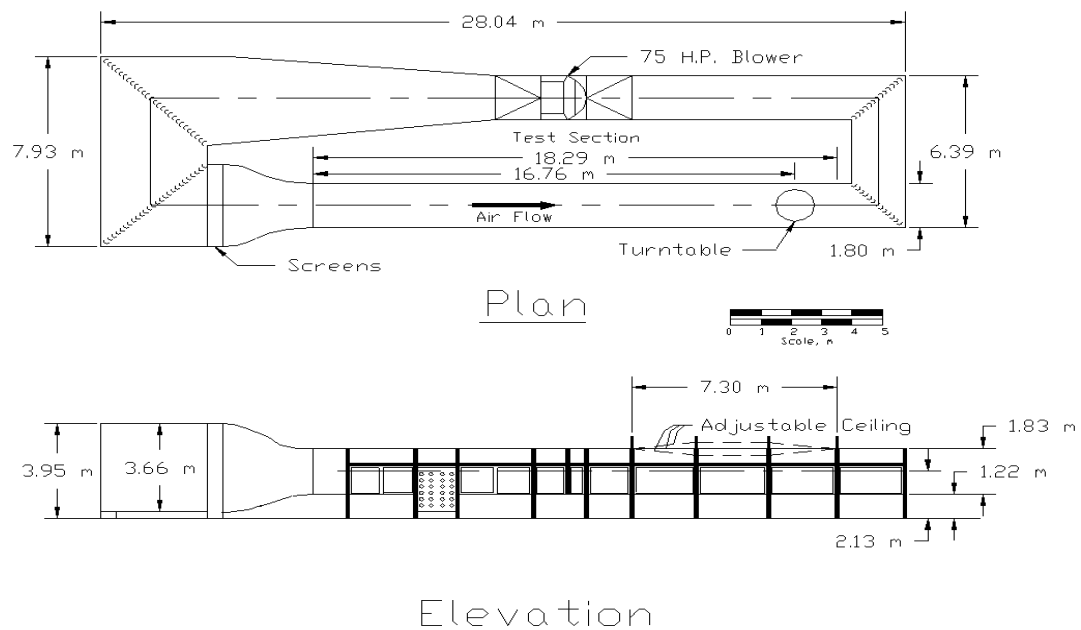


Figure 3.1 Layout of Meteorological Wind Tunnel at Wind Engineering and Fluids Laboratory (WEFL), Colorado State University (CSU)

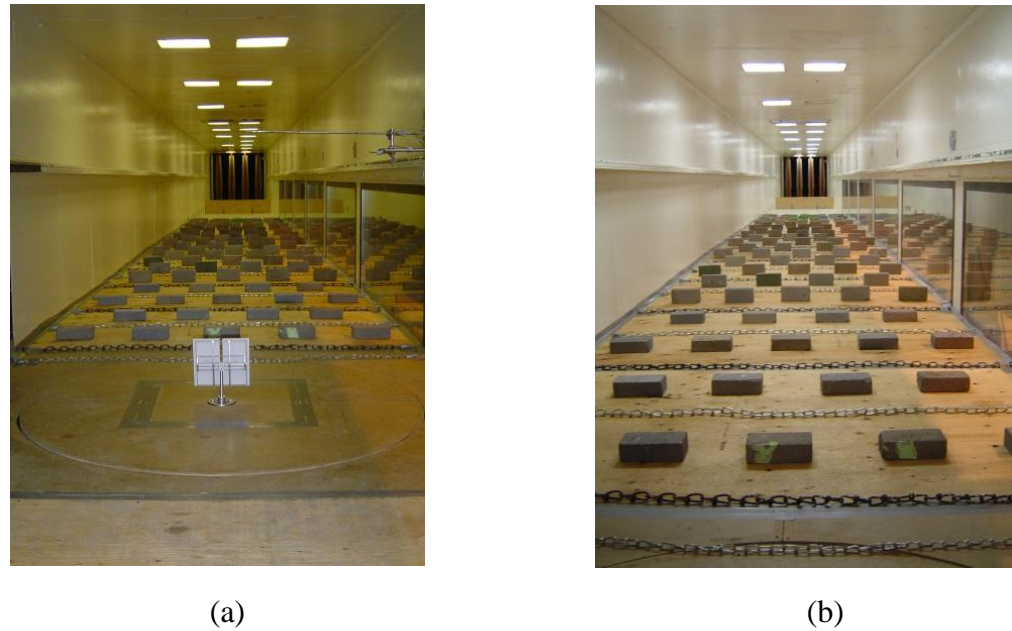


Figure 3.2 Experimental configuration developed for wind tunnel testing

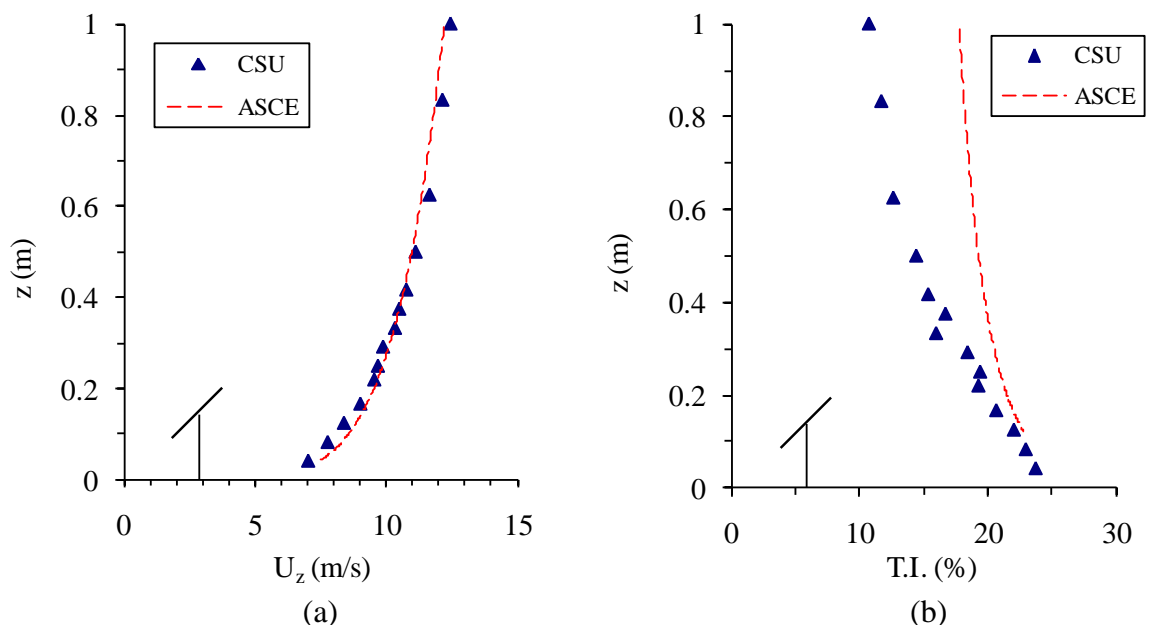


Figure 3.3 (a) Wind velocity and (b) Turbulence intensity profiles



Figure 3.4 High frequency force balance

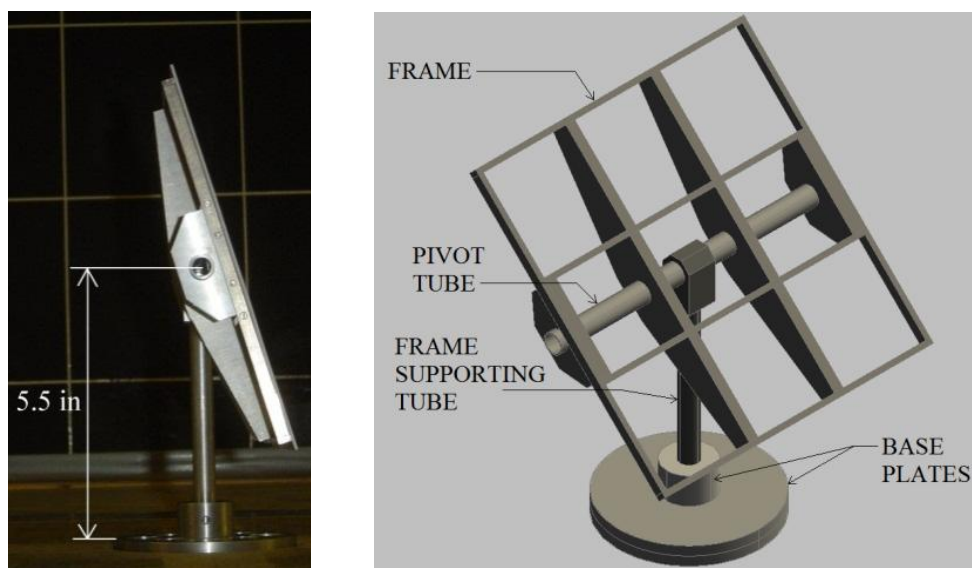


Figure 3.5 Structural components of PVT model

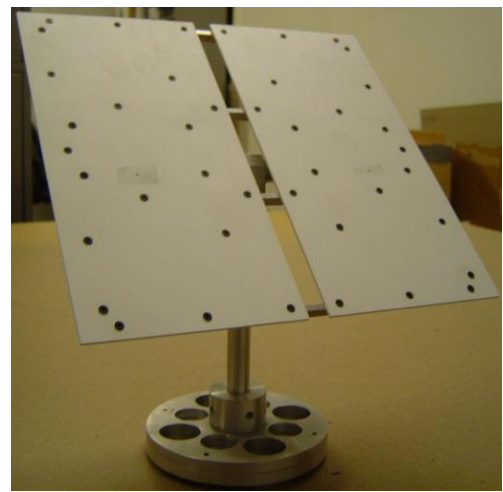


Figure 3.6 Overall view of PVT model with PV panel assembly

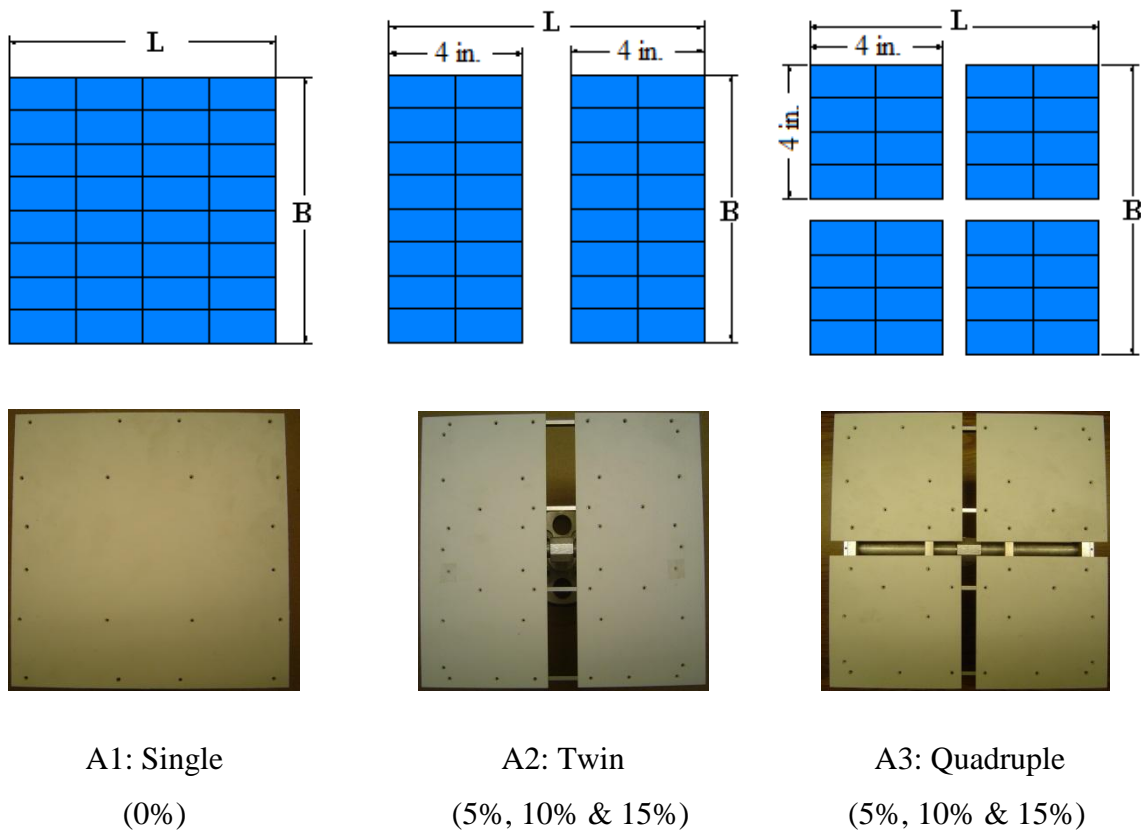


Figure 3.7 PVT configurations and porosities of PV panel assembly

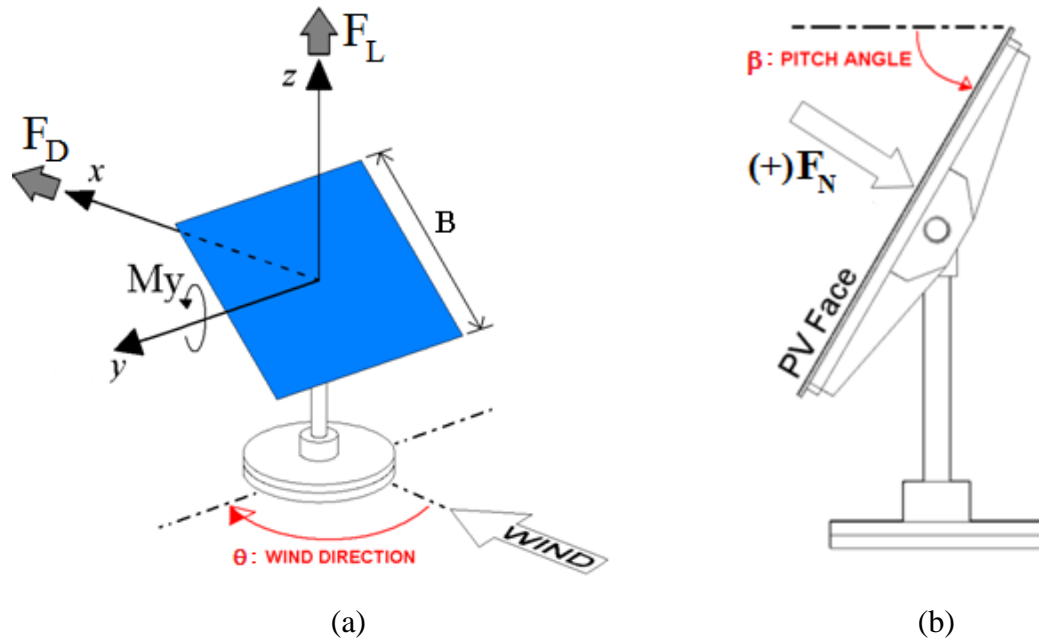


Figure 3.8 Definition of PVT position angles and wind loading components

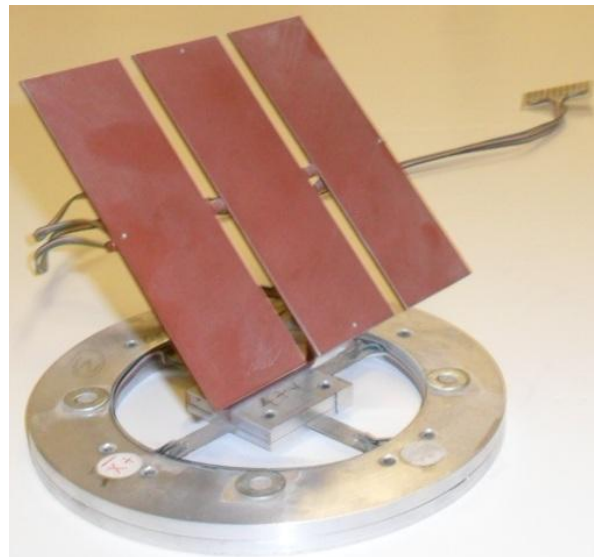


Figure 4.1 Heliostat model used by Peterka et al. [9]

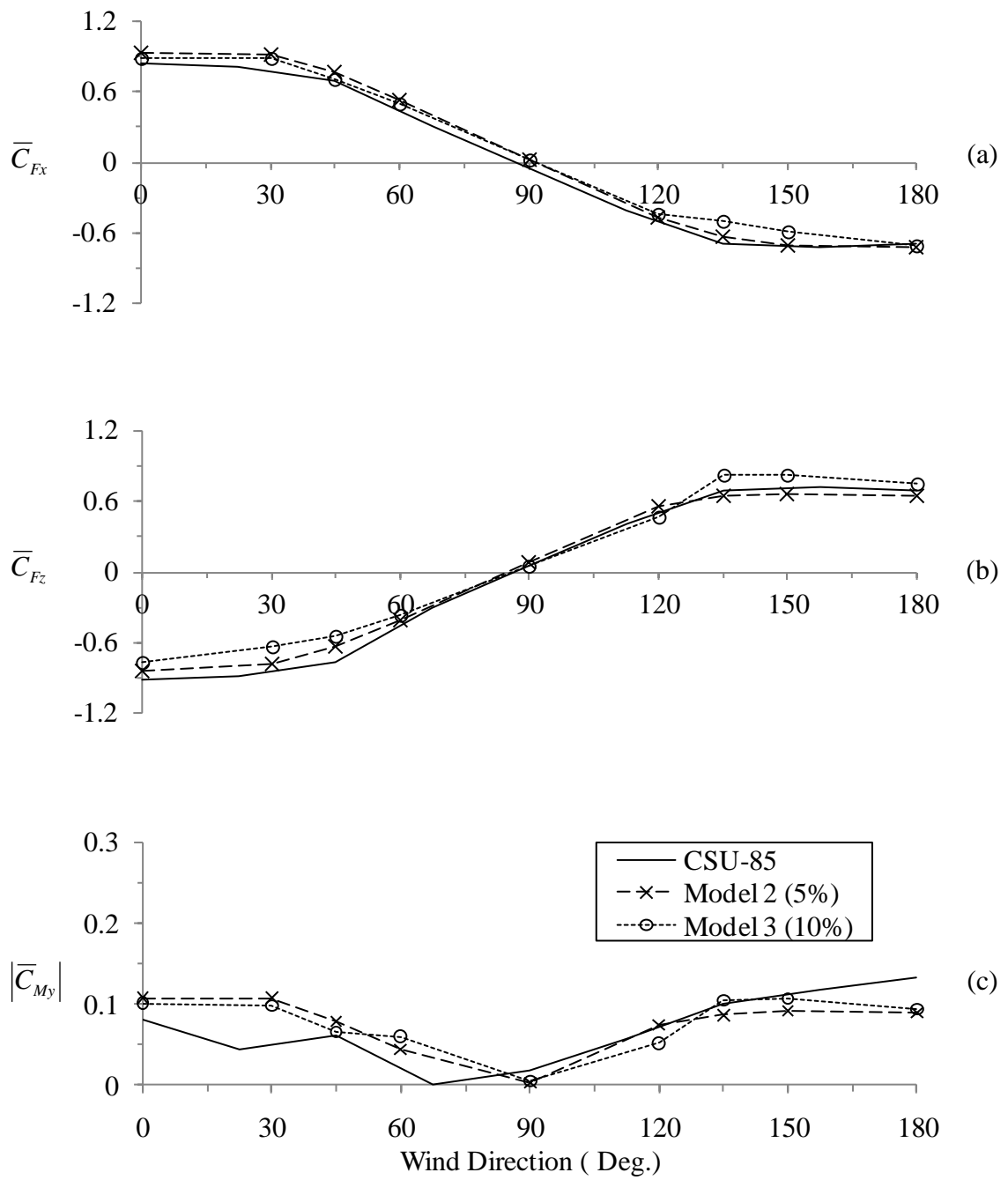


Figure 4.2 Comparison of mean (a) force along x-axis, (b) force along z-axis and (c) pitching moment coefficients, Arrangement A2 & CSU-85, Pitch Angle 45°

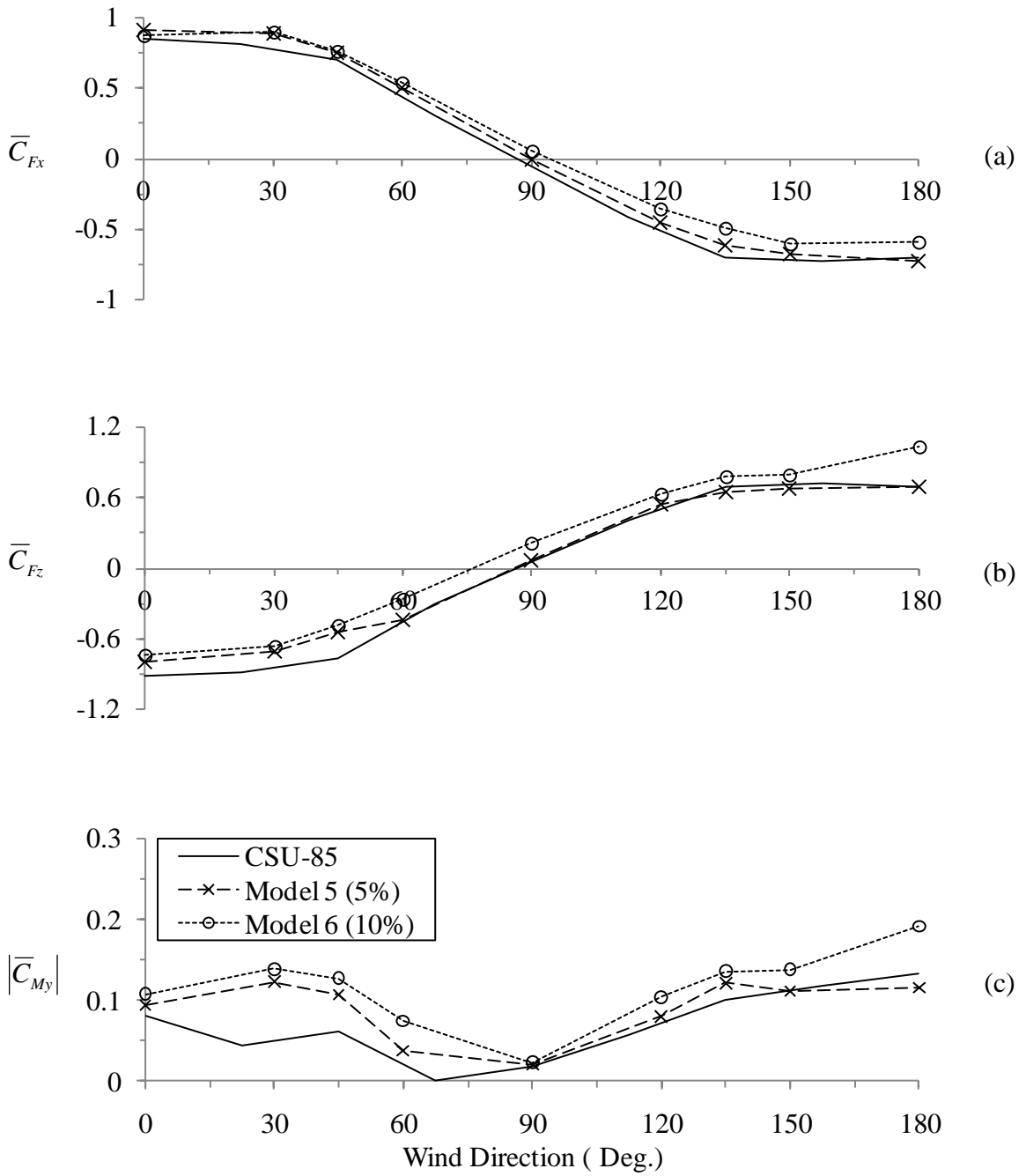


Figure 4.3 Comparison of mean (a) force along x-axis, (b) force along z-axis and (c) pitching moment coefficient, Arrangement A3 & CSU-85, Pitch Angle 45°

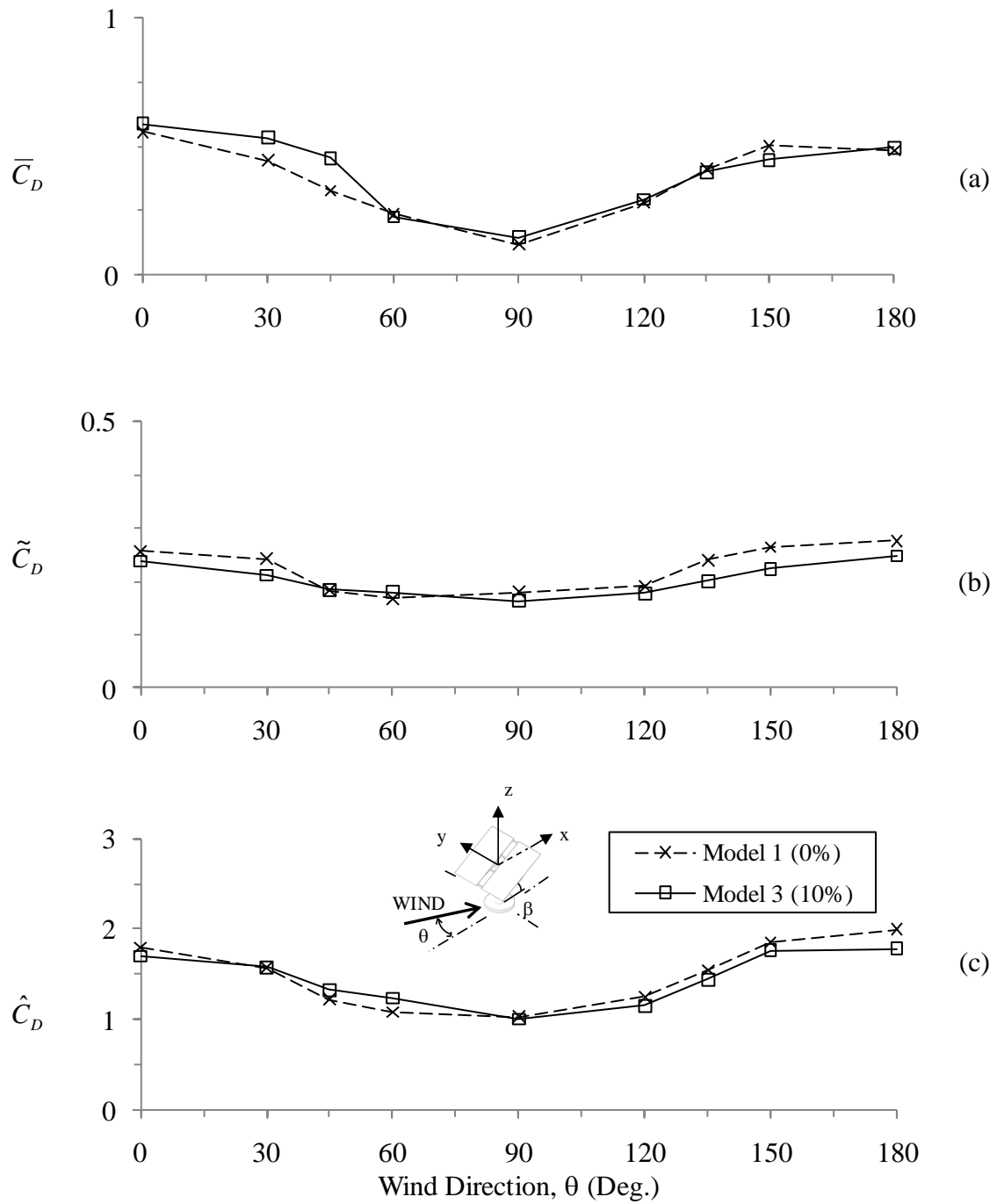


Figure 4.4 Effects of porosity on (a) mean, (b) standard deviation and (c) peak drag force coefficients, Arrangement A2, Pitch Angle 30°

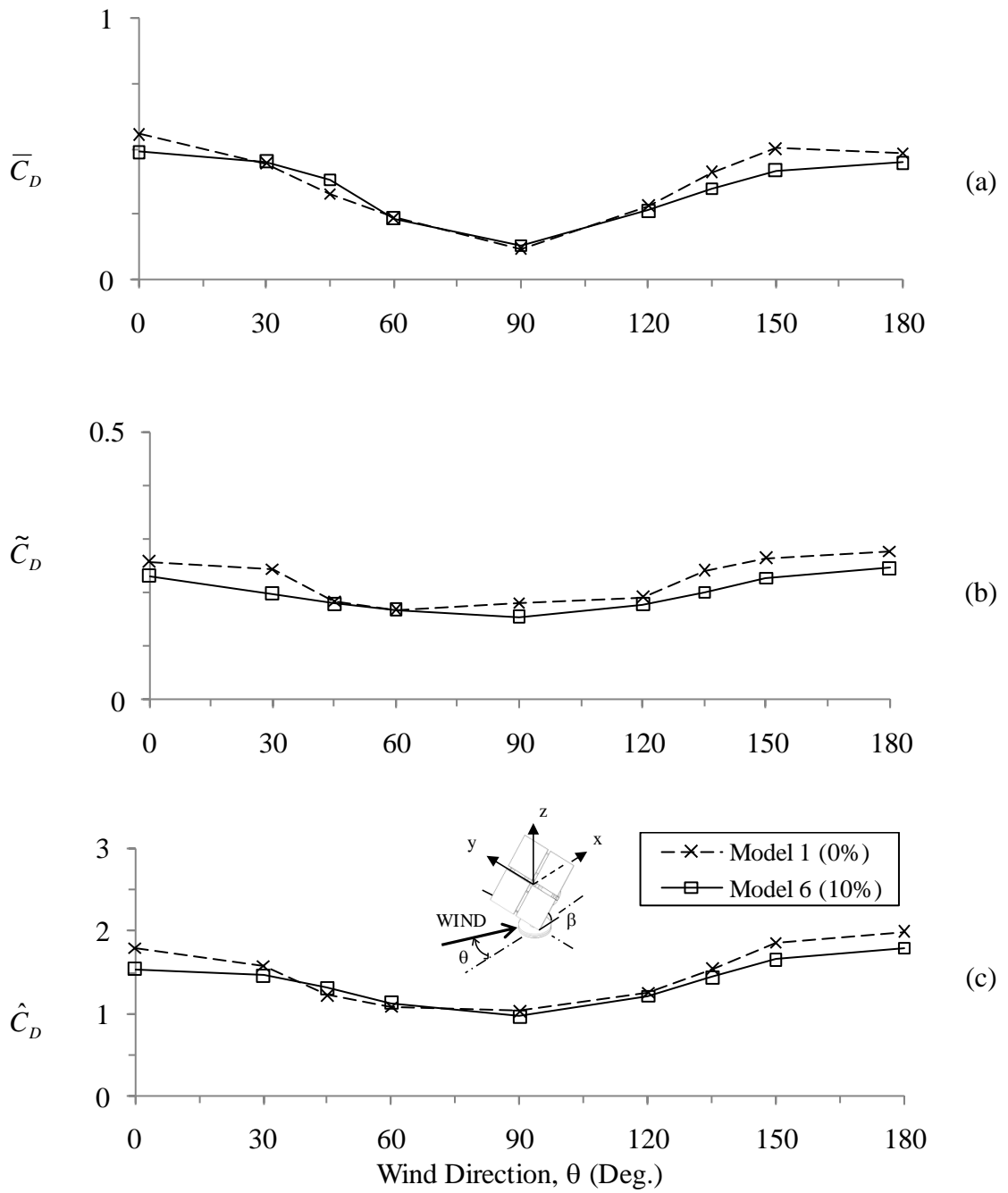


Figure 4.5 Effects of porosity on (a) mean, (b) standard deviation and (c) peak drag force coefficients, Arrangement A3, Pitch Angle 30°

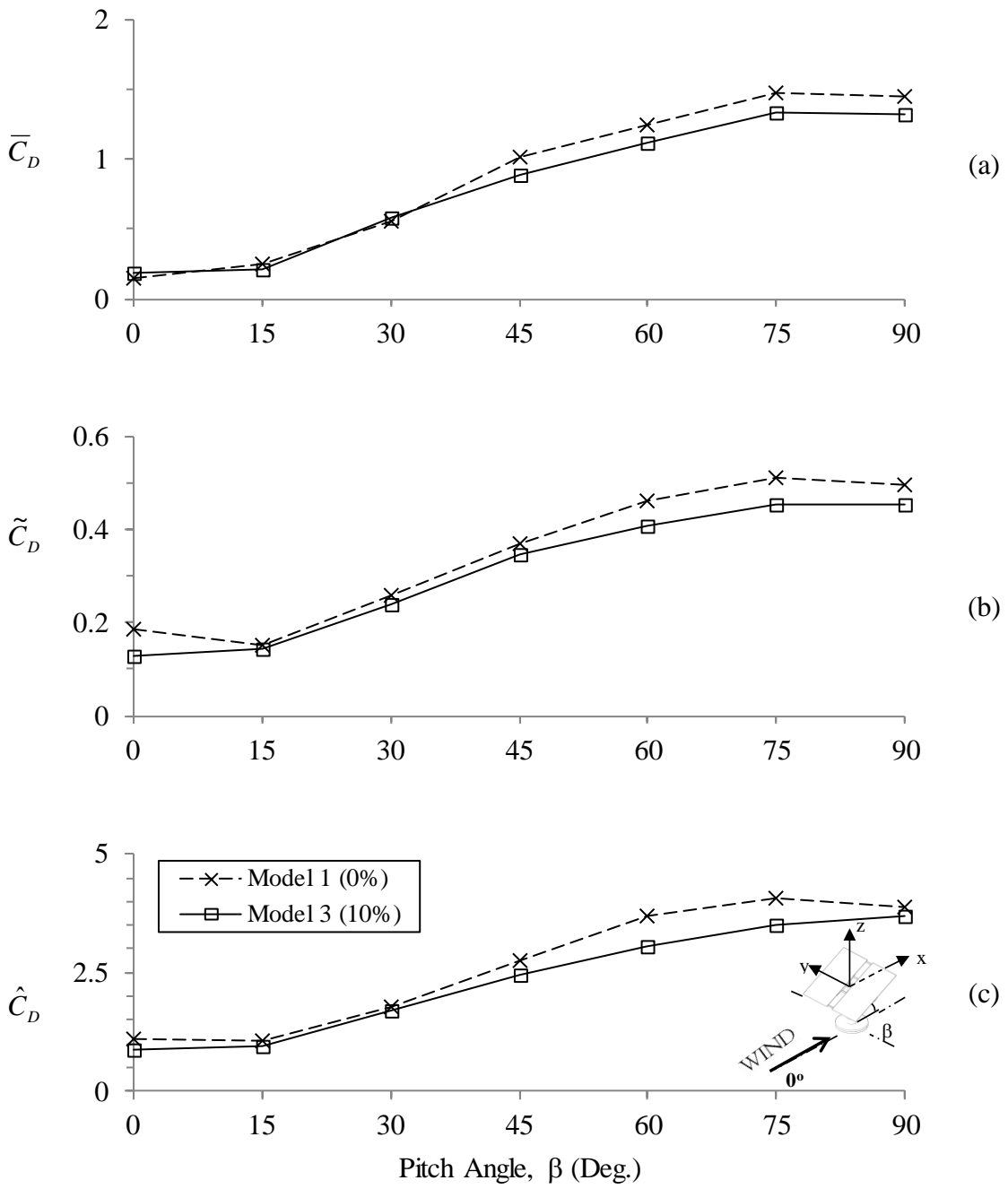


Figure 4.6 Effects of porosity on (a) mean, (b) standard deviation and (c) peak drag force coefficients, Arrangement A2, Wind Direction 0°

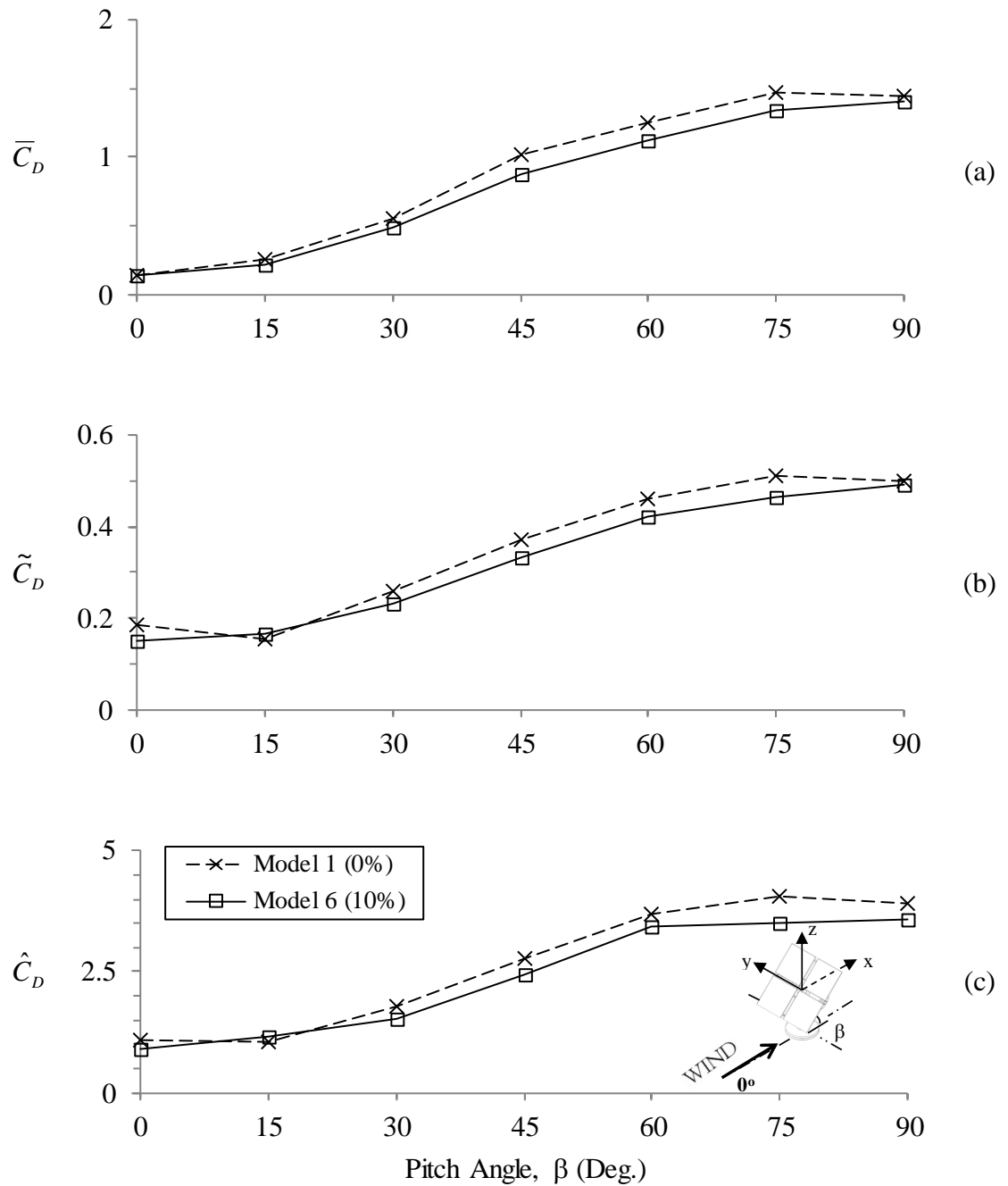


Figure 4.7 Effects of porosity on (a) mean, (b) standard deviation and (c) peak drag force coefficients, Arrangement A3, Wind Direction 0°

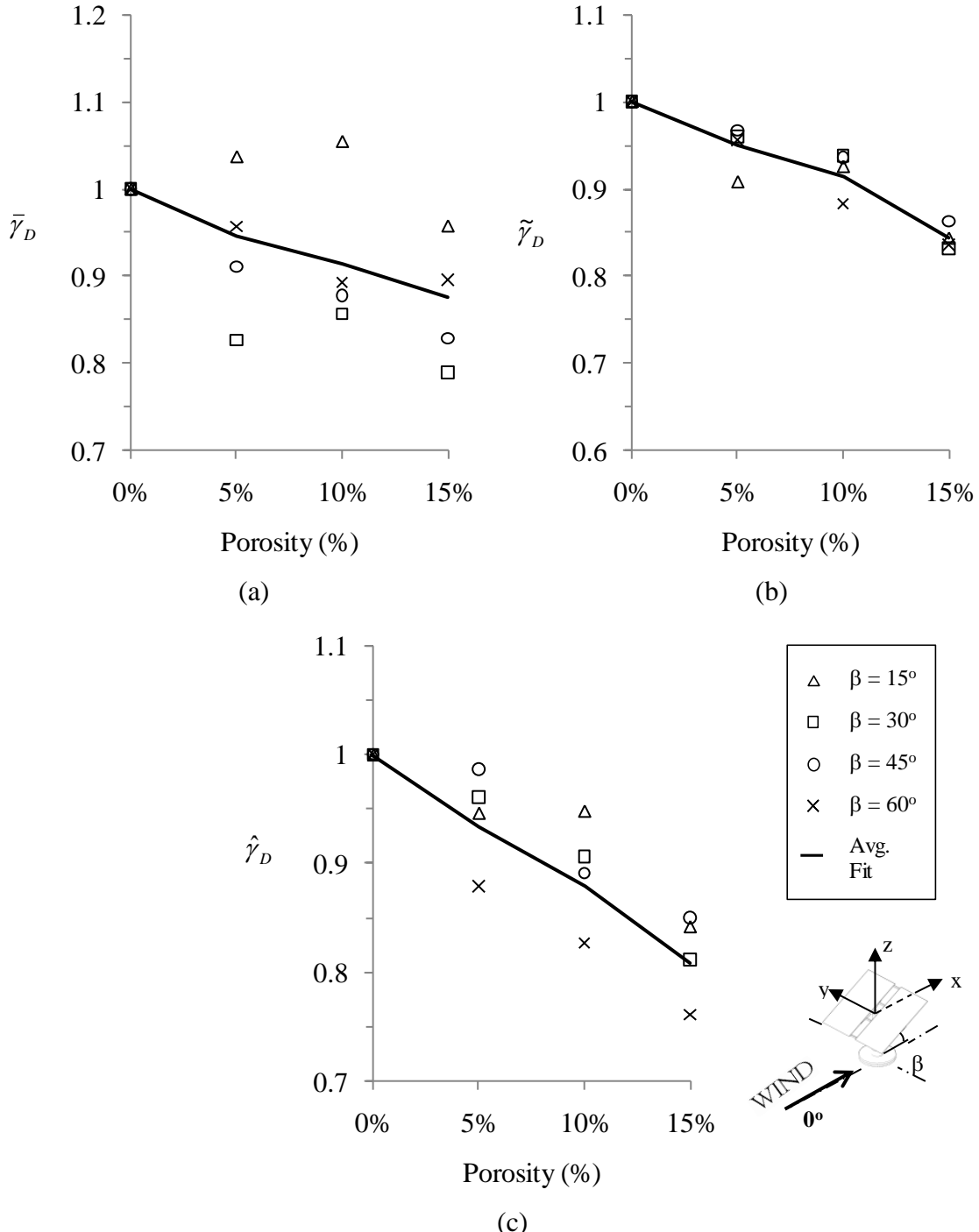


Figure 4.8 Drag force reduction factor: (a) mean, (b) standard deviation and (c) peak,
Arrangement A2, Wind Direction 0°

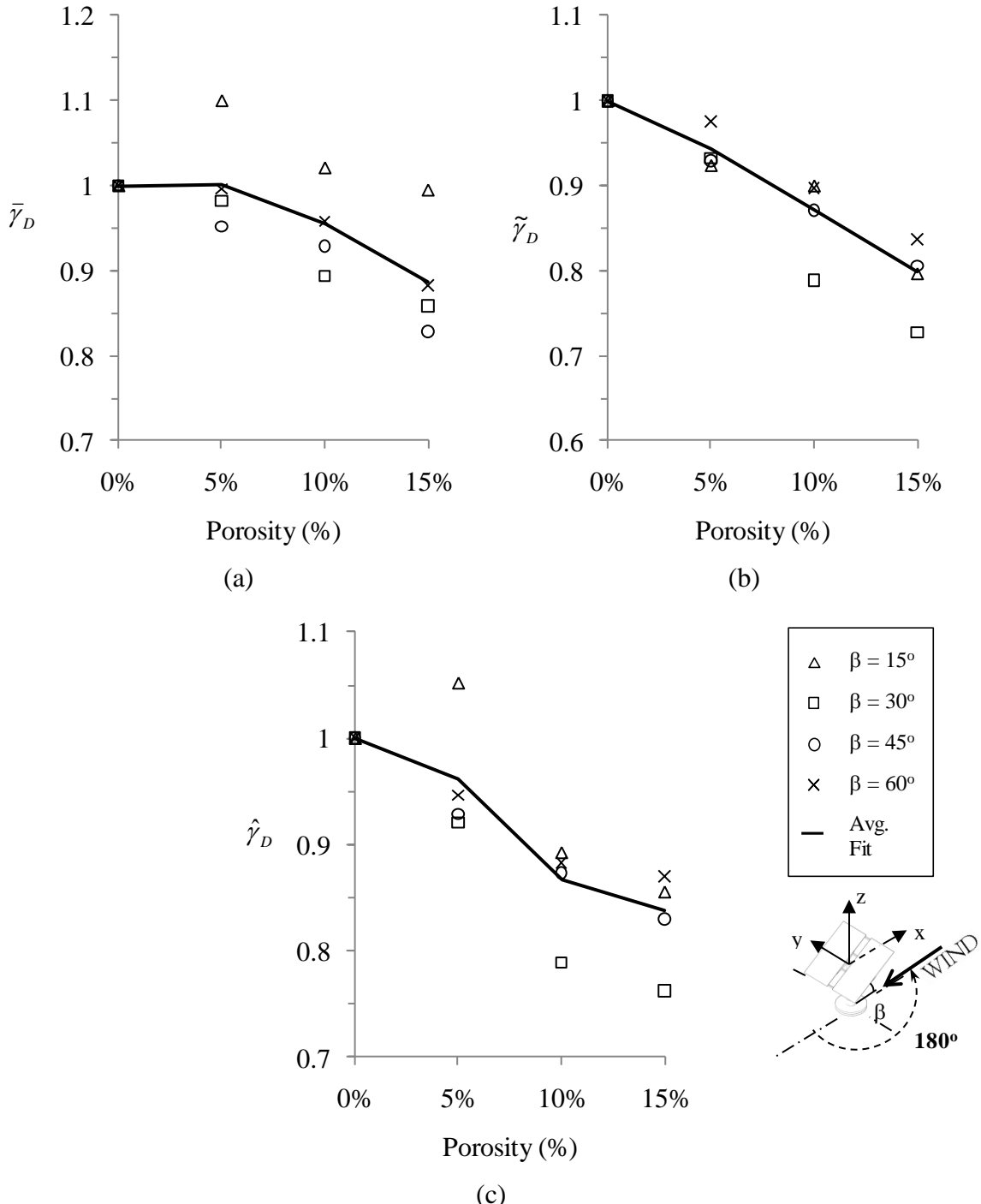


Figure 4.9 Drag force reduction factor: (a) mean, (b) standard deviation and (c) peak,
Arrangement A2, Wind Direction 180°

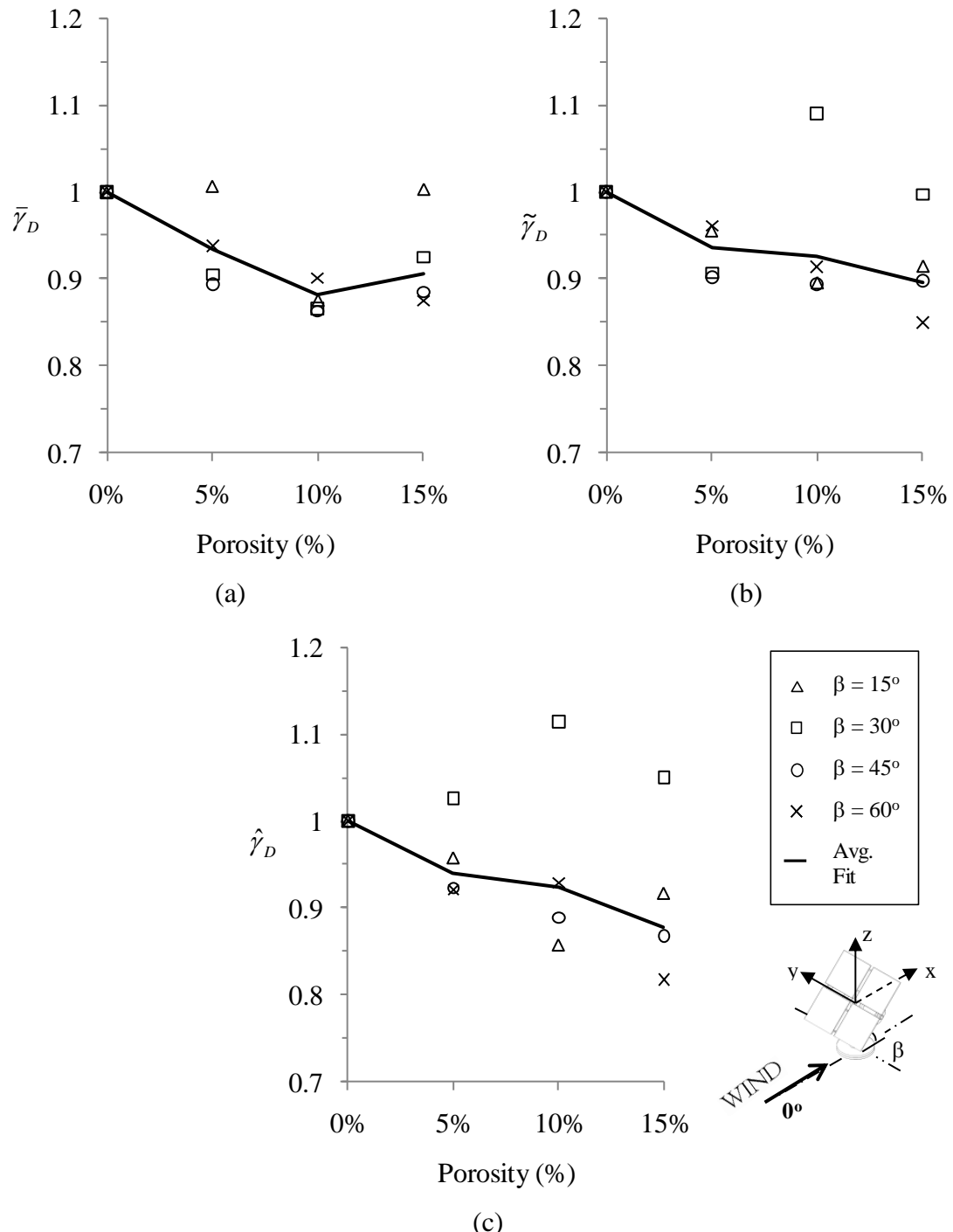


Figure 4.10 Drag force reduction factor: (a) mean, (b) standard deviation and (c) peak, Arrangement A3, Wind Direction 0°

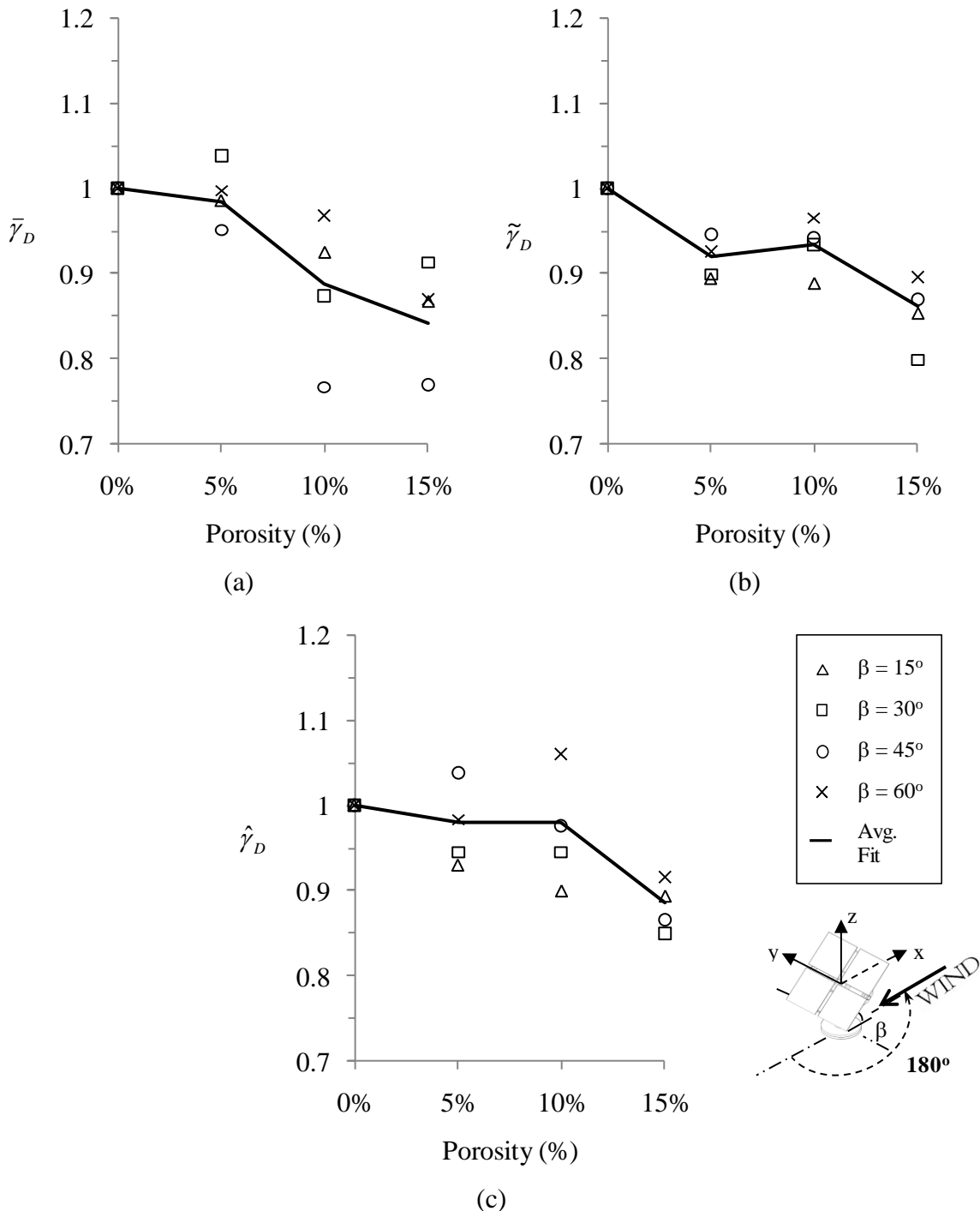


Figure 4.11 Drag force reduction factor: (a) mean, (b) standard deviation and (c) peak,
Arrangement A3, Wind Direction 180°

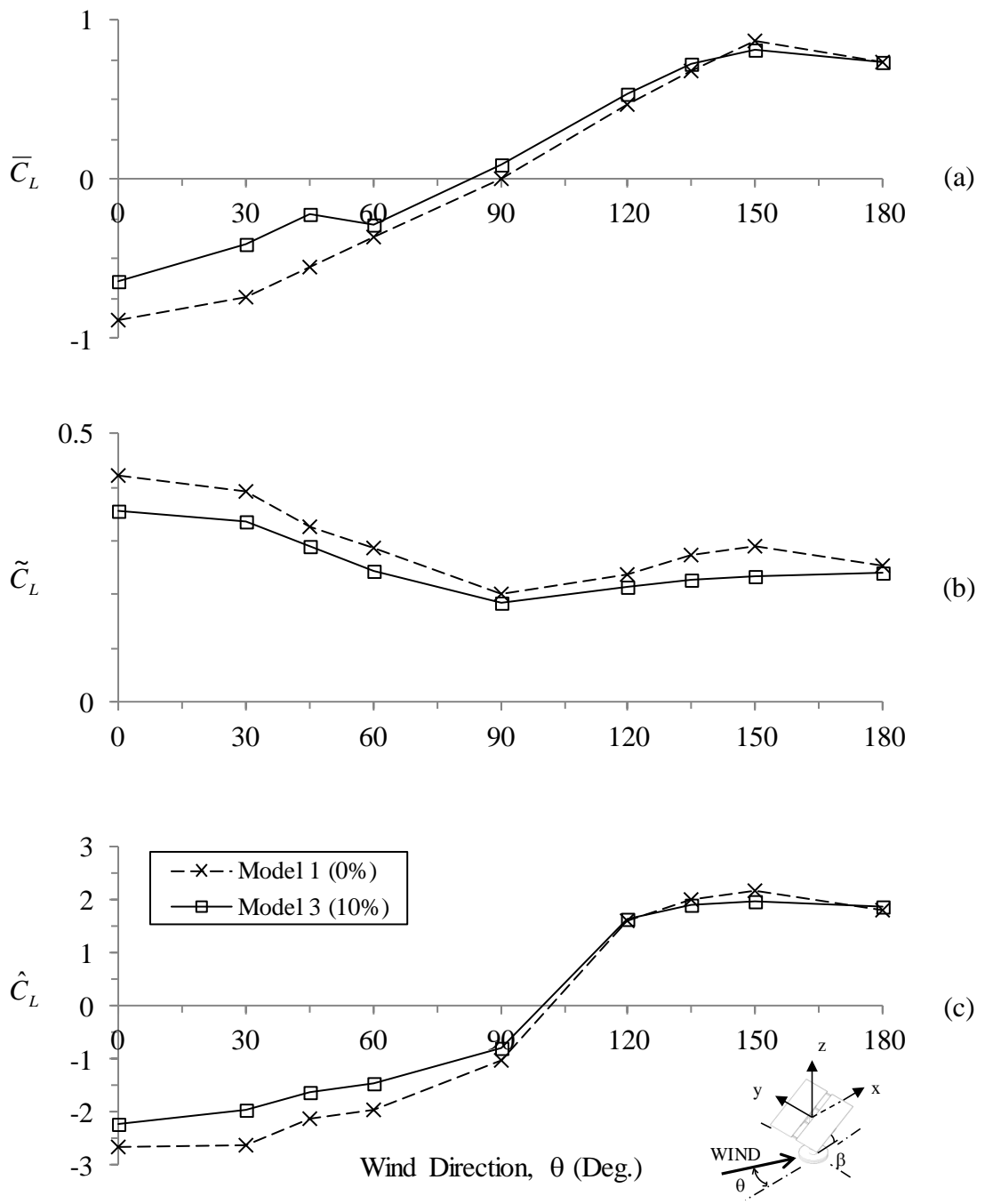


Figure 4.12 Effects of porosity on (a) mean, (b) standard deviation and (c) peak lift force coefficients, Arrangement A2, Pitch Angle 30°

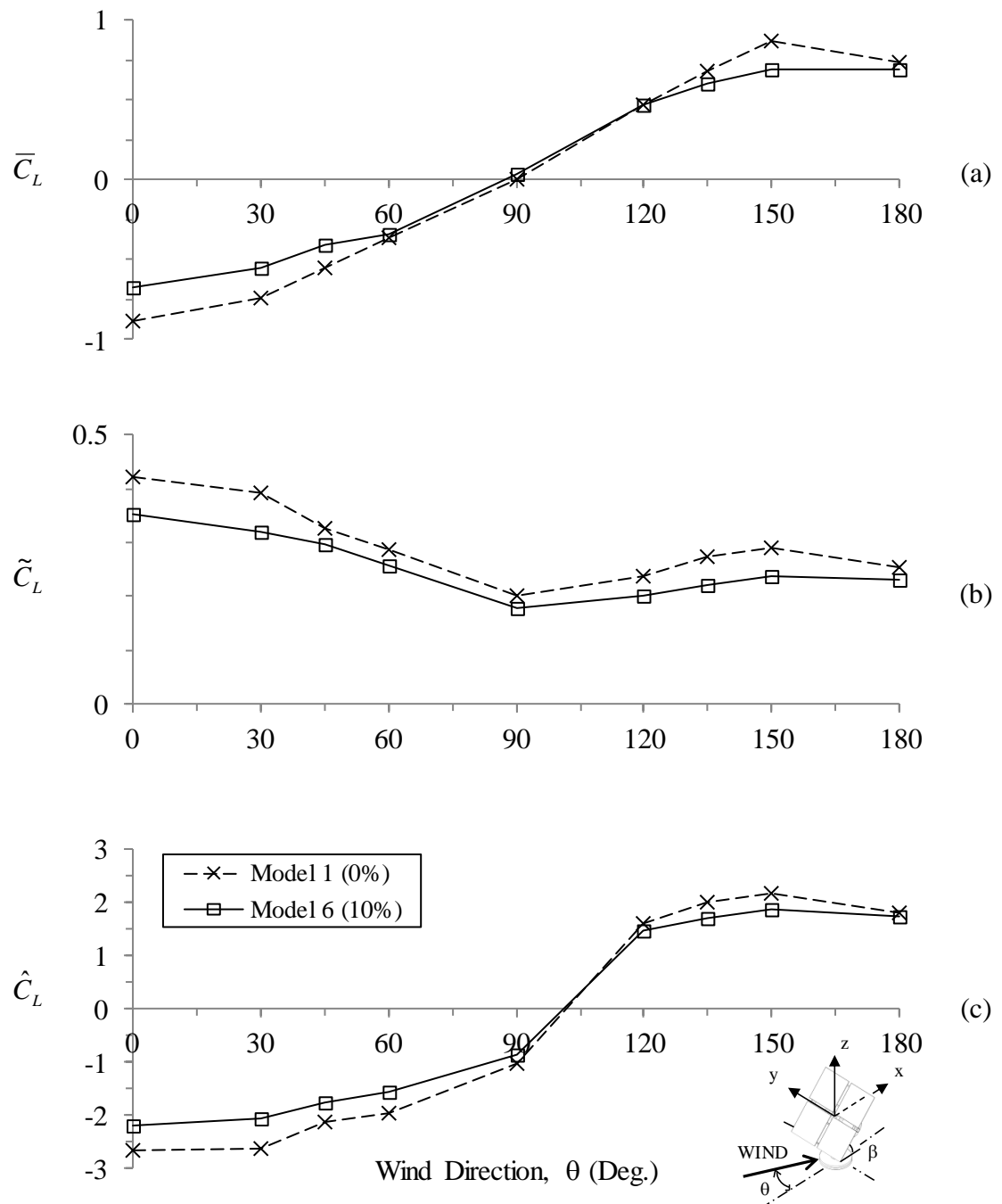


Figure 4.13 Effects of porosity on (a) mean, (b) standard deviation and (c) peak lift force coefficients, Arrangement A3, Pitch Angle 30°

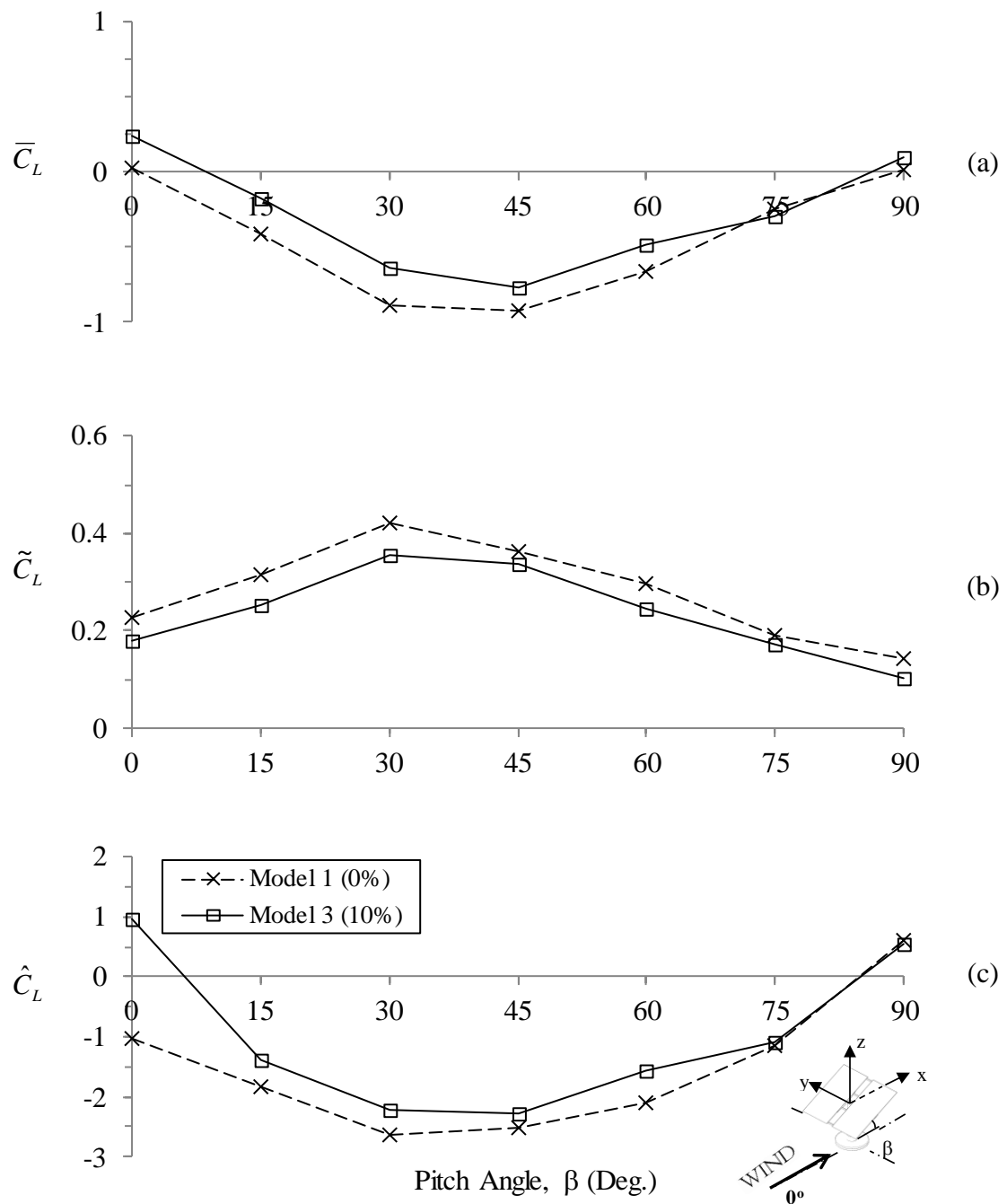


Figure 4.14 Effects of porosity on (a) mean, (b) standard deviation and (c) peak lift force coefficients, Arrangement A2, Wind Direction 0°

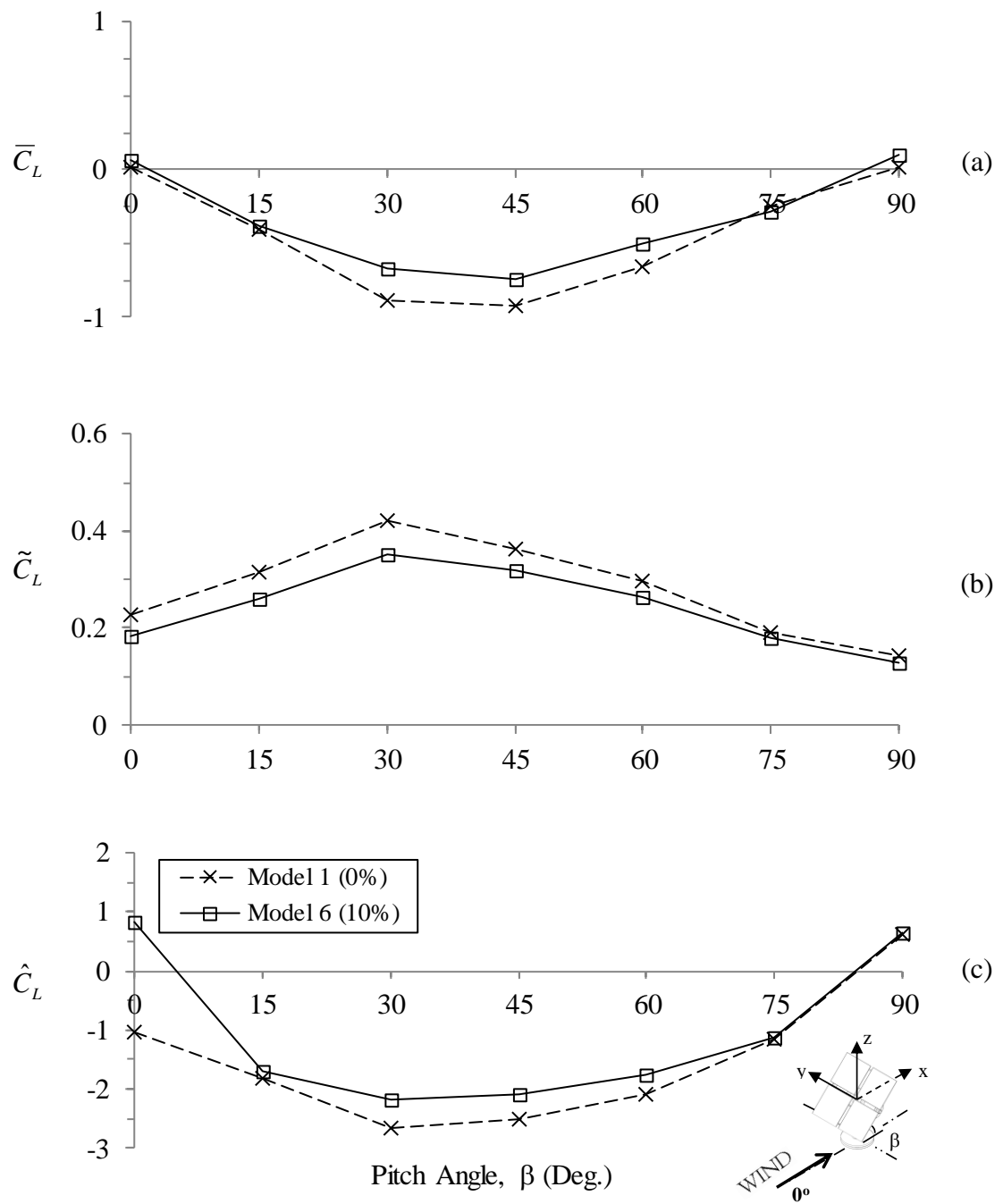


Figure 4.15 Effects of porosity on (a) mean, (b) standard deviation and (c) peak lift force coefficients, Arrangement A3, Wind Direction 0°

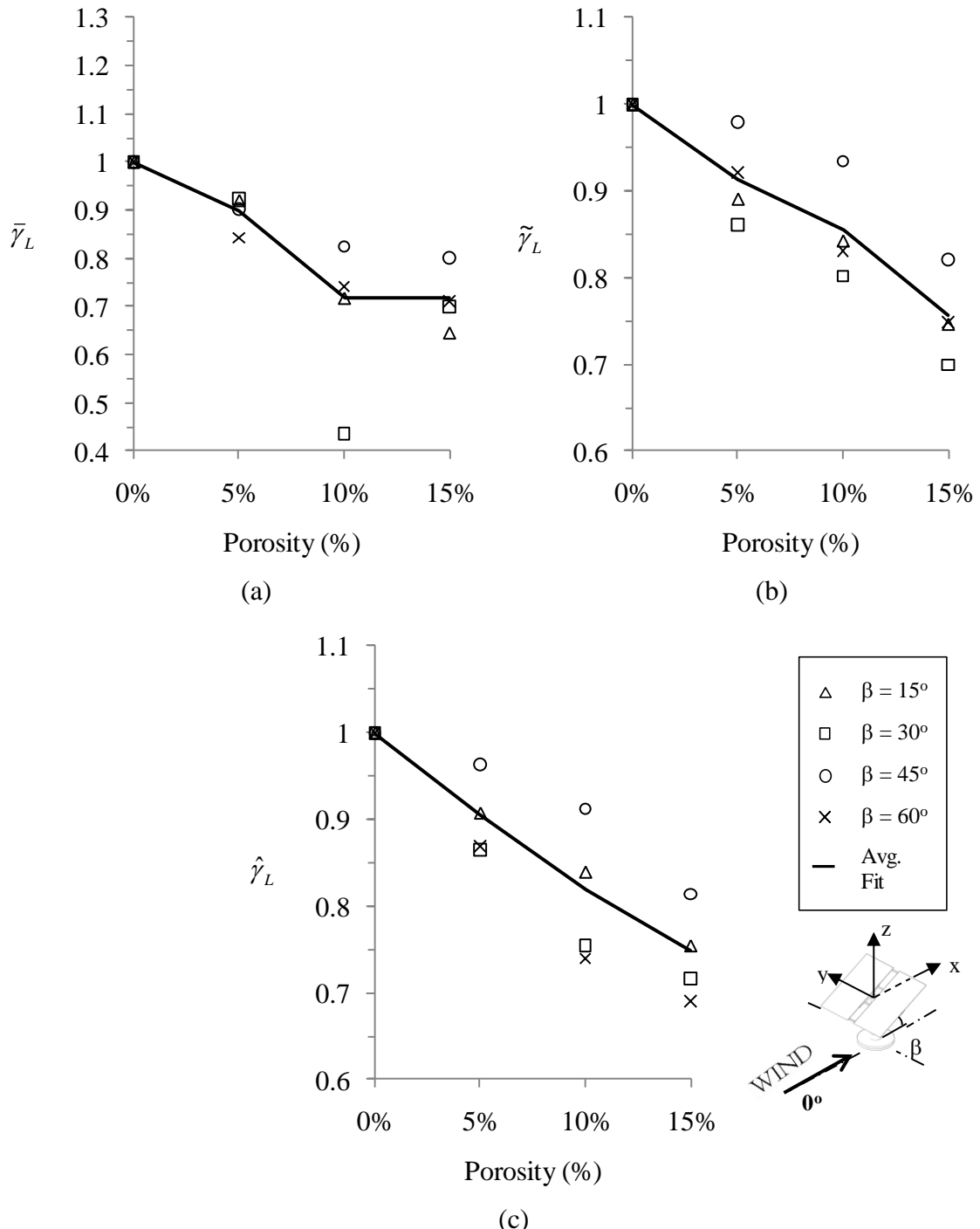


Figure 4.16 Lift force reduction factor: (a) mean, (b) standard deviation and (c) peak, Arrangement A2, Wind Direction 0°

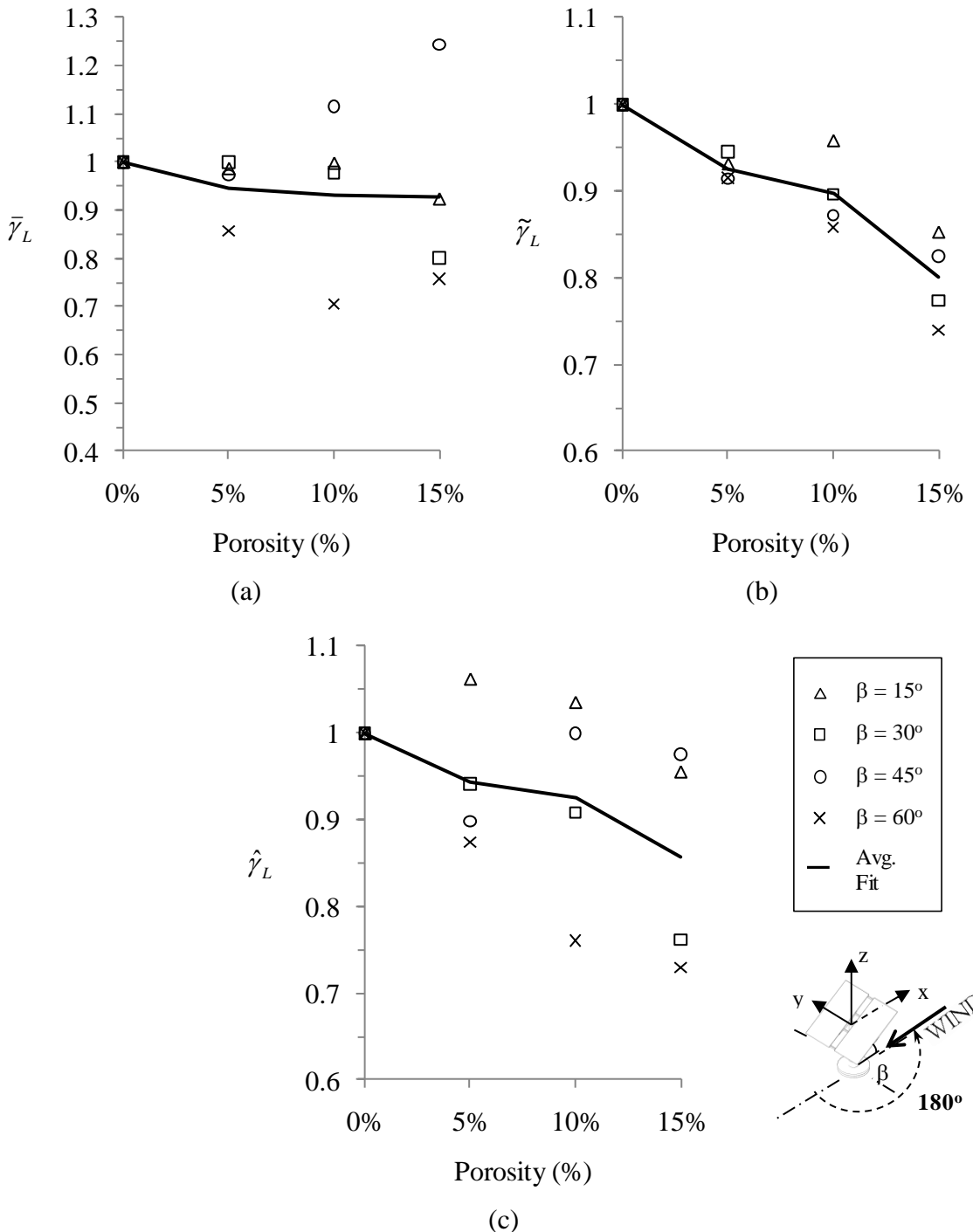


Figure 4.17 Lift force reduction factor: (a) mean, (b) standard deviation and (c) peak,
Arrangement A2, Wind Direction 180°

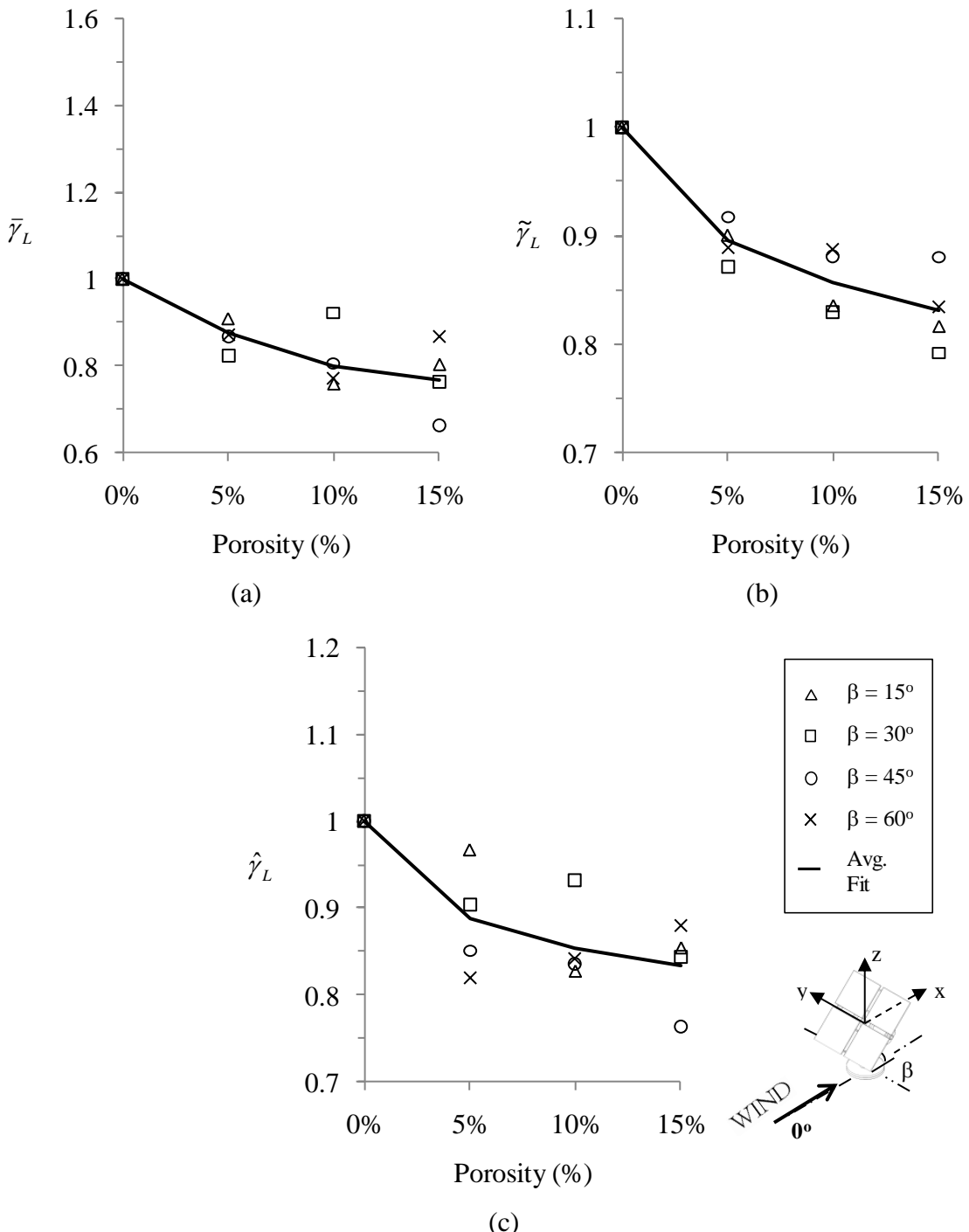


Figure 4.18 Lift force reduction factor: (a) mean, (b) standard deviation and (c) peak, Arrangement A3, Wind Direction 0°

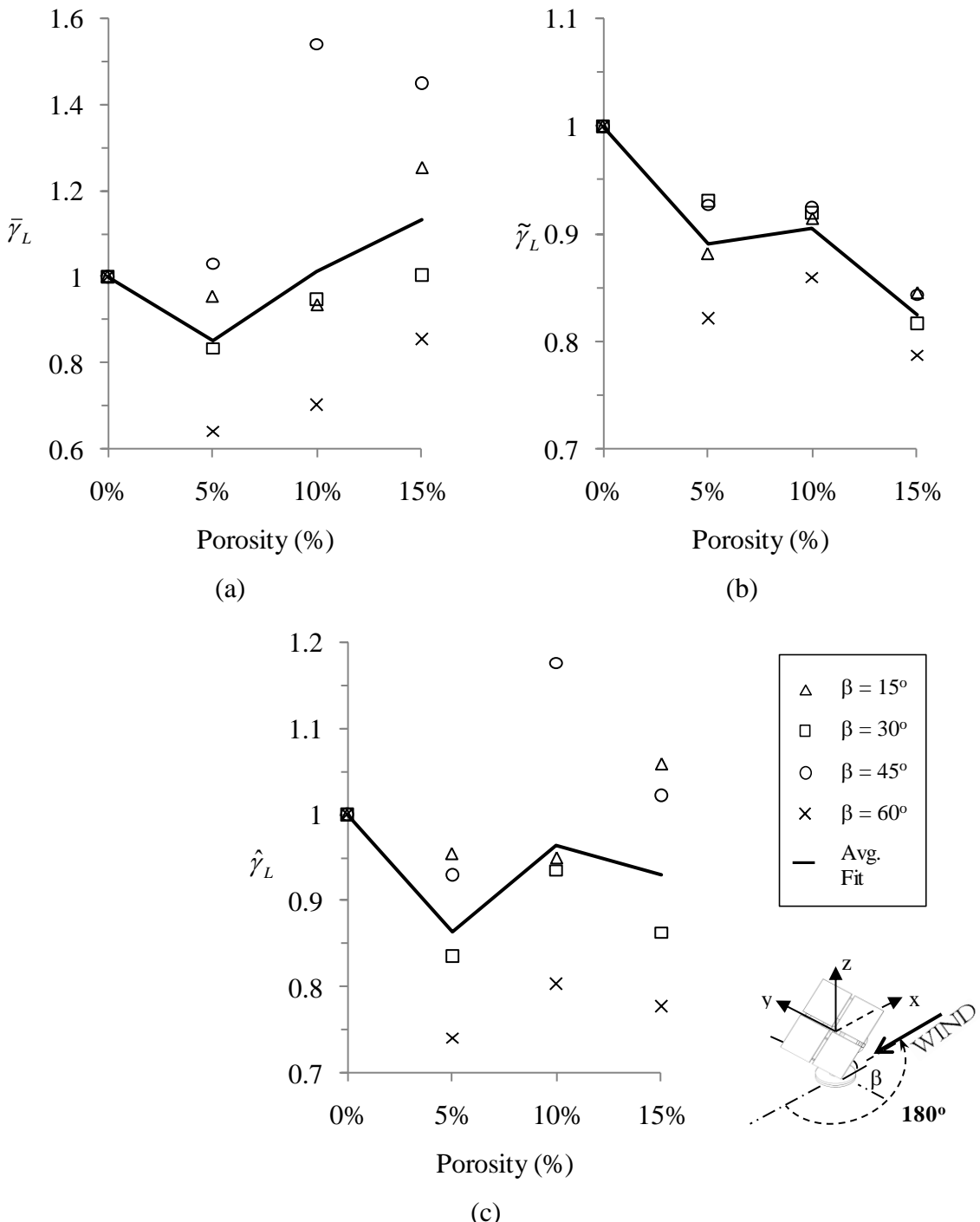


Figure 4.19 Lift force reduction factor: (a) mean, (b) standard deviation and (c) peak,
Arrangement A3, Wind Direction 180°

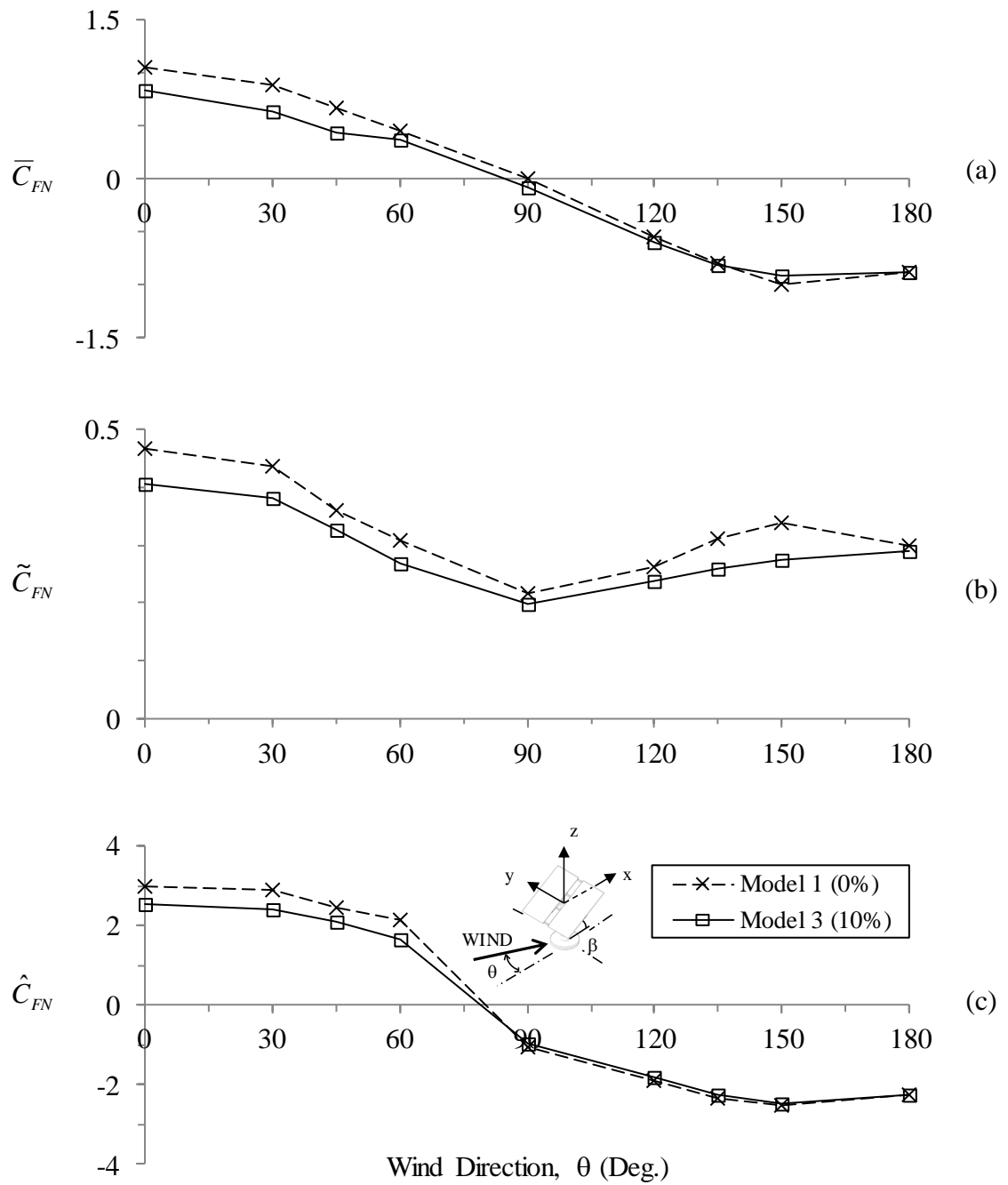


Figure 4.20 Effects of porosity on (a) mean, (b) standard deviation and (c) peak normal force coefficients, Arrangement A2, Pitch Angle 30°

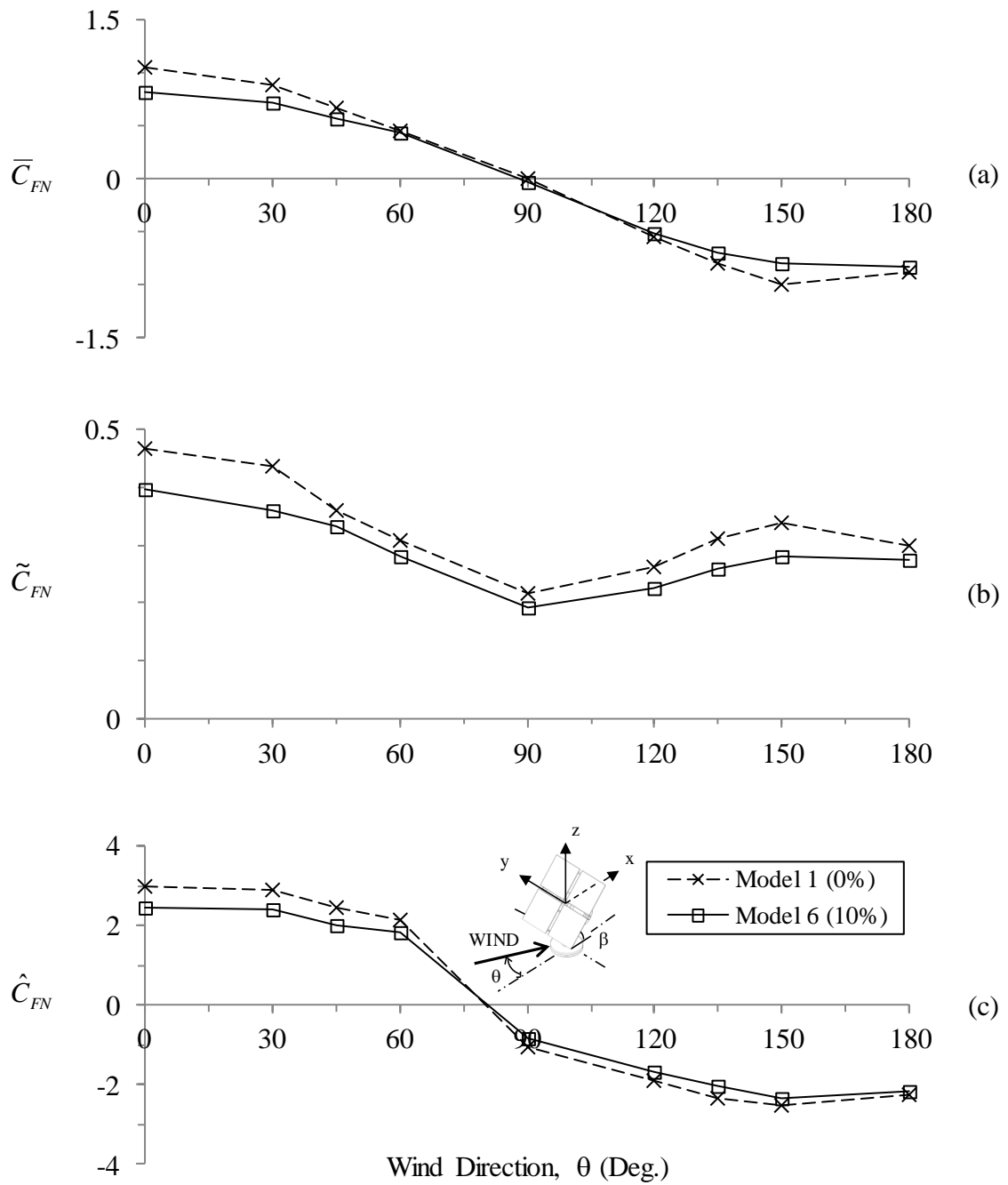


Figure 4.21 Effects of porosity on (a) mean, (b) standard deviation and (c) peak normal force coefficients, Arrangement A3, Pitch Angle 30°

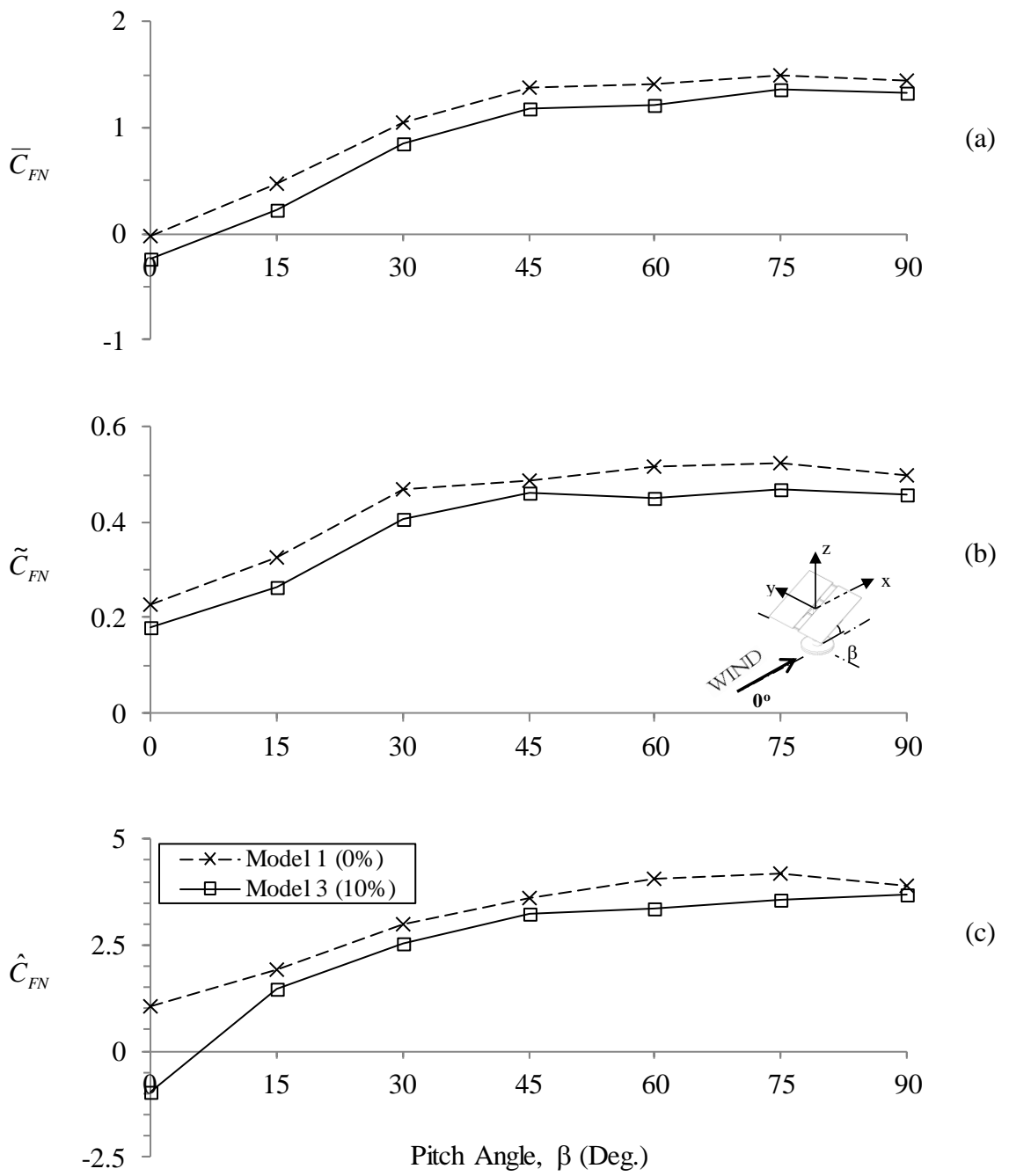


Figure 4.22 Effects of porosity on (a) mean, (b) standard deviation and (c) peak normal force coefficients, Arrangement A2, Wind Direction 0°

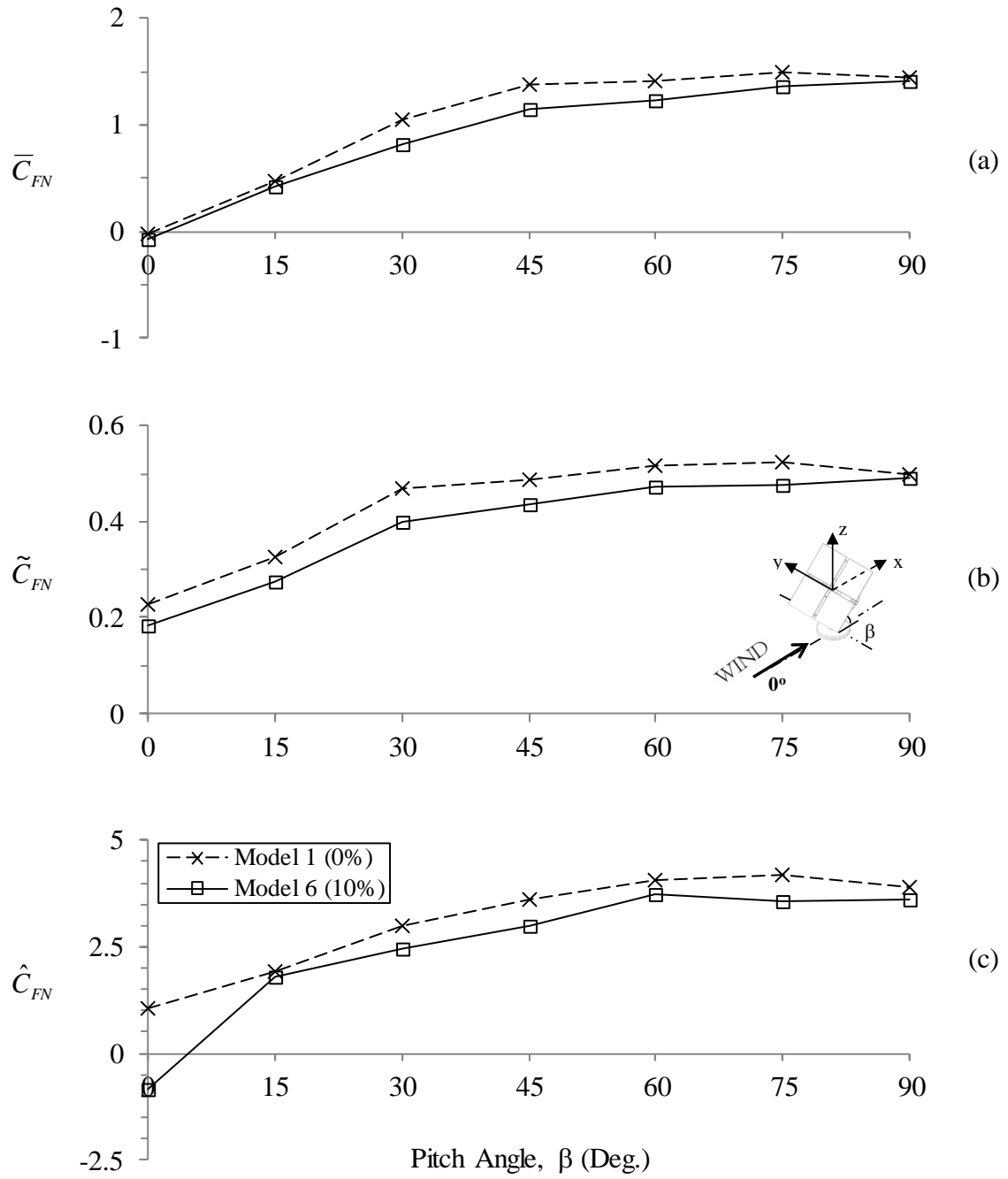


Figure 4.23 Effects of porosity on (a) mean, (b) standard deviation and (c) peak normal force coefficients, Arrangement A3, Wind Direction 0°

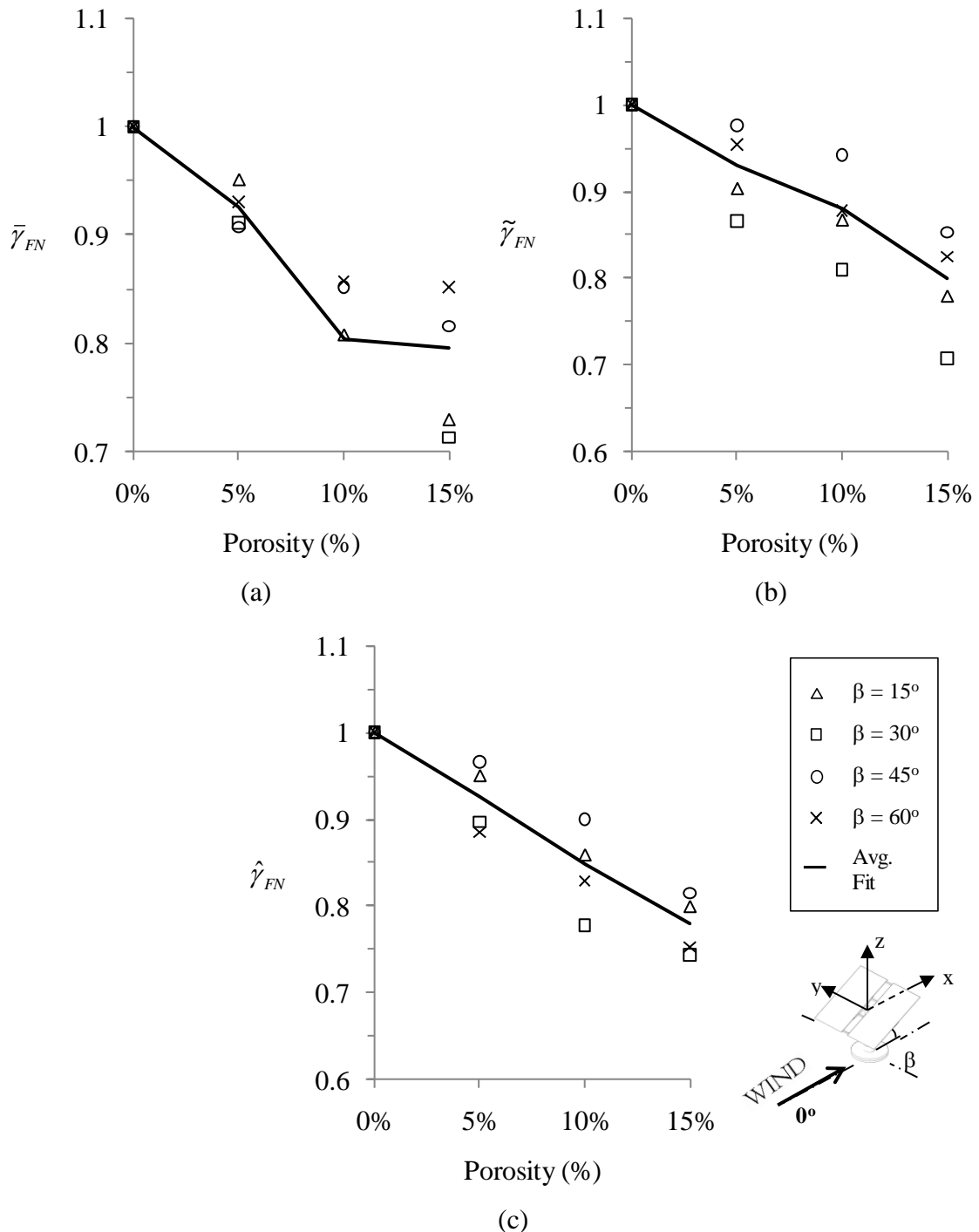


Figure 4.24 Normal force reduction factor: (a) mean, (b) standard deviation and (c) peak,
Arrangement A2, Wind Direction 0°

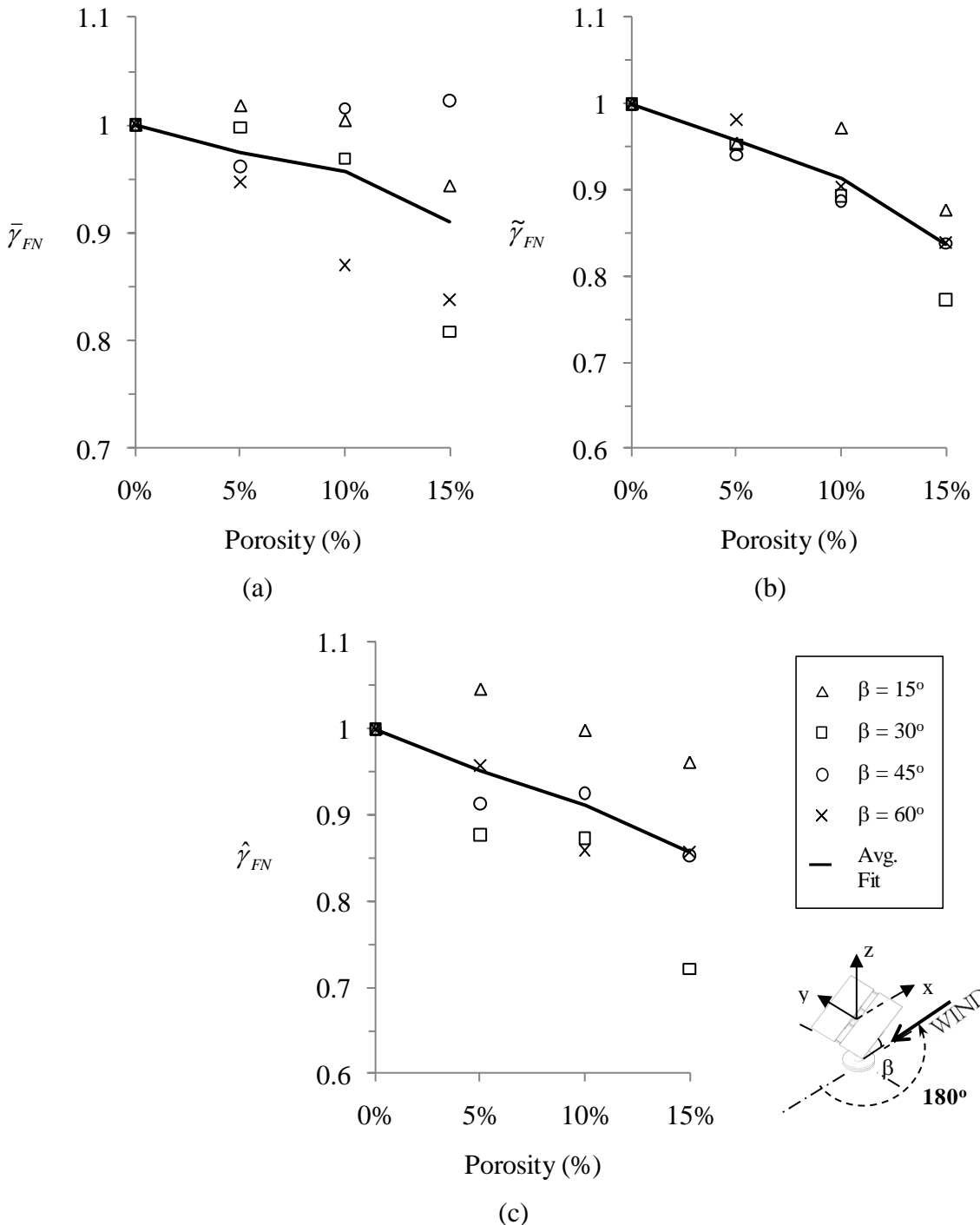


Figure 4.25 Normal force reduction factor: (a) mean, (b) standard deviation and (c) peak,
Arrangement A2, Wind Direction 180°

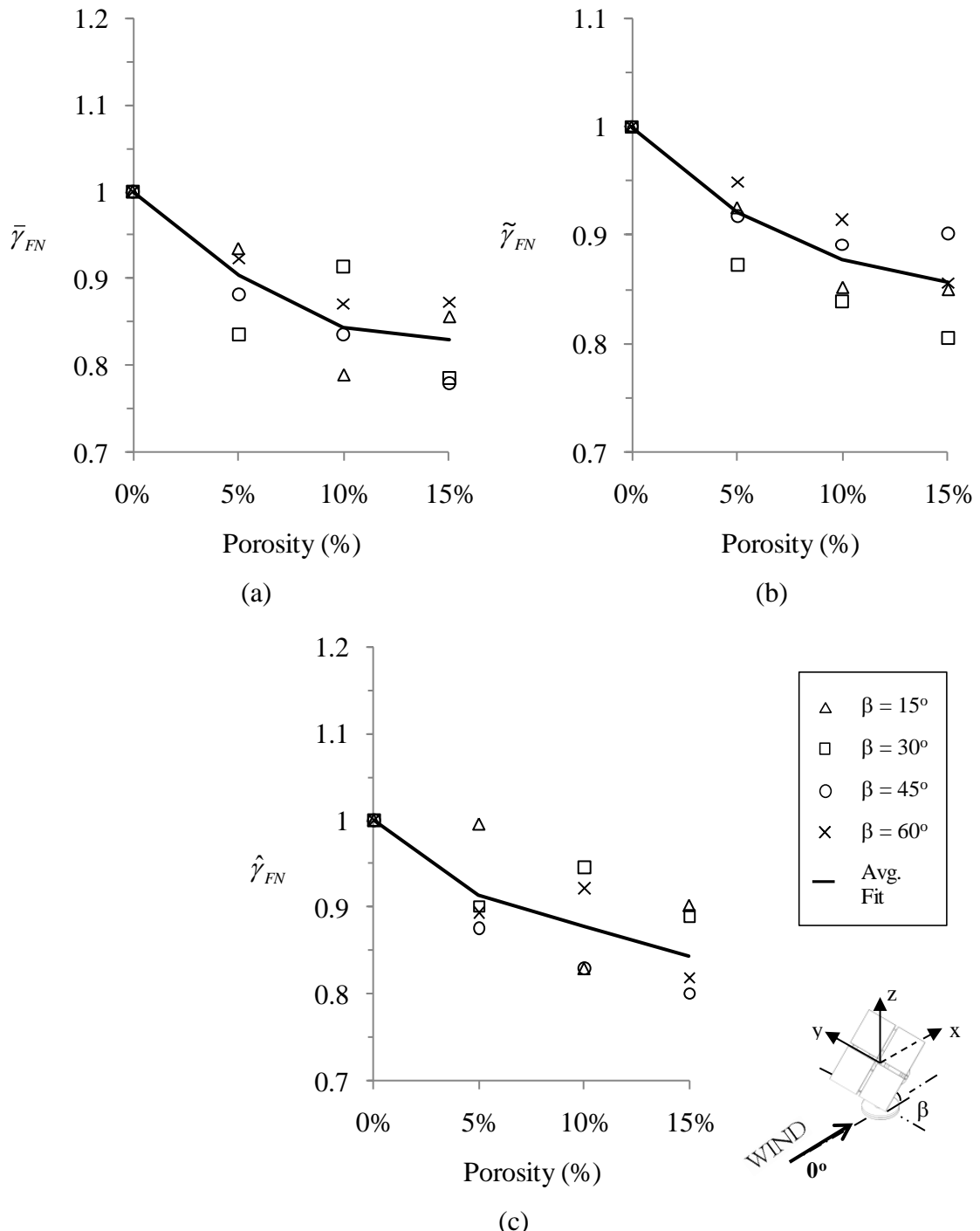


Figure 4.26 Normal force reduction factor: (a) mean, (b) standard deviation and (c) peak, Arrangement A3, Wind Direction 0°

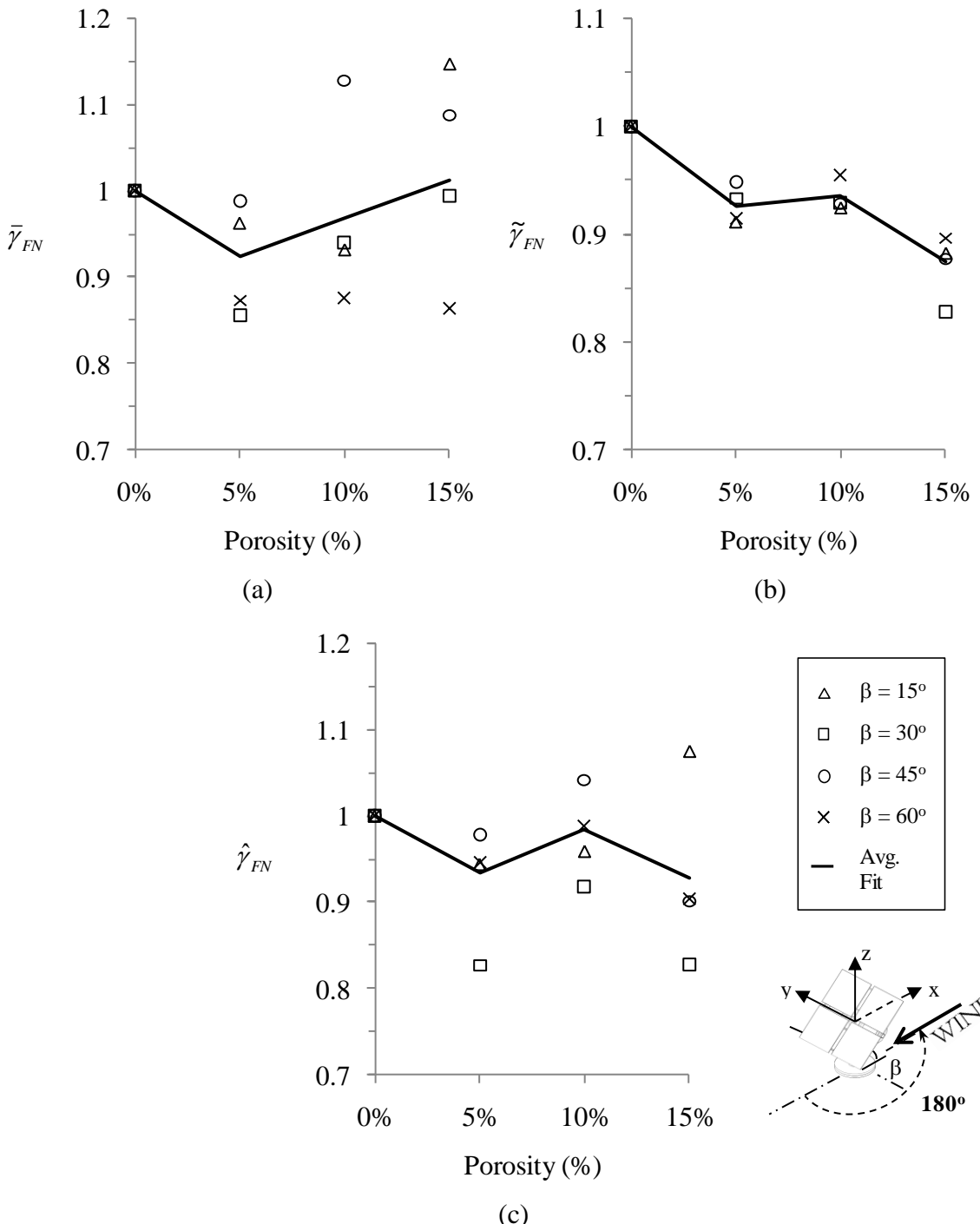


Figure 4.27 Normal force reduction factor: (a) mean, (b) standard deviation and (c) peak,
Arrangement A3, Wind Direction 180°

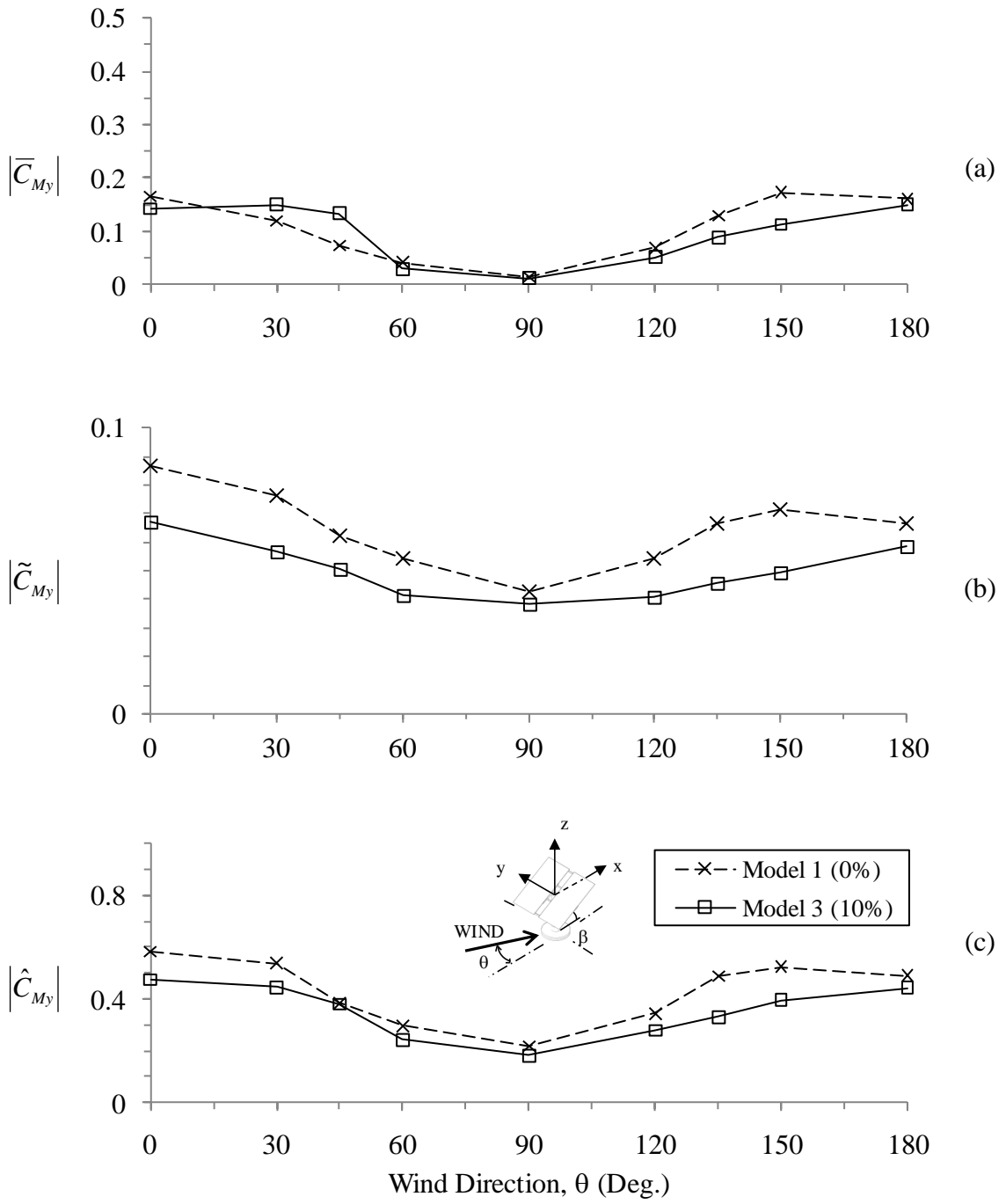


Figure 4.28 Effects of porosity on (a) mean, (b) standard deviation and (c) peak pitching moment coefficients, Arrangement A2, Pitch Angle 30°

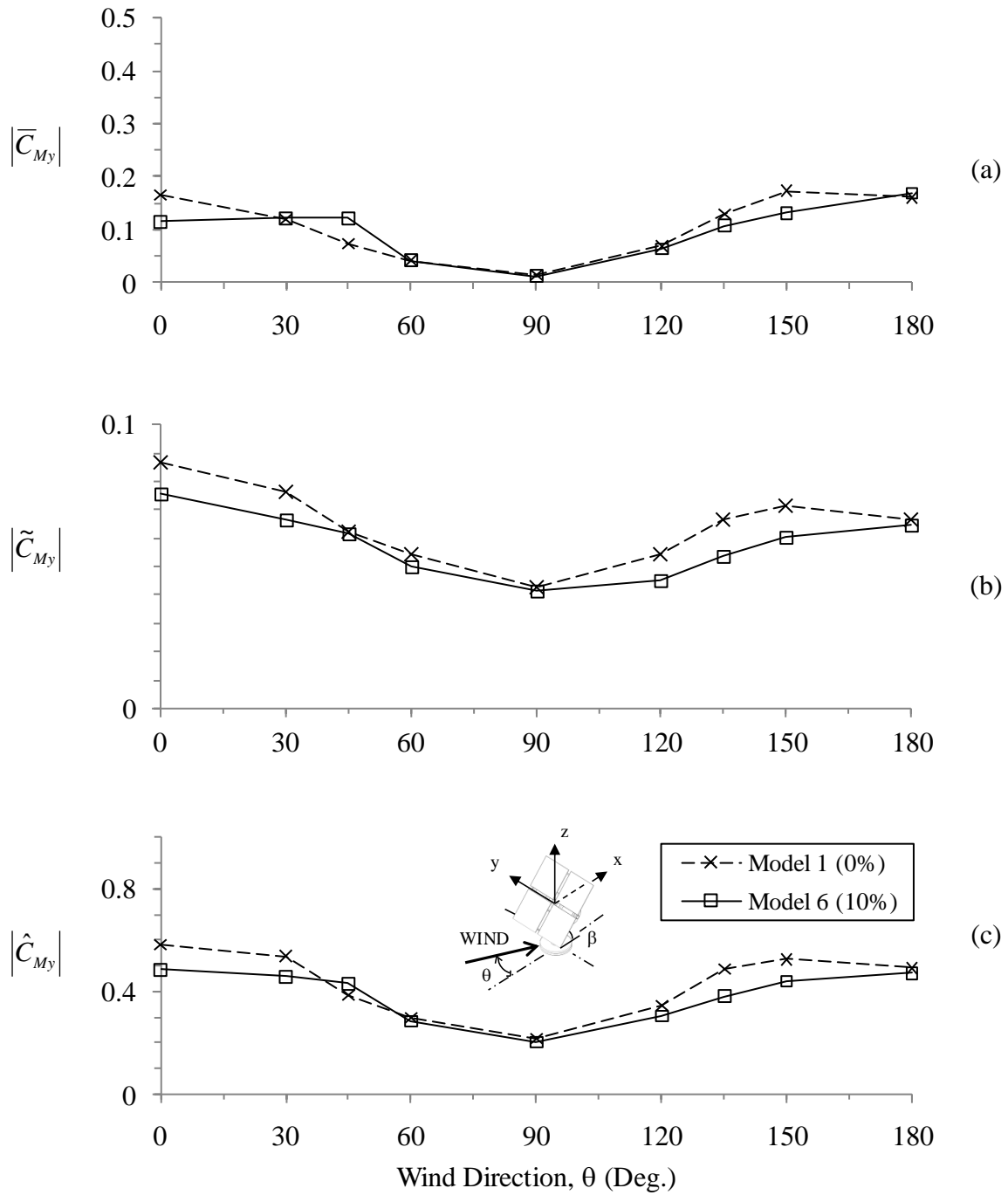


Figure 4.29 Effects of porosity on (a) mean, (b) standard deviation and (c) peak pitching moment coefficients, Arrangement A3, Pitch Angle 30°

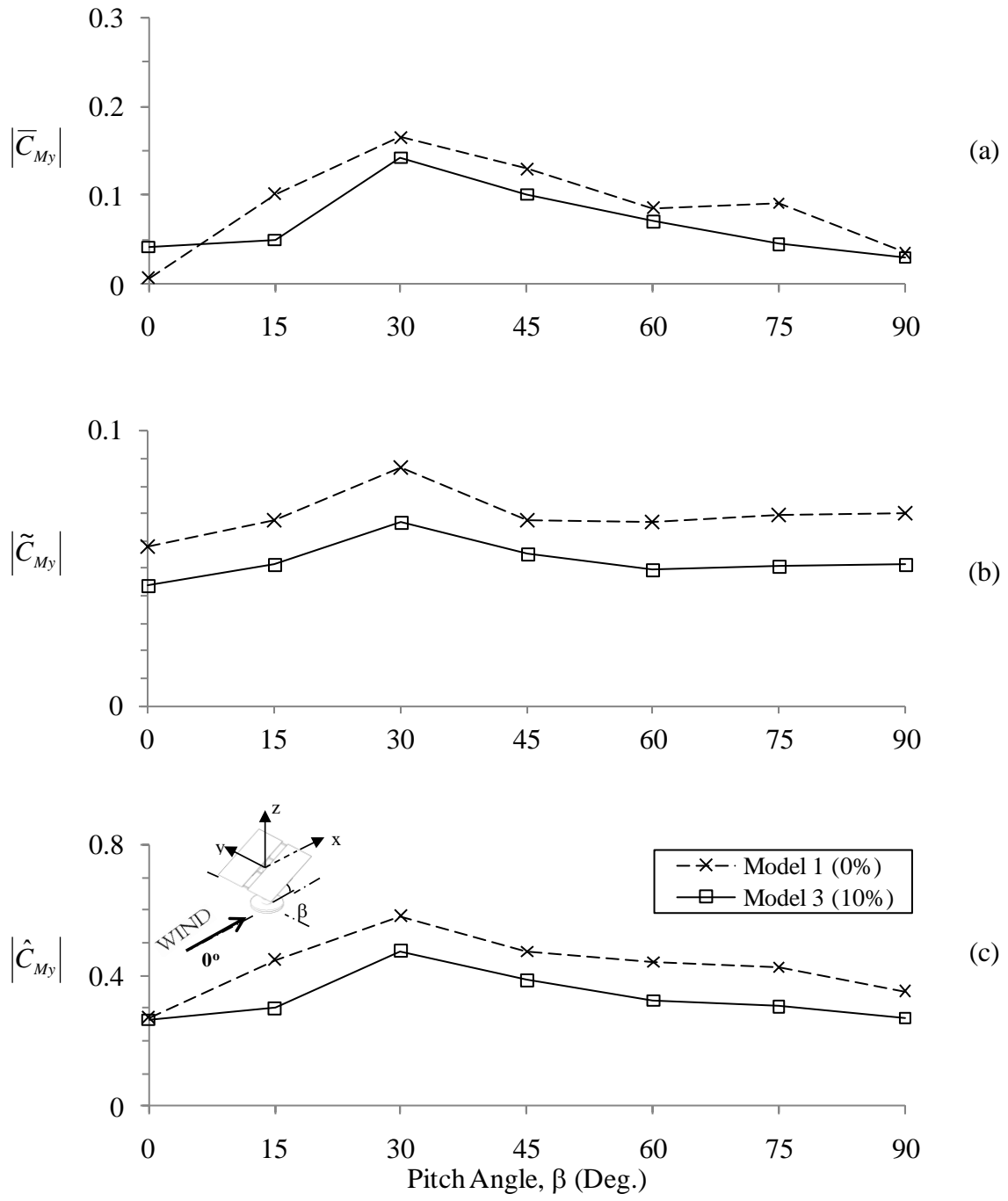


Figure 4.30 Effects of porosity on (a) mean, (b) standard deviation and (c) peak pitching moment coefficients, Arrangement A2, Wind Direction 0°

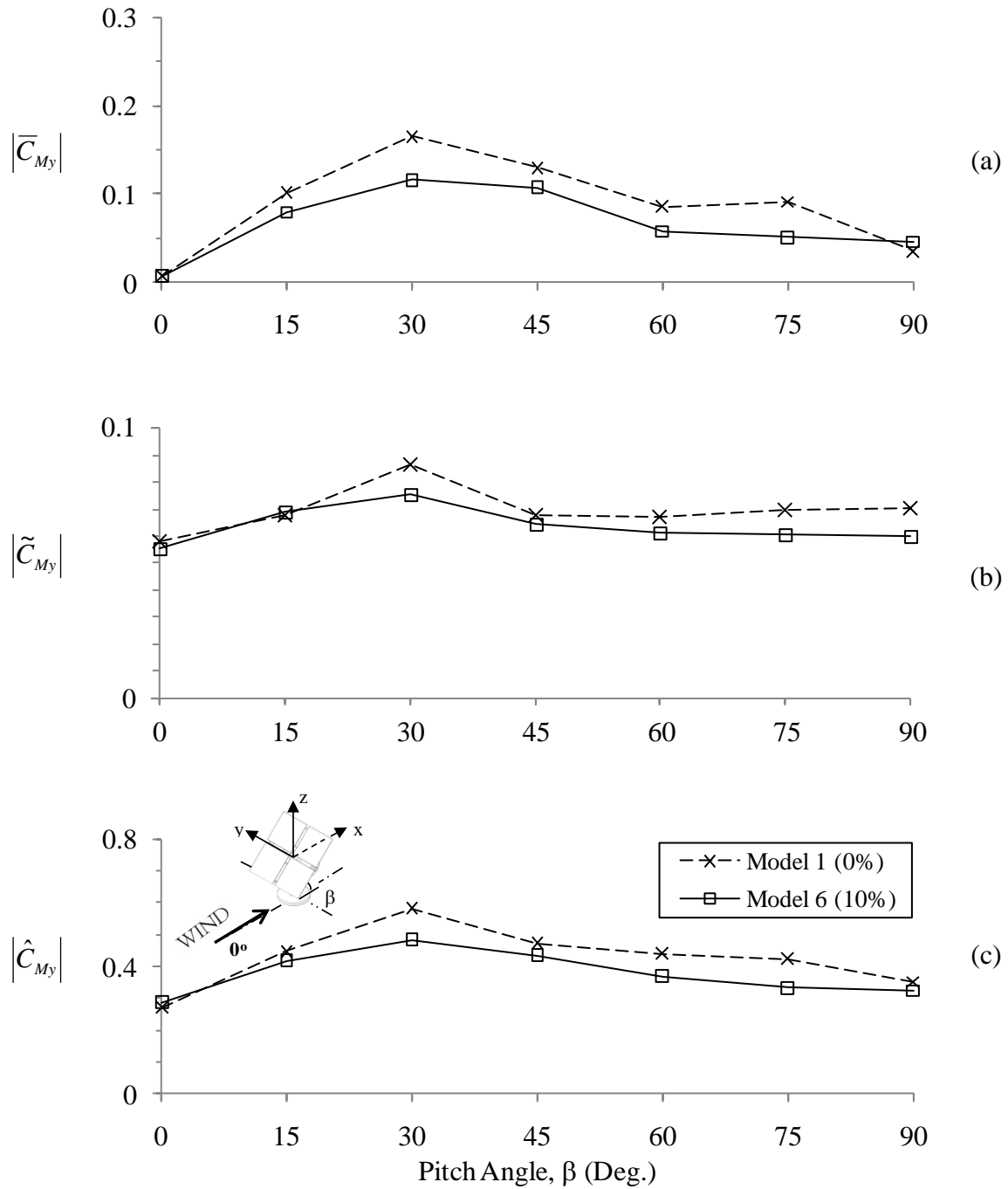


Figure 4.31 Effects of porosity on (a) mean, (b) standard deviation and (c) peak pitching moment coefficients, Arrangement A3, Wind Direction 0°

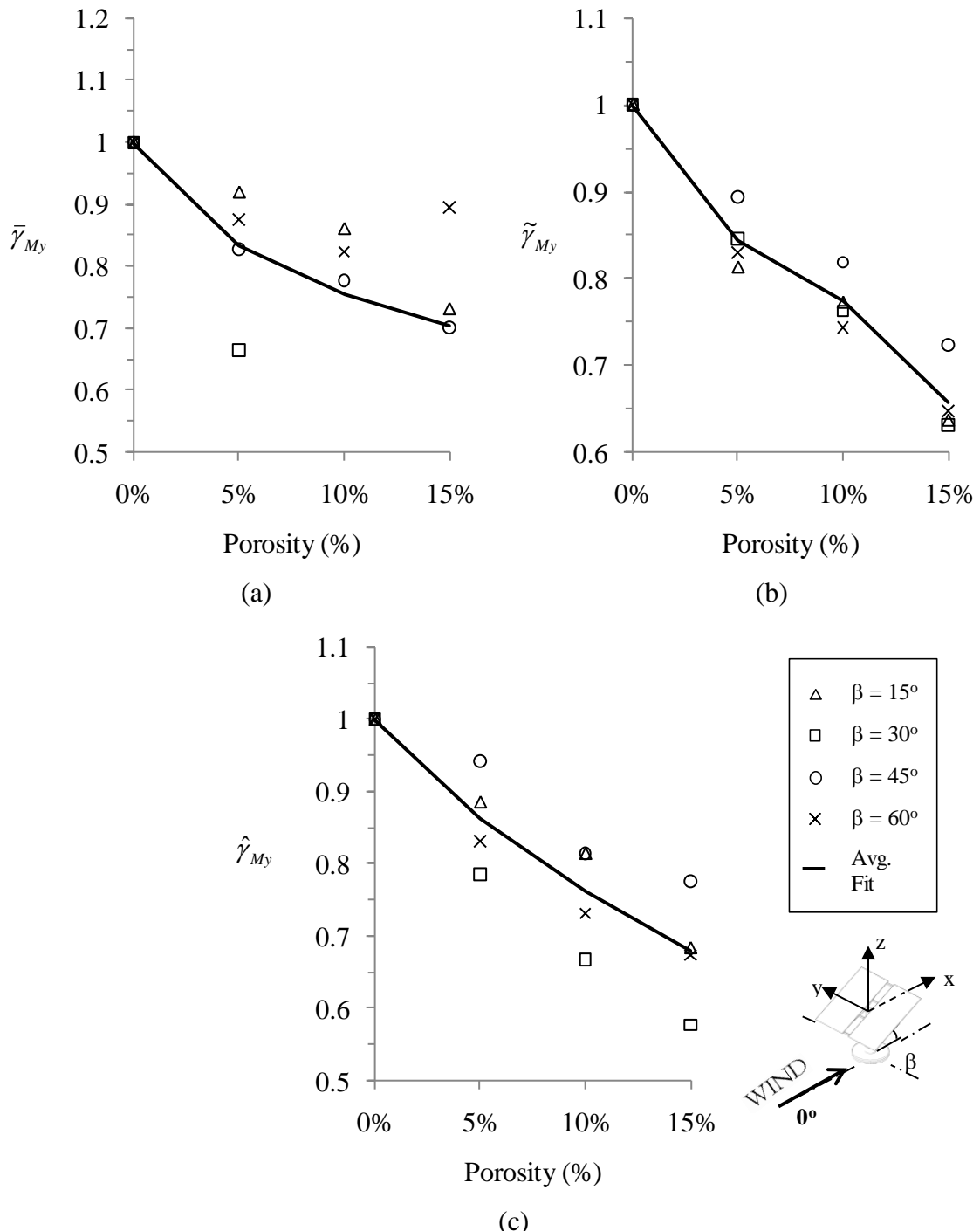


Figure 4.32 Pitching moment reduction factor: (a) mean, (b) standard deviation and (c) peak, Arrangement A2, Wind Direction 0°

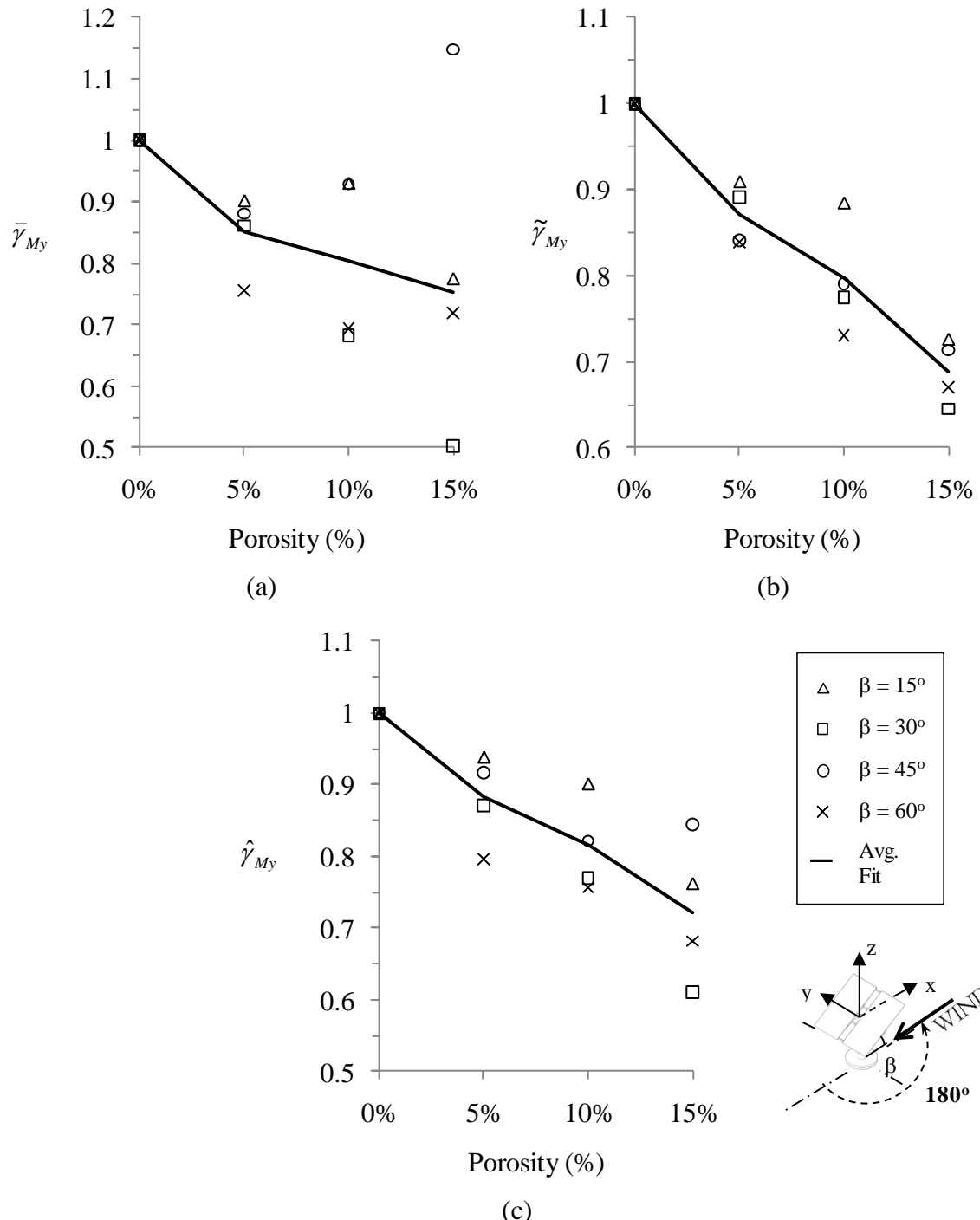


Figure 4.33 Pitching moment reduction factor: (a) mean, (b) standard deviation and (c) peak, Arrangement A2, Wind Direction 180°

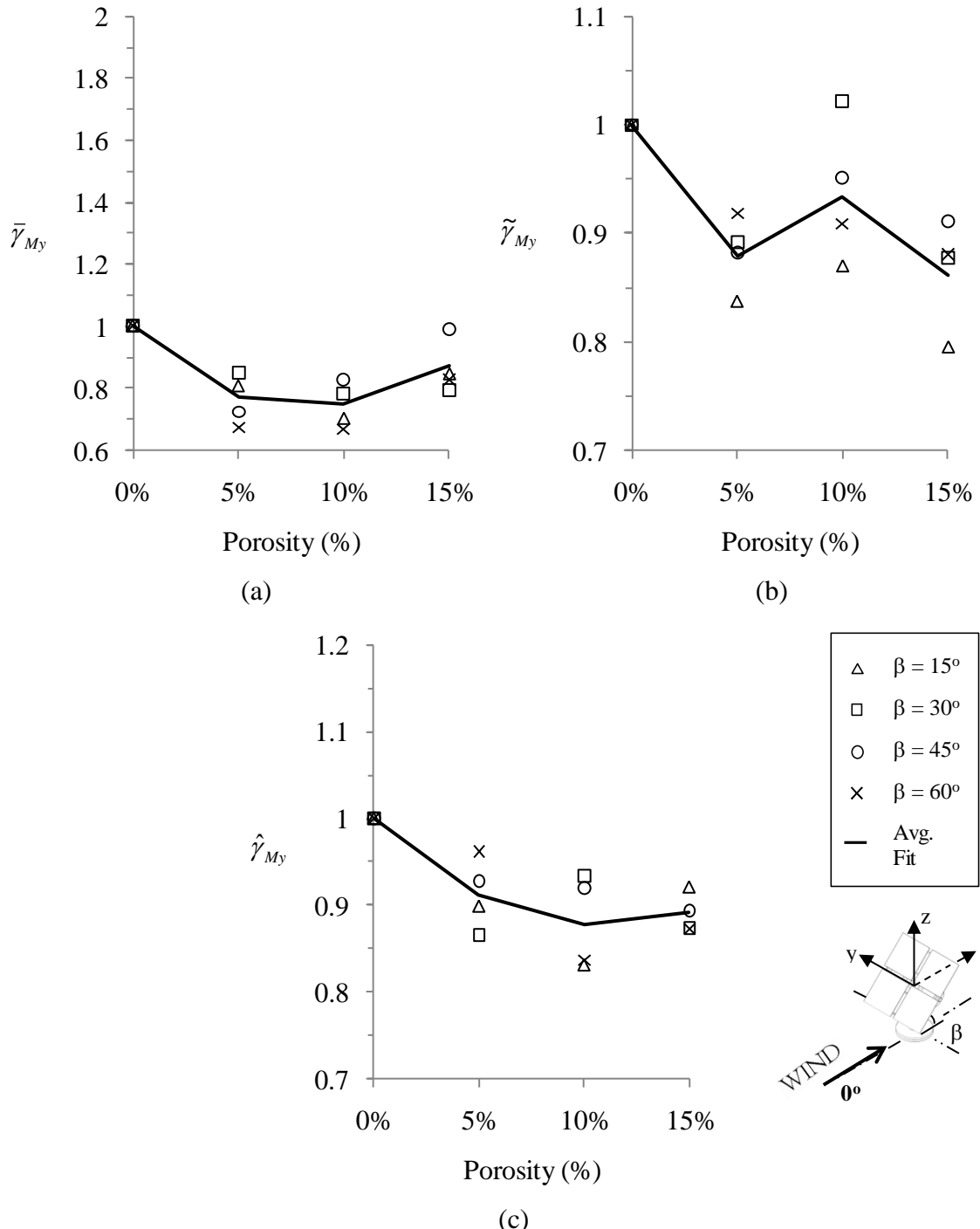


Figure 4.34 Pitching moment reduction factor: (a) mean, (b) standard deviation and (c) peak, Arrangement A3, Wind Direction 0°

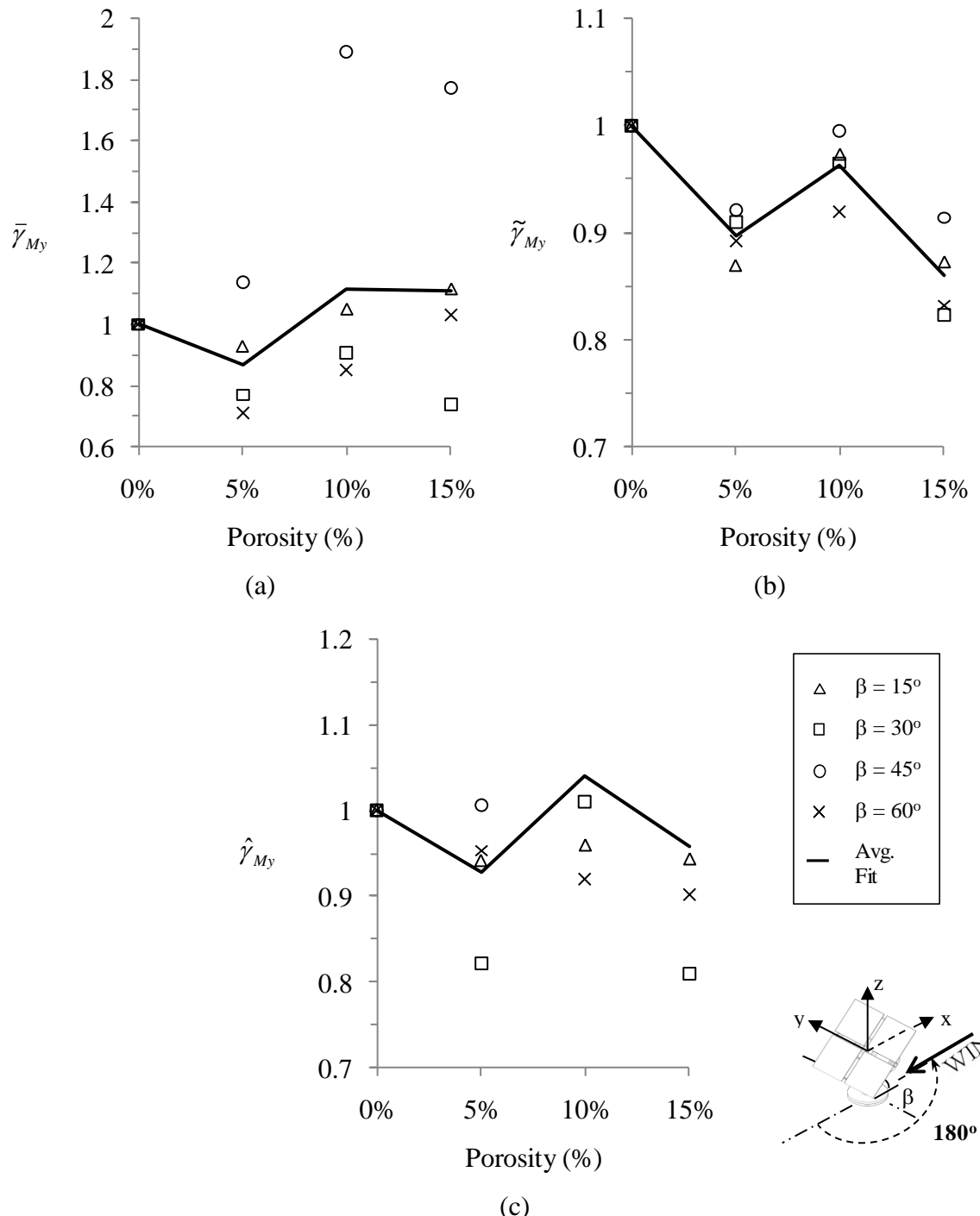
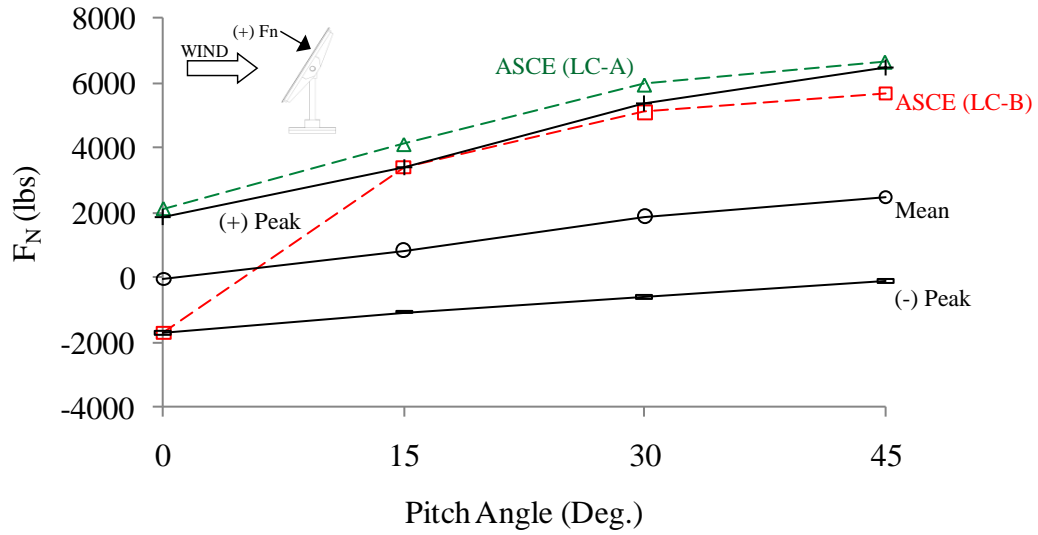
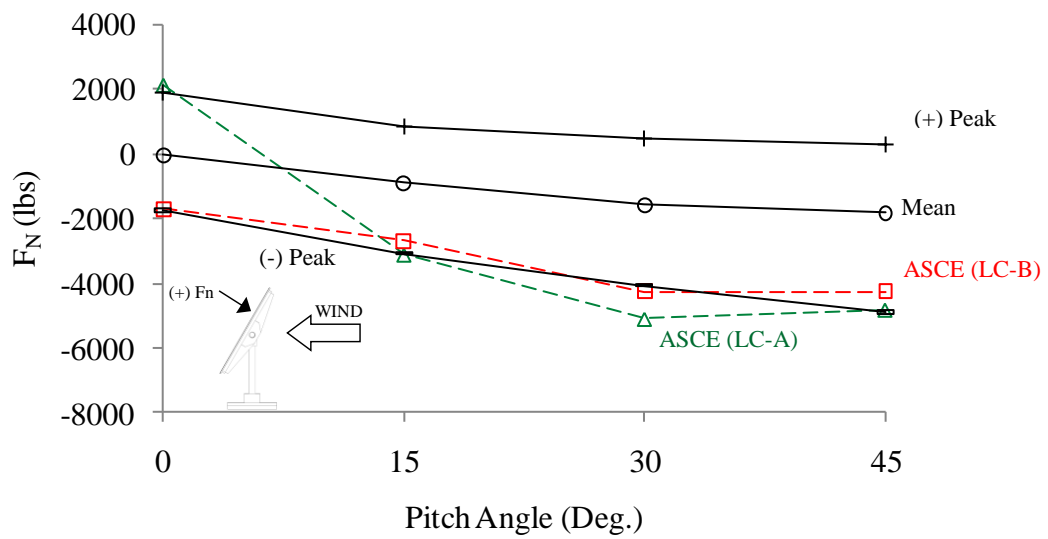


Figure 4.35 Pitching moment reduction factor: (a) mean, (b) standard deviation and (c) peak, Arrangement A3, Wind Direction 180°



(a) Wind Direction = 0°



(b) Wind Direction = 180°

Figure 4.36 Comparison of prototype design wind loads on PVT

REFERENCES

- [1] altE store – making renewable do-able, 2010, “Passive Solar Panel Trackers”, <http://www.altestore.com/store/Solar-Panel-Mounts-Trackers/Passive-Solar-Panel-Trackers/Zomeworks-Utrf168-Universal-Solar-Tracker/p2294/>
- [2] ASCE 7, 2005, “Minimum Design Loads for Buildings and Other Structures”, American Society of Civil Engineers, ASCE, New York, USA.
- [3] Energreen Systems – renewable energy systems, 2010, “Wattsun Active Mounds”, <http://www.energreensystems.ca/products-details.php?prod=129>
- [4] Goosens, D., Offer, Z.Y., and Zangvil, A., 1993, “Wind Tunnel Experiments and Field Investigations of Eolian Dust Deposition on Photovoltaic Solar Collectors”, Solar Energy, Vol. 50, No. 1, pp 75-84.
- [5] Hernandez, S., Mendez, J., Nieto, F. and Jurado, J.A., 2009, “Aerodynamic Analysis of a Photovoltaic Solar Tracker”, Proc. 5th EACWE, Florence, Italy.
- [6] Hosoya, N., and Peterka, J.A., 2008, “Wind Tunnel Tests of Parabolic Trough Solar Collectors”, Technical Report No. NREL/SR-550-32282, Ceremak Peterka Petersen, Inc., Fort Collins, CO.
- [7] Kvasznica, Z., and Elmer,G., 2006, “Optimising Solar Tracking Systems for Solar Cells”, 4th Serbian-Hungarian Joint Symposium on Intelligent Systems, SISY, pp.167-180.
- [8] Mahboub, C., Moummi, N., Moummi, A. and Youcef-Ali, S., 2011, “Effect of Angle of Attack on the Wind Convection Coefficient”, Solar Energy, doi: 10.1016/j.solener.2011.01.008
- [9] Peterka, J.A, Hosoya, N., Bienkiewicz, B., and Cermak, J.E., 1986, “Wind Load Reduction for Heliostats”, Solar Energy Research Institute Report SERI/STR-253-2859, Golden, CO.

- [10] Peterka, J.A, Tan, Z., Bienkiewicz, B., and Cermak , J.E., 1987, “Mean and Peak Wind Load Reduction on Heliostats”, Solar Energy Research Institute Report SERI/STR-253-3431, Golden, CO.
- [11] Renewable Energy Development, 2008, “Solar Energy”,
<http://renewableenergydev.com/red/solar-energy-pennsylvania-solar-park/>
- [12] Scaletchi, I., Visa, I., and Velicu, R., 2010, “Modeling Wind Action on Solar Tracking Platforms”, Bulletin of The Transilvania University of Brasov, Vol.3 (52), Brasov, Romania, http://but.unitbv.ro/Bulletin/Series%20I/Contents_I.html
- [13] Shademan, M., and Hangan, H., 2009, “Wind Loading on Solar Panels at Different Inclination Angles”, Proc. 11th Americas Conference on Wind Engineering, San Juan, Puerto Rico, <http://www.iawe.org/iaweconf.html>
- [14] Shingleton, J., 2008, “One-Axis Trackers – Improved Reliability, Durability, Performance, and Cost Reduction”, Technical Report No. NREL/SR-520-42769, Shingleton Design, LLC, Auburn, NY.
- [15] Solarco, 2010, “Services & Projects”, <http://www.solarco.biz/Services.html>
- [16] Velicu, R., Moldovean, G., Scaletchi, I. and Butuc, B.R., 2010, “Wind Loads on an Azimuthal Photovoltaic Platform. Experimental Study,” International Conf. on Renewable Energies and Power Quality, EA4EPQ, Granada, Spain, <http://www.icrepq.com/papers3-icrepq10.html>
- [17] Velicu, R., Lates, M., and Moldovean, G., 2009, “Loading Cases and Forces on Azimuthal Solar Tracking Systems with Linear Actuator,” Proc. 10th International Symposium on Science of Mechanisms and Machines, Brasov, Romania.
- [18] World Energy Statistics, 2010, “Global Solar Energy Statistics”, <http://energy-statistics.blogspot.com/2010/09/global-solar-energy-statistics.html>

APPENDIX A

A1. DRAG AND LIFT FORCE COEFFICIENTS

Model 1		C _D			C _L				
β (deg.)	θ (deg.)	(+) Peak	Mean	(-) Peak	S.D.	(+) Peak	Mean	(-) Peak	S.D.
0	0	1.09	0.14	-0.75	0.19	0.95	0.02	-1.04	0.23
0	30	0.95	0.17	-0.49	0.16	1.10	0.09	-1.05	0.23
0	45	0.99	0.18	-0.53	0.16	1.06	0.07	-1.04	0.23
0	60	1.18	0.18	-0.72	0.18	1.07	0.07	-1.18	0.25
0	90	1.11	0.20	-0.61	0.18	1.20	0.37	-0.58	0.19
0	120	1.06	0.16	-0.50	0.17	1.06	0.08	-1.01	0.21
0	135	1.01	0.16	-0.58	0.16	1.03	0.08	-1.04	0.23
0	150	1.03	0.15	-0.58	0.19	1.18	0.07	-1.27	0.24
0	180	1.14	0.12	-0.74	0.18	0.98	0.03	-1.03	0.22
15	0	1.05	0.25	-0.33	0.15	0.65	-0.41	-1.83	0.32
15	30	0.94	0.23	-0.30	0.14	0.76	-0.35	-1.86	0.31
15	45	0.95	0.22	-0.31	0.14	0.82	-0.30	-1.64	0.28
15	60	0.95	0.19	-0.43	0.15	0.89	-0.16	-1.46	0.26
15	90	1.07	0.14	-0.71	0.18	0.92	0.05	-0.93	0.21
15	120	1.03	0.20	-0.58	0.19	1.52	0.35	-0.72	0.21
15	135	1.15	0.23	-0.53	0.18	1.47	0.46	-0.52	0.23
15	150	1.23	0.22	-0.62	0.19	1.64	0.54	-0.44	0.21
15	180	1.34	0.21	-0.77	0.21	1.55	0.46	-0.44	0.22
30	0	1.80	0.56	-0.21	0.26	0.49	-0.89	-2.65	0.42
30	30	1.57	0.45	-0.39	0.24	0.61	-0.74	-2.63	0.39
30	45	1.22	0.33	-0.31	0.18	0.57	-0.55	-2.11	0.33
30	60	1.08	0.24	-0.45	0.17	0.76	-0.37	-1.94	0.29
30	90	1.03	0.12	-0.66	0.18	0.92	0.00	-1.01	0.20
30	120	1.25	0.28	-0.48	0.19	1.62	0.47	-0.50	0.24
30	135	1.54	0.41	-0.41	0.24	2.02	0.68	-0.46	0.27
30	150	1.85	0.50	-0.51	0.26	2.17	0.87	-0.20	0.29

Model 1		C _D				C _L			
β (deg.)	θ (deg.)	(+) Peak	Mean	(-) Peak	S.D.	(+) Peak	Mean	(-) Peak	S.D.
30	180	2.00	0.49	-0.54	0.28	1.82	0.74	-0.30	0.25
45	0	2.76	1.02	-0.08	0.37	0.34	-0.93	-2.51	0.36
45	30	2.49	0.84	-0.19	0.33	0.52	-0.82	-2.50	0.37
45	45	1.88	0.59	-0.27	0.26	0.56	-0.66	-2.23	0.34
45	60	1.28	0.37	-0.38	0.20	0.63	-0.43	-1.84	0.29
45	90	1.00	0.15	-0.53	0.17	1.10	0.08	-0.85	0.21
45	120	1.60	0.42	-0.42	0.22	1.75	0.60	-0.44	0.25
45	135	1.94	0.64	-0.44	0.28	1.93	0.74	-0.36	0.27
45	150	2.10	0.71	-0.34	0.29	1.79	0.69	-0.31	0.24
45	180	2.40	0.77	-0.34	0.32	1.76	0.67	-0.34	0.24
60	0	3.70	1.25	-0.16	0.46	0.38	-0.66	-2.10	0.30
60	30	2.93	1.02	-0.22	0.38	0.36	-0.63	-1.99	0.29
60	45	2.13	0.75	-0.24	0.31	0.45	-0.60	-1.89	0.28
60	60	1.60	0.44	-0.44	0.23	0.53	-0.41	-1.60	0.24
60	90	0.93	0.14	-0.52	0.15	0.82	0.03	-0.73	0.18
60	120	1.75	0.53	-0.28	0.23	1.32	0.45	-0.40	0.21
60	135	2.03	0.73	-0.24	0.27	1.38	0.50	-0.39	0.21
60	150	2.40	0.84	-0.22	0.33	1.91	1.00	0.14	0.22
60	180	2.75	0.95	-0.25	0.36	1.90	0.87	-0.09	0.22
75	0	4.07	1.47	0.01	0.51	0.50	-0.24	-1.15	0.19
75	30	3.13	1.17	-0.13	0.42	0.52	-0.26	-1.06	0.18
75	45	2.46	0.87	-0.26	0.34	0.49	-0.24	-1.05	0.17
75	60	1.69	0.53	-0.28	0.24	0.57	-0.18	-0.96	0.18
75	90	0.77	0.15	-0.39	0.12	0.77	0.10	-0.53	0.14
75	120	1.79	0.59	-0.26	0.24	1.01	0.34	-0.35	0.16
75	135	2.35	0.83	-0.11	0.30	1.05	0.36	-0.30	0.16
75	150	2.78	1.01	-0.06	0.36	1.03	0.37	-0.29	0.15
75	180	2.99	1.18	-0.09	0.41	1.04	0.35	-0.32	0.16
90	0	3.90	1.45	-0.05	0.50	0.62	0.02	-0.58	0.14
90	30	3.10	1.21	-0.11	0.42	0.64	0.07	-0.51	0.13
90	45	2.64	0.88	-0.18	0.34	0.66	0.04	-0.54	0.14
90	60	1.90	0.54	-0.32	0.24	0.60	0.00	-0.61	0.13
90	90	0.71	0.11	-0.36	0.11	0.59	0.03	-0.62	0.14
90	120	1.77	0.56	-0.26	0.24	0.69	0.08	-0.52	0.14
90	135	2.30	0.87	-0.13	0.31	0.68	0.11	-0.46	0.14
90	150	2.98	1.11	-0.13	0.40	0.76	0.16	-0.44	0.14
90	180	3.54	1.25	-0.19	0.47	0.76	0.12	-0.48	0.14

Model 2		C _D				C _L			
β (deg.)	θ (deg.)	(+) Peak	Mean	(-) Peak	S.D.	(+) Peak	Mean	(-) Peak	S.D.
0	0	0.97	0.21	-0.44	0.14	1.22	0.32	-0.58	0.20
0	30	0.90	0.17	-0.43	0.14	1.05	0.06	-0.99	0.22
0	45	0.93	0.16	-0.44	0.15	0.97	0.03	-1.04	0.21
0	60	1.10	0.16	-0.61	0.17	0.96	0.03	-1.00	0.22
0	90	1.05	0.13	-0.74	0.20	0.91	0.01	-0.91	0.20
0	120	1.09	0.15	-0.53	0.16	0.92	0.06	-0.96	0.21
0	135	0.89	0.15	-0.45	0.14	1.09	0.06	-1.01	0.21
0	150	0.87	0.13	-0.49	0.14	1.02	0.05	-1.02	0.21
0	180	1.01	0.11	-0.63	0.14	0.93	0.02	-1.02	0.20
15	0	1.01	0.21	-0.36	0.15	0.58	-0.38	-1.58	0.27
15	30	1.01	0.28	-0.27	0.14	0.61	-0.35	-1.56	0.26
15	45	1.02	0.25	-0.32	0.15	0.67	-0.27	-1.47	0.25
15	60	1.10	0.19	-0.49	0.16	0.73	-0.18	-1.36	0.23
15	90	1.08	0.19	-0.52	0.17	1.14	0.25	-0.74	0.20
15	120	1.08	0.20	-0.57	0.17	1.47	0.48	-0.47	0.20
15	135	1.17	0.22	-0.48	0.17	1.55	0.50	-0.49	0.20
15	150	1.15	0.22	-0.49	0.18	1.50	0.56	-0.32	0.20
15	180	1.24	0.21	-0.54	0.19	1.46	0.46	-0.42	0.20
30	0	1.70	0.58	-0.15	0.23	0.43	-0.82	-2.40	0.38
30	30	1.49	0.49	-0.15	0.20	0.46	-0.63	-2.14	0.35
30	45	1.22	0.33	-0.34	0.18	0.54	-0.49	-1.83	0.31
30	60	1.17	0.23	-0.45	0.17	0.75	-0.26	-1.54	0.27
30	90	1.02	0.15	-0.59	0.17	0.94	0.05	-0.92	0.19
30	120	1.25	0.28	-0.46	0.18	1.56	0.47	-0.48	0.22
30	135	1.54	0.40	-0.41	0.21	1.83	0.66	-0.27	0.24
30	150	1.92	0.50	-0.36	0.24	1.93	0.74	-0.24	0.25
30	180	2.10	0.53	-0.68	0.26	1.94	0.73	-0.17	0.24
45	0	2.72	0.93	-0.08	0.36	0.36	-0.84	-2.42	0.36
45	30	2.43	0.79	-0.20	0.32	0.43	-0.79	-2.40	0.36
45	45	1.77	0.57	-0.29	0.25	0.45	-0.64	-2.01	0.31
45	60	1.30	0.34	-0.54	0.20	0.56	-0.41	-1.63	0.27
45	90	0.92	0.14	-0.57	0.17	1.00	0.08	-0.79	0.19
45	120	1.54	0.41	-0.45	0.21	1.62	0.56	-0.35	0.22
45	135	1.88	0.59	-0.34	0.25	1.78	0.65	-0.27	0.22

Model 2		C _D				C _L			
β (deg.)	θ (deg.)	(+) Peak	Mean	(-) Peak	S.D.	(+) Peak	Mean	(-) Peak	S.D.
45	150	2.18	0.70	-0.20	0.28	1.69	0.67	-0.20	0.22
45	180	2.23	0.73	-0.30	0.30	1.58	0.65	-0.22	0.21
60	0	3.25	1.19	-0.04	0.44	0.40	-0.56	-1.83	0.27
60	30	3.08	1.01	-0.09	0.38	0.49	-0.58	-1.81	0.27
60	45	2.09	0.73	-0.33	0.31	0.48	-0.52	-1.62	0.26
60	60	1.46	0.42	-0.44	0.23	0.54	-0.37	-1.46	0.23
60	90	0.86	0.13	-0.47	0.15	0.89	0.08	-0.67	0.17
60	120	1.66	0.50	-0.34	0.23	1.27	0.42	-0.36	0.19
60	135	2.00	0.70	-0.25	0.28	1.36	0.46	-0.33	0.19
60	150	2.33	0.86	-0.08	0.31	1.41	0.53	-0.27	0.19
60	180	2.60	0.94	-0.18	0.36	1.66	0.75	-0.03	0.20
75	0	3.66	1.36	0.06	0.47	0.41	-0.28	-1.11	0.18
75	30	3.06	1.18	-0.06	0.41	0.49	-0.21	-1.02	0.18
75	45	2.58	0.81	-0.22	0.33	0.39	-0.27	-1.09	0.17
75	60	1.73	0.45	-0.35	0.23	0.47	-0.18	-0.96	0.17
75	90	0.68	0.13	-0.36	0.12	0.70	0.08	-0.47	0.13
75	120	1.73	0.51	-0.22	0.22	1.04	0.44	-0.14	0.14
75	135	2.13	0.77	-0.15	0.30	1.10	0.35	-0.29	0.15
75	150	2.63	0.95	-0.19	0.35	1.20	0.44	-0.24	0.15
75	180	2.91	1.05	-0.06	0.37	1.09	0.37	-0.28	0.15
90	0	3.79	1.49	0.08	0.49	0.54	0.03	-0.51	0.11
90	30	3.27	1.23	0.05	0.41	0.61	0.11	-0.36	0.11
90	45	2.43	0.89	-0.08	0.34	0.57	0.04	-0.50	0.11
90	60	1.60	0.52	-0.23	0.22	0.62	0.09	-0.47	0.12
90	90	0.62	0.13	-0.32	0.11	0.64	0.09	-0.44	0.12
90	120	1.72	0.57	-0.29	0.24	0.79	0.20	-0.37	0.13
90	135	2.41	0.81	-0.19	0.31	0.79	0.27	-0.29	0.12
90	150	2.90	1.01	-0.12	0.37	0.85	0.33	-0.23	0.12
90	180	3.22	1.14	-0.10	0.42	0.69	0.14	-0.40	0.12

Model 3		C _D				C _L			
β (deg.)	θ (deg.)	(+) Peak	Mean	(-) Peak	S.D.	(+) Peak	Mean	(-) Peak	S.D.
0	0	0.89	0.19	-0.37	0.13	0.97	0.24	-0.71	0.18
0	30	0.98	0.29	-0.26	0.14	1.14	0.34	-0.63	0.20
0	45	1.12	0.32	-0.32	0.15	1.33	0.40	-0.55	0.20
0	60	0.91	0.16	-0.53	0.16	1.01	0.06	-0.94	0.20
0	90	1.18	0.15	-0.68	0.18	0.86	0.08	-0.76	0.18
0	120	1.12	0.17	-0.55	0.17	0.98	0.15	-0.73	0.19
0	135	0.85	0.15	-0.47	0.15	0.94	0.08	-0.80	0.19
0	150	0.77	0.13	-0.42	0.13	0.99	0.11	-0.84	0.19
0	180	0.73	0.09	-0.55	0.14	0.90	0.10	-0.80	0.18
15	0	0.95	0.22	-0.34	0.14	0.70	-0.18	-1.38	0.25
15	30	0.93	0.24	-0.37	0.14	0.70	-0.16	-1.31	0.24
15	45	0.92	0.20	-0.42	0.15	0.73	-0.15	-1.28	0.23
15	60	1.03	0.19	-0.48	0.17	0.73	-0.13	-1.23	0.21
15	90	0.97	0.12	-0.59	0.16	0.86	0.03	-0.78	0.18
15	120	0.96	0.16	-0.60	0.16	1.12	0.25	-0.61	0.19
15	135	0.94	0.20	-0.40	0.15	1.49	0.55	-0.25	0.19
15	150	1.04	0.20	-0.44	0.15	1.46	0.53	-0.30	0.19
15	180	1.06	0.19	-0.50	0.16	1.41	0.45	-0.34	0.19
30	0	1.70	0.59	-0.17	0.24	0.52	-0.64	-2.22	0.36
30	30	1.58	0.54	-0.23	0.21	0.71	-0.40	-1.97	0.34
30	45	1.33	0.45	-0.22	0.18	0.86	-0.22	-1.61	0.29
30	60	1.23	0.23	-0.59	0.18	0.64	-0.28	-1.44	0.24
30	90	1.01	0.15	-0.55	0.16	0.91	0.09	-0.78	0.18
30	120	1.15	0.29	-0.43	0.18	1.63	0.54	-0.37	0.22
30	135	1.44	0.40	-0.43	0.20	1.92	0.73	-0.14	0.23
30	150	1.77	0.45	-0.39	0.22	1.97	0.81	-0.13	0.23
30	180	1.78	0.50	-0.41	0.25	1.89	0.74	-0.22	0.24
45	0	2.46	0.89	-0.11	0.35	0.36	-0.77	-2.29	0.34
45	30	2.28	0.77	-0.25	0.31	0.46	-0.64	-2.18	0.33
45	45	1.80	0.53	-0.30	0.24	0.53	-0.54	-1.88	0.30
45	60	1.38	0.34	-0.47	0.21	0.52	-0.37	-1.44	0.24
45	90	1.02	0.14	-0.54	0.16	0.92	0.05	-0.73	0.18
45	120	1.36	0.38	-0.37	0.20	1.48	0.47	-0.38	0.20
45	135	1.73	0.54	-0.20	0.23	1.70	0.83	-0.02	0.20
45	150	2.06	0.63	-0.23	0.26	1.77	0.83	0.01	0.20
45	180	2.10	0.71	-0.34	0.28	1.76	0.75	-0.05	0.20
60	0	3.06	1.11	-0.08	0.41	0.38	-0.49	-1.55	0.25

Model 3		C _D				C _L			
β (deg.)	θ (deg.)	(+) Peak	Mean	(-) Peak	S.D.	(+) Peak	Mean	(-) Peak	S.D.
60	30	2.76	0.96	-0.24	0.36	0.39	-0.50	-1.82	0.25
60	45	2.24	0.73	-0.19	0.30	0.48	-0.40	-1.52	0.25
60	60	1.54	0.44	-0.36	0.22	0.63	-0.21	-1.22	0.21
60	90	0.84	0.14	-0.48	0.15	0.80	0.08	-0.64	0.15
60	120	1.49	0.47	-0.29	0.21	1.34	0.52	-0.23	0.17
60	135	1.92	0.63	-0.17	0.25	1.47	0.68	0.02	0.17
60	150	2.23	0.82	-0.18	0.30	1.34	0.53	-0.16	0.18
60	180	2.42	0.91	-0.14	0.33	1.44	0.62	-0.09	0.19
75	0	3.50	1.34	-0.02	0.46	0.39	-0.29	-1.08	0.17
75	30	3.01	1.07	-0.14	0.39	0.49	-0.25	-0.99	0.17
75	45	2.25	0.81	-0.15	0.32	0.41	-0.26	-1.01	0.17
75	60	1.50	0.45	-0.40	0.22	0.42	-0.19	-0.97	0.16
75	90	0.71	0.12	-0.39	0.12	0.60	0.05	-0.54	0.13
75	120	1.62	0.50	-0.26	0.23	0.83	0.24	-0.33	0.13
75	135	2.14	0.75	-0.11	0.28	0.95	0.31	-0.37	0.14
75	150	2.49	0.92	-0.04	0.33	1.09	0.43	-0.16	0.14
75	180	2.89	1.07	-0.02	0.36	1.01	0.43	-0.15	0.14
90	0	3.68	1.32	0.00	0.46	0.55	0.10	-0.35	0.10
90	30	3.15	1.15	-0.07	0.39	0.73	0.25	-0.24	0.11
90	45	2.41	0.85	-0.15	0.32	0.54	0.06	-0.39	0.11
90	60	1.57	0.49	-0.33	0.22	0.54	0.06	-0.45	0.11
90	90	0.62	0.11	-0.32	0.11	0.51	0.06	-0.40	0.10
90	120	1.57	0.51	-0.25	0.22	0.64	0.12	-0.38	0.11
90	135	2.16	0.78	-0.19	0.29	0.78	0.29	-0.25	0.11
90	150	2.51	0.96	-0.08	0.34	0.70	0.16	-0.36	0.11
90	180	3.13	1.13	-0.11	0.38	0.62	0.12	-0.38	0.11

Model 4		C _D				C _L			
β (deg.)	θ (deg.)	(+) Peak	Mean	(-) Peak	S.D.	(+) Peak	Mean	(-) Peak	S.D.
0	0	0.81	0.17	-0.39	0.12	0.83	0.17	-0.50	0.14
0	30	0.90	0.25	-0.29	0.12	0.93	0.25	-0.57	0.16
0	45	0.81	0.16	-0.38	0.13	0.74	0.07	-0.75	0.17
0	60	0.91	0.16	-0.50	0.16	0.89	0.11	-0.78	0.17
0	90	1.06	0.12	-0.71	0.18	0.67	-0.03	-0.83	0.16
0	120	1.03	0.15	-0.50	0.16	0.76	0.05	-0.75	0.16
0	135	0.82	0.15	-0.46	0.14	0.83	0.09	-0.79	0.16
0	150	0.76	0.13	-0.40	0.13	0.73	0.10	-0.64	0.16
0	180	0.77	0.08	-0.45	0.12	0.74	0.10	-0.62	0.16
15	0	0.85	0.20	-0.29	0.13	0.48	-0.29	-1.31	0.22
15	30	0.85	0.19	-0.29	0.13	0.50	-0.25	-1.27	0.21
15	45	0.99	0.19	-0.48	0.15	0.56	-0.20	-1.11	0.20
15	60	1.00	0.16	-0.62	0.16	0.66	-0.10	-1.06	0.19
15	90	1.11	0.13	-0.74	0.18	0.81	0.07	-0.70	0.16
15	120	0.98	0.17	-0.48	0.16	1.06	0.24	-0.58	0.17
15	135	0.94	0.19	-0.43	0.15	1.14	0.34	-0.42	0.16
15	150	1.08	0.20	-0.51	0.15	1.11	0.37	-0.35	0.16
15	180	1.03	0.18	-0.45	0.15	1.18	0.37	-0.32	0.17
30	0	1.51	0.53	-0.14	0.22	0.33	-0.57	-1.99	0.31
30	30	1.42	0.50	-0.20	0.20	0.51	-0.37	-1.57	0.28
30	45	1.20	0.30	-0.37	0.19	0.43	-0.40	-1.52	0.24
30	60	1.31	0.22	-0.59	0.20	0.54	-0.19	-1.19	0.21
30	90	1.04	0.15	-0.67	0.18	0.89	0.10	-0.62	0.15
30	120	1.31	0.28	-0.40	0.17	1.39	0.50	-0.20	0.19
30	135	1.29	0.35	-0.43	0.19	1.44	0.60	-0.14	0.19
30	150	1.43	0.40	-0.34	0.20	1.67	0.66	-0.05	0.19
30	180	1.71	0.48	-0.29	0.22	1.74	0.68	-0.11	0.22
45	0	2.35	0.84	-0.15	0.32	0.22	-0.74	-2.04	0.30
45	30	2.09	0.66	-0.36	0.28	0.20	-0.65	-1.91	0.29
45	45	1.62	0.47	-0.34	0.23	0.29	-0.53	-1.65	0.26
45	60	1.39	0.31	-0.56	0.21	0.52	-0.29	-1.29	0.21
45	90	0.93	0.11	-0.58	0.16	0.74	0.03	-0.62	0.14
45	120	1.37	0.34	-0.39	0.19	1.23	0.42	-0.21	0.17
45	135	1.74	0.51	-0.28	0.22	1.33	0.51	-0.16	0.17
45	150	1.70	0.60	-0.37	0.23	1.37	0.57	-0.16	0.17
45	180	1.99	0.63	-0.20	0.26	1.71	0.84	0.07	0.19
60	0	2.81	1.12	-0.03	0.39	0.32	-0.47	-1.45	0.22

Model 4		C _D				C _L			
β (deg.)	θ (deg.)	(+) Peak	Mean	(-) Peak	S.D.	(+) Peak	Mean	(-) Peak	S.D.
60	30	2.51	0.95	-0.03	0.33	0.40	-0.38	-1.38	0.21
60	45	2.07	0.74	-0.12	0.28	0.49	-0.30	-1.29	0.21
60	60	1.37	0.39	-0.38	0.21	0.40	-0.27	-1.18	0.19
60	90	0.87	0.15	-0.46	0.14	0.77	0.12	-0.50	0.13
60	120	1.54	0.45	-0.25	0.20	1.02	0.37	-0.16	0.14
60	135	1.80	0.62	-0.13	0.24	1.06	0.44	-0.12	0.14
60	150	2.12	0.76	-0.11	0.27	1.25	0.58	-0.04	0.15
60	180	2.39	0.83	-0.07	0.30	1.38	0.66	0.01	0.16
75	0	3.44	1.23	0.05	0.43	0.32	-0.30	-1.04	0.16
75	30	2.81	1.00	-0.15	0.37	0.35	-0.27	-0.96	0.15
75	45	2.29	0.73	-0.26	0.30	0.32	-0.24	-0.89	0.15
75	60	1.55	0.41	-0.39	0.21	0.38	-0.18	-0.83	0.14
75	90	0.71	0.11	-0.41	0.13	0.54	0.03	-0.47	0.12
75	120	1.69	0.47	-0.27	0.22	0.71	0.20	-0.30	0.12
75	135	2.02	0.71	-0.16	0.27	0.90	0.34	-0.20	0.12
75	150	2.33	0.89	-0.05	0.31	0.95	0.37	-0.20	0.13
75	180	2.95	1.04	0.07	0.34	0.93	0.36	-0.16	0.13
90	0	3.47	1.35	0.07	0.43	0.69	0.23	-0.23	0.11
90	30	2.82	1.08	-0.01	0.36	0.55	0.06	-0.47	0.11
90	45	2.27	0.82	-0.10	0.30	0.56	0.04	-0.49	0.11
90	60	1.52	0.46	-0.27	0.21	0.54	0.04	-0.43	0.11
90	90	0.58	0.10	-0.31	0.11	0.55	0.03	-0.48	0.11
90	120	1.60	0.51	-0.26	0.22	0.64	0.12	-0.34	0.11
90	135	1.99	0.72	-0.12	0.26	0.60	0.13	-0.35	0.11
90	150	2.59	0.93	-0.02	0.33	0.65	0.15	-0.32	0.11
90	180	2.82	1.08	-0.06	0.37	0.57	0.10	-0.44	0.11

Model 5		C _D				C _L			
β (deg.)	θ (deg.)	(+) Peak	Mean	(-) Peak	S.D.	(+) Peak	Mean	(-) Peak	S.D.
0	0	1.00	0.14	-0.52	0.14	0.90	0.07	-0.85	0.20
0	30	0.86	0.16	-0.41	0.13	1.10	0.09	-0.82	0.20
0	45	0.87	0.16	-0.44	0.15	0.96	0.09	-0.84	0.20
0	60	0.93	0.17	-0.57	0.16	0.95	0.08	-0.86	0.20
0	90	1.02	0.14	-0.70	0.18	0.85	0.03	-0.89	0.19
0	120	1.02	0.16	-0.52	0.16	0.97	0.04	-0.98	0.20
0	135	0.80	0.15	-0.47	0.14	0.86	0.02	-1.00	0.21
0	150	0.87	0.14	-0.42	0.13	0.94	0.01	-0.98	0.21
0	180	0.91	0.11	-0.52	0.13	0.87	-0.02	-1.06	0.20
15	0	1.08	0.23	-0.36	0.14	0.67	-0.34	-1.65	0.27
15	30	1.04	0.21	-0.43	0.14	0.62	-0.32	-1.62	0.26
15	45	0.92	0.20	-0.33	0.14	0.64	-0.26	-1.44	0.25
15	60	0.95	0.19	-0.46	0.15	0.94	-0.10	-1.23	0.22
15	90	1.07	0.15	-0.56	0.16	0.93	0.07	-0.82	0.18
15	120	1.01	0.19	-0.53	0.17	1.26	0.28	-0.59	0.19
15	135	1.00	0.21	-0.45	0.17	1.37	0.38	-0.53	0.20
15	150	1.12	0.24	-0.45	0.18	1.44	0.44	-0.42	0.21
15	180	1.27	0.22	-0.64	0.19	1.30	0.39	-0.48	0.20
30	0	1.72	0.56	-0.24	0.25	0.49	-0.80	-2.56	0.38
30	30	1.59	0.50	-0.14	0.21	0.46	-0.70	-2.36	0.35
30	45	1.41	0.37	-0.27	0.18	0.47	-0.56	-1.99	0.31
30	60	1.13	0.26	-0.42	0.17	0.59	-0.33	-1.50	0.25
30	90	0.86	0.15	-0.50	0.15	1.02	0.07	-0.78	0.19
30	120	1.25	0.28	-0.40	0.17	1.57	0.45	-0.41	0.21
30	135	1.44	0.40	-0.32	0.20	1.68	0.62	-0.33	0.23
30	150	1.85	0.50	-0.39	0.24	1.88	0.78	-0.19	0.24
30	180	1.86	0.48	-0.41	0.25	1.74	0.70	-0.15	0.22
45	0	2.55	0.91	-0.05	0.33	0.38	-0.81	-2.13	0.33
45	30	2.14	0.77	-0.07	0.30	0.43	-0.72	-2.13	0.34
45	45	1.78	0.59	-0.26	0.24	0.52	-0.55	-1.92	0.30
45	60	1.47	0.33	-0.50	0.21	0.56	-0.44	-1.71	0.26
45	90	0.90	0.14	-0.55	0.16	1.00	0.07	-0.84	0.19
45	120	1.50	0.39	-0.37	0.20	1.65	0.55	-0.30	0.21
45	135	1.75	0.56	-0.29	0.25	1.58	0.66	-0.23	0.22
45	150	2.04	0.67	-0.29	0.27	1.71	0.69	-0.13	0.22
45	180	2.49	0.73	-0.46	0.31	1.63	0.69	-0.15	0.22
60	0	3.40	1.17	-0.12	0.44	0.40	-0.57	-1.72	0.26

Model 5		C_D				C_L			
β (deg.)	θ (deg.)	(+) Peak	Mean	(-) Peak	S.D.	(+) Peak	Mean	(-) Peak	S.D.
60	30	2.96	1.01	-0.15	0.38	0.36	-0.57	-1.72	0.26
60	45	2.23	0.77	-0.20	0.31	0.43	-0.50	-1.66	0.25
60	60	1.74	0.46	-0.37	0.23	0.49	-0.36	-1.48	0.22
60	90	0.82	0.14	-0.42	0.14	0.80	0.07	-0.71	0.16
60	120	1.83	0.49	-0.30	0.22	1.31	0.45	-0.29	0.18
60	135	1.91	0.66	-0.16	0.25	1.23	0.48	-0.21	0.17
60	150	2.57	0.83	-0.23	0.31	1.43	0.53	-0.24	0.18
60	180	2.70	0.94	-0.10	0.34	1.40	0.56	-0.18	0.18
75	0	3.74	1.31	-0.01	0.47	0.45	-0.26	-1.12	0.19
75	30	3.15	1.14	-0.07	0.41	0.51	-0.22	-1.08	0.18
75	45	2.68	0.88	-0.14	0.33	0.51	-0.22	-1.05	0.17
75	60	1.65	0.51	-0.29	0.23	0.52	-0.14	-0.85	0.16
75	90	0.76	0.12	-0.41	0.13	0.60	0.00	-0.60	0.13
75	120	1.55	0.49	-0.27	0.22	0.97	0.27	-0.33	0.14
75	135	1.99	0.72	-0.17	0.28	1.00	0.31	-0.35	0.15
75	150	2.77	0.95	-0.13	0.34	1.09	0.31	-0.33	0.15
75	180	2.88	1.07	-0.06	0.39	1.01	0.34	-0.29	0.15
90	0	3.74	1.39	0.05	0.50	0.67	0.12	-0.47	0.13
90	30	3.33	1.22	0.02	0.41	0.72	0.15	-0.43	0.13
90	45	2.66	0.94	-0.13	0.34	0.70	0.16	-0.37	0.12
90	60	1.78	0.53	-0.28	0.23	0.55	0.00	-0.50	0.12
90	90	0.65	0.11	-0.34	0.12	0.56	0.04	-0.46	0.12
90	120	1.67	0.51	-0.27	0.23	0.63	0.10	-0.41	0.12
90	135	2.05	0.76	-0.06	0.29	0.74	0.21	-0.28	0.12
90	150	2.64	1.00	0.00	0.36	0.78	0.23	-0.34	0.12
90	180	3.00	1.09	-0.05	0.40	0.72	0.20	-0.41	0.12

Model 6		C _D				C _L			
β (deg.)	θ (deg.)	(+) Peak	Mean	(-) Peak	S.D.	(+) Peak	Mean	(-) Peak	S.D.
0	0	0.91	0.13	-0.50	0.15	0.84	0.07	-0.78	0.18
0	30	0.88	0.19	-0.38	0.14	0.91	0.08	-0.89	0.19
0	45	0.96	0.20	-0.40	0.15	0.95	0.09	-0.85	0.20
0	60	0.92	0.15	-0.59	0.15	0.86	0.05	-0.98	0.19
0	90	1.08	0.15	-0.72	0.16	0.84	0.08	-0.80	0.18
0	120	0.81	0.16	-0.45	0.15	0.86	0.06	-0.88	0.18
0	135	0.94	0.14	-0.52	0.15	0.94	0.11	-0.88	0.19
0	150	0.91	0.12	-0.58	0.14	1.03	0.11	-0.78	0.20
0	180	0.89	0.09	-0.59	0.14	0.92	0.08	-0.79	0.19
15	0	1.17	0.22	-0.44	0.17	0.53	-0.38	-1.70	0.26
15	30	0.98	0.24	-0.34	0.15	0.65	-0.33	-1.56	0.26
15	45	0.99	0.23	-0.39	0.15	0.69	-0.25	-1.49	0.25
15	60	0.94	0.17	-0.52	0.16	0.67	-0.19	-1.23	0.22
15	90	0.97	0.13	-0.57	0.16	0.81	0.03	-0.93	0.18
15	120	1.12	0.17	-0.59	0.16	1.17	0.25	-0.56	0.18
15	135	1.16	0.20	-0.53	0.17	1.26	0.36	-0.50	0.19
15	150	1.10	0.22	-0.43	0.17	1.39	0.43	-0.41	0.20
15	180	1.27	0.18	-0.73	0.19	1.45	0.44	-0.44	0.20
30	0	1.54	0.49	-0.24	0.23	0.50	-0.67	-2.19	0.35
30	30	1.46	0.45	-0.26	0.20	0.51	-0.55	-2.05	0.32
30	45	1.31	0.38	-0.25	0.18	0.66	-0.41	-1.76	0.30
30	60	1.13	0.23	-0.41	0.17	0.57	-0.34	-1.55	0.26
30	90	0.97	0.13	-0.64	0.16	0.80	0.03	-0.87	0.18
30	120	1.21	0.26	-0.48	0.18	1.47	0.47	-0.33	0.20
30	135	1.44	0.35	-0.43	0.20	1.71	0.60	-0.24	0.22
30	150	1.66	0.42	-0.43	0.23	1.88	0.69	-0.23	0.24
30	180	1.80	0.45	-0.57	0.25	1.73	0.69	-0.39	0.23
45	0	2.45	0.88	-0.12	0.33	0.33	-0.75	-2.10	0.32
45	30	2.20	0.79	-0.20	0.30	0.44	-0.66	-2.02	0.32
45	45	1.78	0.61	-0.22	0.26	0.58	-0.49	-1.84	0.30
45	60	1.35	0.39	-0.40	0.20	0.70	-0.26	-1.49	0.25
45	90	0.97	0.17	-0.51	0.16	1.00	0.21	-0.57	0.18
45	120	1.41	0.37	-0.41	0.20	1.55	0.64	-0.20	0.20
45	135	1.77	0.51	-0.36	0.24	1.72	0.78	-0.05	0.22
45	150	2.16	0.62	-0.30	0.28	1.83	0.80	-0.05	0.22
45	180	2.34	0.59	-0.51	0.31	2.06	1.04	0.16	0.22
60	0	3.43	1.13	-0.04	0.42	0.54	-0.51	-1.77	0.26

Model 6		C_D				C_L			
β (deg.)	θ (deg.)	(+) Peak	Mean	(-) Peak	S.D.	(+) Peak	Mean	(-) Peak	S.D.
60	30	2.94	1.00	-0.09	0.37	0.48	-0.51	-1.80	0.26
60	45	2.44	0.77	-0.19	0.31	0.57	-0.45	-1.62	0.25
60	60	1.56	0.46	-0.43	0.23	0.57	-0.27	-1.42	0.22
60	90	0.85	0.16	-0.44	0.15	0.86	0.15	-0.59	0.16
60	120	1.50	0.48	-0.30	0.22	1.26	0.49	-0.18	0.17
60	135	1.96	0.65	-0.23	0.26	1.28	0.51	-0.21	0.17
60	150	2.23	0.78	-0.17	0.30	1.42	0.57	-0.17	0.18
60	180	2.91	0.92	-0.29	0.35	1.52	0.61	-0.16	0.19
75	0	3.51	1.34	0.06	0.46	0.47	-0.28	-1.12	0.18
75	30	2.98	1.14	-0.08	0.40	0.42	-0.26	-1.09	0.17
75	45	2.42	0.86	-0.18	0.32	0.42	-0.22	-1.03	0.17
75	60	1.68	0.51	-0.34	0.23	0.46	-0.14	-0.91	0.15
75	90	0.76	0.16	-0.36	0.13	0.70	0.12	-0.44	0.12
75	120	1.73	0.50	-0.25	0.23	0.84	0.26	-0.30	0.13
75	135	1.91	0.71	-0.17	0.27	1.03	0.43	-0.09	0.13
75	150	2.84	0.93	-0.05	0.33	1.09	0.48	-0.13	0.14
75	180	2.83	1.03	-0.09	0.38	1.11	0.48	-0.10	0.14
90	0	3.59	1.41	0.09	0.49	0.64	0.09	-0.57	0.13
90	30	3.19	1.28	0.07	0.42	0.77	0.27	-0.24	0.12
90	45	2.48	0.97	-0.01	0.31	0.81	0.29	-0.18	0.11
90	60	1.68	0.63	-0.10	0.22	0.81	0.32	-0.16	0.11
90	90	0.68	0.23	-0.16	0.11	0.88	0.37	-0.14	0.11
90	120	1.68	0.56	-0.15	0.22	0.87	0.43	-0.06	0.10
90	135	2.25	0.80	-0.15	0.29	0.99	0.47	-0.11	0.11
90	150	2.83	1.01	-0.10	0.36	1.00	0.49	-0.03	0.12
90	180	2.92	1.07	-0.10	0.39	1.01	0.48	-0.05	0.12

Model 7		C _D				C _L			
β (deg.)	θ (deg.)	(+) Peak	Mean	(-) Peak	S.D.	(+) Peak	Mean	(-) Peak	S.D.
0	0	0.88	0.11	-0.51	0.15	0.85	0.07	-0.69	0.16
0	30	0.83	0.16	-0.44	0.13	0.82	0.07	-0.70	0.16
0	45	0.87	0.17	-0.44	0.15	0.89	0.08	-0.79	0.17
0	60	0.95	0.18	-0.52	0.15	0.83	0.14	-0.71	0.16
0	90	0.93	0.14	-0.49	0.15	0.72	0.05	-0.75	0.15
0	120	0.87	0.14	-0.45	0.14	0.71	0.04	-0.76	0.16
0	135	0.84	0.14	-0.43	0.14	0.83	0.09	-0.84	0.18
0	150	0.81	0.12	-0.45	0.14	0.83	0.07	-0.85	0.18
0	180	0.80	0.08	-0.53	0.14	0.79	0.05	-0.79	0.18
15	0	1.10	0.23	-0.42	0.15	0.48	-0.31	-1.54	0.25
15	30	1.06	0.27	-0.30	0.14	0.48	-0.29	-1.44	0.23
15	45	0.97	0.25	-0.32	0.15	0.57	-0.21	-1.22	0.22
15	60	1.01	0.21	-0.35	0.14	0.62	-0.09	-1.05	0.19
15	90	0.98	0.14	-0.64	0.15	0.72	0.06	-0.64	0.15
15	120	0.95	0.18	-0.41	0.15	1.15	0.34	-0.39	0.16
15	135	0.99	0.21	-0.38	0.15	1.31	0.45	-0.33	0.18
15	150	1.12	0.22	-0.43	0.16	1.43	0.49	-0.30	0.19
15	180	1.14	0.19	-0.54	0.17	1.34	0.46	-0.30	0.18
30	0	1.65	0.56	-0.18	0.24	0.34	-0.71	-2.26	0.34
30	30	1.58	0.48	-0.20	0.20	0.37	-0.56	-1.96	0.30
30	45	1.27	0.39	-0.16	0.17	0.43	-0.42	-1.58	0.27
30	60	1.16	0.29	-0.35	0.15	0.54	-0.21	-1.39	0.23
30	90	0.92	0.17	-0.43	0.14	0.84	0.15	-0.59	0.15
30	120	1.22	0.27	-0.34	0.16	1.46	0.51	-0.15	0.18
30	135	1.45	0.36	-0.36	0.19	1.56	0.66	-0.13	0.20
30	150	1.82	0.43	-0.46	0.22	1.86	0.74	-0.15	0.22
30	180	1.78	0.42	-0.50	0.24	1.93	0.93	0.15	0.21
45	0	2.40	0.90	-0.10	0.33	0.37	-0.62	-1.91	0.32
45	30	2.32	0.79	-0.09	0.29	0.43	-0.54	-2.03	0.31
45	45	1.74	0.61	-0.18	0.24	0.51	-0.40	-1.73	0.28
45	60	1.39	0.39	-0.29	0.19	0.67	-0.16	-1.28	0.24
45	90	0.93	0.18	-0.44	0.14	1.02	0.24	-0.49	0.16
45	120	1.32	0.38	-0.29	0.18	1.54	0.64	-0.15	0.18
45	135	1.89	0.53	-0.28	0.23	1.71	0.76	-0.09	0.20
45	150	2.07	0.61	-0.26	0.26	1.77	0.78	-0.02	0.21
45	180	2.08	0.59	-0.36	0.28	1.79	0.98	0.19	0.20
60	0	3.02	1.09	-0.02	0.39	0.32	-0.57	-1.85	0.25

Model 7		C_D				C_L			
β (deg.)	θ (deg.)	(+) Peak	Mean	(-) Peak	S.D.	(+) Peak	Mean	(-) Peak	S.D.
60	30	2.64	0.93	-0.12	0.35	0.31	-0.55	-1.64	0.25
60	45	2.04	0.70	-0.21	0.28	0.33	-0.45	-1.43	0.23
60	60	1.41	0.42	-0.43	0.21	0.46	-0.28	-1.18	0.20
60	90	0.82	0.15	-0.41	0.13	0.84	0.11	-0.53	0.15
60	120	1.41	0.43	-0.25	0.20	1.15	0.43	-0.21	0.16
60	135	1.82	0.61	-0.16	0.24	1.28	0.50	-0.18	0.16
60	150	2.17	0.76	-0.26	0.29	1.32	0.56	-0.20	0.17
60	180	2.51	0.82	-0.24	0.33	1.47	0.75	0.07	0.17
75	0	3.56	1.30	0.00	0.46	0.48	-0.21	-1.03	0.17
75	30	2.86	1.07	-0.18	0.38	0.44	-0.19	-1.02	0.16
75	45	2.33	0.80	-0.14	0.30	0.51	-0.16	-0.95	0.15
75	60	1.54	0.50	-0.27	0.22	0.50	-0.13	-0.78	0.14
75	90	0.70	0.14	-0.34	0.11	0.57	0.07	-0.46	0.12
75	120	1.65	0.49	-0.18	0.21	0.80	0.27	-0.24	0.12
75	135	2.03	0.73	-0.13	0.27	1.07	0.44	-0.14	0.13
75	150	2.41	0.91	-0.10	0.33	1.09	0.47	-0.08	0.13
75	180	2.96	1.05	0.04	0.37	1.05	0.47	-0.11	0.13
90	0	3.73	1.37	0.12	0.46	0.56	0.09	-0.41	0.11
90	30	3.06	1.15	0.03	0.39	0.60	0.11	-0.37	0.11
90	45	2.34	0.89	-0.06	0.30	0.60	0.12	-0.30	0.10
90	60	1.53	0.49	-0.22	0.21	0.50	0.05	-0.42	0.10
90	90	0.61	0.14	-0.26	0.10	0.55	0.12	-0.31	0.10
90	120	1.52	0.50	-0.16	0.21	0.62	0.19	-0.23	0.10
90	135	2.24	0.75	-0.12	0.28	0.61	0.19	-0.25	0.10
90	150	2.91	0.99	-0.04	0.35	0.72	0.20	-0.28	0.11
90	180	3.01	1.13	0.00	0.40	0.67	0.17	-0.33	0.11

A2. NORMAL FORCE AND PITCHING MOMENT COEFFICIENTS

Model 1		C _{FN}				C _{My}			
β (deg.)	θ (deg.)	(+) Peak	Mean	(-) Peak	S.D.	(+) Peak	Mean	(-) Peak	S.D.
0	0	1.04	-0.02	-0.95	0.23	0.27	0.01	-0.27	0.06
0	30	1.05	-0.09	-1.10	0.23	0.23	-0.01	-0.27	0.06
0	45	1.04	-0.07	-1.06	0.23	0.24	0.00	-0.24	0.05
0	60	1.18	-0.07	-1.07	0.25	0.23	-0.01	-0.28	0.05
0	90	0.58	-0.37	-1.20	0.19	0.19	-0.05	-0.25	0.05
0	120	1.01	-0.08	-1.06	0.21	0.20	-0.01	-0.21	0.04
0	135	1.04	-0.08	-1.03	0.23	0.22	-0.02	-0.23	0.05
0	150	1.27	-0.07	-1.18	0.24	0.25	-0.03	-0.27	0.06
0	180	1.03	-0.03	-0.98	0.22	0.25	-0.03	-0.28	0.06
15	0	1.90	0.46	-0.59	0.33	0.14	-0.10	-0.45	0.07
15	30	1.92	0.40	-0.73	0.31	0.15	-0.08	-0.38	0.06
15	45	1.68	0.34	-0.81	0.29	0.17	-0.06	-0.36	0.05
15	60	1.53	0.19	-0.87	0.27	0.16	-0.03	-0.27	0.05
15	90	0.97	-0.04	-0.95	0.21	0.17	0.00	-0.20	0.04
15	120	0.77	-0.37	-1.61	0.22	0.16	-0.06	-0.33	0.05
15	135	0.52	-0.49	-1.58	0.23	0.14	-0.10	-0.40	0.05
15	150	0.43	-0.57	-1.71	0.22	0.13	-0.13	-0.42	0.06
15	180	0.45	-0.50	-1.71	0.23	0.10	-0.15	-0.46	0.06
30	0	2.98	1.05	-0.33	0.47	0.13	-0.17	-0.58	0.09
30	30	2.91	0.89	-0.43	0.44	0.14	-0.12	-0.54	0.08
30	45	2.45	0.67	-0.48	0.36	0.17	-0.07	-0.39	0.06
30	60	2.17	0.46	-0.71	0.31	0.18	-0.04	-0.30	0.05
30	90	1.02	0.00	-1.07	0.22	0.22	0.01	-0.17	0.04
30	120	0.55	-0.55	-1.88	0.26	0.14	-0.07	-0.34	0.05
30	135	0.40	-0.80	-2.36	0.31	0.13	-0.13	-0.49	0.07
30	150	0.23	-1.00	-2.52	0.34	0.09	-0.17	-0.53	0.07
30	180	0.27	-0.88	-2.26	0.30	0.08	-0.16	-0.49	0.07
45	0	3.60	1.38	-0.06	0.49	0.14	-0.13	-0.47	0.07
45	30	3.56	1.27	-0.21	0.50	0.15	-0.13	-0.49	0.07
45	45	3.19	1.03	-0.34	0.45	0.18	-0.09	-0.45	0.07
45	60	2.41	0.70	-0.48	0.36	0.20	-0.05	-0.32	0.06
45	90	1.21	-0.04	-1.23	0.24	0.21	0.00	-0.21	0.05
45	120	0.42	-0.78	-2.53	0.32	0.16	-0.09	-0.39	0.06

Model 1		C _{FN}				C _{My}			
β (deg.)	θ (deg.)	(+) Peak	Mean	(-) Peak	S.D.	(+) Peak	Mean	(-) Peak	S.D.
45	135	0.20	-1.04	-2.71	0.36	0.14	-0.12	-0.43	0.06
45	150	0.11	-1.00	-2.67	0.34	0.16	-0.10	-0.38	0.06
45	180	0.15	-1.02	-2.71	0.34	0.14	-0.10	-0.39	0.06
60	0	4.05	1.41	-0.03	0.52	0.19	-0.09	-0.44	0.07
60	30	3.76	1.36	-0.17	0.50	0.21	-0.08	-0.40	0.07
60	45	3.37	1.24	-0.13	0.48	0.19	-0.08	-0.41	0.07
60	60	2.78	0.87	-0.40	0.39	0.24	-0.03	-0.31	0.06
60	90	1.23	-0.01	-1.30	0.26	0.22	0.01	-0.20	0.05
60	120	0.30	-0.84	-2.49	0.34	0.21	-0.05	-0.31	0.06
60	135	0.20	-0.98	-2.64	0.34	0.18	-0.05	-0.30	0.06
60	150	-0.02	-1.21	-3.02	0.37	0.10	-0.15	-0.43	0.06
60	180	-0.01	-1.26	-3.07	0.38	0.11	-0.13	-0.42	0.06
75	0	4.18	1.49	-0.02	0.52	0.19	-0.09	-0.42	0.07
75	30	3.80	1.40	-0.06	0.50	0.22	-0.06	-0.37	0.07
75	45	3.62	1.30	-0.13	0.50	0.23	-0.05	-0.35	0.07
75	60	3.22	1.03	-0.36	0.44	0.25	-0.03	-0.33	0.06
75	90	1.31	-0.02	-1.52	0.29	0.26	0.00	-0.26	0.06
75	120	0.38	-0.88	-2.52	0.37	0.23	-0.03	-0.32	0.06
75	135	0.11	-1.03	-2.91	0.38	0.23	-0.03	-0.32	0.06
75	150	0.05	-1.14	-3.13	0.40	0.22	-0.03	-0.32	0.06
75	180	0.06	-1.23	-3.02	0.42	0.24	-0.04	-0.31	0.06
90	0	3.90	1.45	-0.05	0.50	0.29	-0.04	-0.35	0.07
90	30	3.56	1.40	-0.04	0.48	0.27	-0.04	-0.37	0.07
90	45	3.84	1.28	-0.14	0.48	0.27	-0.02	-0.34	0.07
90	60	3.76	1.09	-0.28	0.45	0.26	-0.02	-0.31	0.06
90	90	1.38	-0.01	-1.32	0.30	0.28	0.02	-0.27	0.06
90	120	0.44	-0.85	-2.89	0.38	0.29	0.01	-0.27	0.06
90	135	0.27	-1.06	-2.93	0.39	0.25	0.01	-0.26	0.06
90	150	0.20	-1.19	-3.29	0.44	0.27	0.00	-0.26	0.06
90	180	0.19	-1.25	-3.54	0.47	0.28	0.00	-0.27	0.06

Model 2		C _{FN}				C _{My}			
β (deg.)	θ (deg.)	(+) Peak	Mean	(-) Peak	S.D.	(+) Peak	Mean	(-) Peak	S.D.
0	0	0.58	-0.32	-1.22	0.20	0.17	-0.04	-0.28	0.05
0	30	0.99	-0.06	-1.05	0.22	0.20	-0.01	-0.22	0.05
0	45	1.04	-0.03	-0.97	0.21	0.21	0.00	-0.21	0.05
0	60	1.00	-0.03	-0.96	0.22	0.18	-0.01	-0.22	0.04
0	90	0.91	-0.01	-0.91	0.20	0.18	0.00	-0.17	0.04
0	120	0.96	-0.06	-0.92	0.21	0.18	-0.01	-0.18	0.04
0	135	1.01	-0.06	-1.09	0.21	0.19	-0.01	-0.20	0.04
0	150	1.02	-0.05	-1.02	0.21	0.20	-0.02	-0.22	0.05
0	180	1.02	-0.02	-0.93	0.20	0.19	-0.03	-0.26	0.05
15	0	1.71	0.42	-0.54	0.28	0.14	-0.07	-0.35	0.06
15	30	1.69	0.41	-0.59	0.27	0.10	-0.12	-0.37	0.05
15	45	1.54	0.32	-0.67	0.25	0.10	-0.10	-0.33	0.05
15	60	1.44	0.20	-0.73	0.23	0.14	-0.04	-0.24	0.04
15	90	0.79	-0.22	-1.12	0.20	0.13	-0.04	-0.23	0.04
15	120	0.51	-0.48	-1.49	0.21	0.12	-0.07	-0.26	0.04
15	135	0.50	-0.52	-1.60	0.21	0.12	-0.08	-0.30	0.04
15	150	0.38	-0.59	-1.55	0.21	0.09	-0.11	-0.36	0.05
15	180	0.44	-0.50	-1.50	0.21	0.10	-0.13	-0.40	0.05
30	0	2.83	1.00	-0.32	0.42	0.09	-0.15	-0.52	0.07
30	30	2.58	0.81	-0.37	0.39	0.10	-0.14	-0.46	0.06
30	45	2.16	0.62	-0.48	0.35	0.16	-0.07	-0.37	0.06
30	60	1.74	0.35	-0.65	0.29	0.17	-0.02	-0.24	0.05
30	90	0.99	-0.04	-1.06	0.21	0.19	0.00	-0.18	0.04
30	120	0.47	-0.54	-1.78	0.24	0.13	-0.06	-0.28	0.04
30	135	0.27	-0.77	-2.19	0.28	0.12	-0.10	-0.37	0.05
30	150	0.27	-0.89	-2.43	0.30	0.12	-0.11	-0.40	0.06
30	180	0.14	-0.90	-2.36	0.29	0.10	-0.15	-0.46	0.06
45	0	3.48	1.25	-0.15	0.48	0.12	-0.11	-0.45	0.06
45	30	3.50	1.22	-0.22	0.49	0.14	-0.11	-0.43	0.06
45	45	2.87	0.99	-0.36	0.42	0.16	-0.08	-0.38	0.06
45	60	2.30	0.67	-0.47	0.35	0.17	-0.04	-0.30	0.05
45	90	1.00	-0.03	-1.17	0.22	0.20	0.00	-0.17	0.04
45	120	0.34	-0.73	-2.13	0.29	0.11	-0.07	-0.31	0.05
45	135	0.16	-0.91	-2.58	0.31	0.11	-0.09	-0.33	0.05
45	150	0.08	-0.98	-2.64	0.32	0.12	-0.09	-0.36	0.05
45	180	0.04	-0.98	-2.48	0.32	0.10	-0.09	-0.36	0.05
60	0	3.58	1.31	-0.08	0.49	0.15	-0.07	-0.37	0.06

Model 2		C_{FN}			C_{My}				
β (deg.)	θ (deg.)	(+) Peak	Mean	(-) Peak	S.D.	(+) Peak	Mean	(-) Peak	S.D.
60	30	3.82	1.32	-0.15	0.49	0.17	-0.07	-0.36	0.06
60	45	3.24	1.17	-0.18	0.47	0.18	-0.05	-0.34	0.06
60	60	2.66	0.85	-0.48	0.39	0.21	-0.03	-0.28	0.05
60	90	1.13	-0.03	-1.29	0.24	0.19	0.00	-0.19	0.04
60	120	0.31	-0.76	-2.75	0.31	0.14	-0.05	-0.26	0.04
60	135	0.21	-0.90	-2.47	0.33	0.16	-0.05	-0.29	0.05
60	150	0.03	-1.04	-2.70	0.35	0.14	-0.06	-0.28	0.05
60	180	-0.03	-1.19	-2.94	0.37	0.13	-0.10	-0.34	0.05
75	0	3.69	1.38	0.05	0.49	0.20	-0.06	-0.34	0.06
75	30	3.55	1.36	-0.05	0.48	0.15	-0.10	-0.39	0.06
75	45	3.56	1.20	-0.14	0.47	0.23	-0.04	-0.32	0.06
75	60	3.09	0.88	-0.43	0.42	0.25	0.02	-0.23	0.05
75	90	1.22	-0.02	-1.45	0.27	0.19	0.00	-0.21	0.05
75	120	0.40	-0.72	-2.45	0.32	0.14	-0.06	-0.27	0.04
75	135	0.21	-0.92	-2.64	0.35	0.17	-0.04	-0.27	0.05
75	150	0.10	-1.05	-2.95	0.38	0.16	-0.06	-0.30	0.05
75	180	-0.02	-1.11	-2.94	0.38	0.18	-0.06	-0.31	0.05
90	0	3.79	1.49	0.08	0.49	0.21	-0.04	-0.34	0.06
90	30	3.73	1.40	0.03	0.47	0.18	-0.09	-0.36	0.06
90	45	3.51	1.28	-0.17	0.48	0.24	-0.02	-0.29	0.06
90	60	3.16	1.00	-0.42	0.43	0.30	0.01	-0.26	0.06
90	90	1.47	0.00	-1.44	0.28	0.30	0.00	-0.27	0.06
90	120	0.55	-0.76	-2.55	0.35	0.25	-0.01	-0.28	0.06
90	135	0.22	-0.89	-2.74	0.36	0.24	-0.03	-0.28	0.06
90	150	0.20	-1.02	-3.10	0.40	0.24	-0.04	-0.31	0.06
90	180	0.10	-1.14	-3.22	0.42	0.28	-0.02	-0.30	0.06

Model 3		C _{FN}				C _{My}			
β (deg.)	θ (deg.)	(+) Peak	Mean	(-) Peak	S.D.	(+) Peak	Mean	(-) Peak	S.D.
0	0	0.71	-0.24	-0.97	0.18	0.14	-0.04	-0.26	0.04
0	30	0.63	-0.34	-1.14	0.20	0.11	-0.09	-0.29	0.04
0	45	0.55	-0.40	-1.33	0.20	0.10	-0.10	-0.32	0.04
0	60	0.94	-0.06	-1.01	0.20	0.18	0.00	-0.19	0.04
0	90	0.76	-0.08	-0.86	0.18	0.17	0.01	-0.13	0.04
0	120	0.73	-0.15	-0.98	0.19	0.16	0.00	-0.15	0.03
0	135	0.80	-0.08	-0.94	0.19	0.17	-0.01	-0.19	0.04
0	150	0.84	-0.11	-0.99	0.19	0.15	-0.03	-0.21	0.04
0	180	0.80	-0.10	-0.90	0.18	0.15	-0.04	-0.24	0.04
15	0	1.48	0.23	-0.67	0.26	0.14	-0.05	-0.30	0.05
15	30	1.40	0.21	-0.68	0.25	0.13	-0.06	-0.31	0.05
15	45	1.36	0.19	-0.72	0.23	0.16	-0.04	-0.25	0.04
15	60	1.31	0.16	-0.72	0.22	0.13	-0.05	-0.23	0.04
15	90	0.80	-0.03	-0.89	0.18	0.16	0.00	-0.16	0.04
15	120	0.64	-0.27	-1.19	0.19	0.14	-0.03	-0.20	0.04
15	135	0.26	-0.56	-1.53	0.19	0.09	-0.09	-0.27	0.04
15	150	0.28	-0.55	-1.53	0.20	0.08	-0.09	-0.29	0.04
15	180	0.37	-0.49	-1.50	0.20	0.09	-0.10	-0.35	0.05
30	0	2.56	0.85	-0.39	0.41	0.09	-0.14	-0.47	0.07
30	30	2.42	0.63	-0.53	0.38	0.06	-0.15	-0.44	0.06
30	45	2.08	0.44	-0.65	0.33	0.06	-0.13	-0.38	0.05
30	60	1.66	0.37	-0.56	0.27	0.15	-0.03	-0.24	0.04
30	90	0.90	-0.07	-0.95	0.20	0.18	0.01	-0.17	0.04
30	120	0.40	-0.60	-1.79	0.24	0.13	-0.05	-0.28	0.04
30	135	0.14	-0.81	-2.23	0.26	0.11	-0.09	-0.33	0.05
30	150	0.11	-0.91	-2.50	0.28	0.07	-0.11	-0.40	0.05
30	180	0.15	-0.89	-2.25	0.29	0.06	-0.15	-0.44	0.06
45	0	3.24	1.17	-0.11	0.46	0.11	-0.10	-0.38	0.06
45	30	3.24	1.08	-0.17	0.45	0.13	-0.10	-0.37	0.06
45	45	2.68	0.89	-0.29	0.40	0.14	-0.07	-0.35	0.05
45	60	2.08	0.62	-0.38	0.31	0.14	-0.06	-0.29	0.05
45	90	0.99	-0.02	-1.10	0.22	0.20	0.00	-0.16	0.04
45	120	0.41	-0.64	-1.92	0.27	0.13	-0.05	-0.26	0.04
45	135	-0.01	-0.93	-2.24	0.28	0.07	-0.10	-0.35	0.04
45	150	0.02	-1.01	-2.54	0.30	0.08	-0.11	-0.33	0.05
45	180	0.05	-1.03	-2.51	0.30	0.11	-0.09	-0.32	0.05

Model 3		C_{FN}				C_{My}			
β (deg.)	θ (deg.)	(+) Peak	Mean	(-) Peak	S.D.	(+) Peak	Mean	(-) Peak	S.D.
60	0	3.35	1.21	-0.10	0.45	0.13	-0.07	-0.32	0.05
60	30	3.49	1.22	-0.18	0.46	0.14	-0.06	-0.32	0.05
60	45	3.21	1.08	-0.17	0.45	0.16	-0.05	-0.31	0.05
60	60	2.50	0.74	-0.39	0.37	0.18	-0.01	-0.24	0.05
60	90	1.16	-0.01	-1.16	0.24	0.17	-0.01	-0.20	0.04
60	120	0.39	-0.71	-2.15	0.28	0.12	-0.06	-0.25	0.04
60	135	0.09	-0.86	-2.27	0.29	0.08	-0.09	-0.26	0.04
60	150	0.00	-0.98	-2.54	0.33	0.11	-0.06	-0.27	0.04
60	180	-0.05	-1.09	-2.64	0.34	0.09	-0.09	-0.32	0.04
75	0	3.56	1.37	-0.03	0.47	0.17	-0.04	-0.30	0.05
75	30	3.54	1.28	-0.08	0.46	0.17	-0.04	-0.28	0.05
75	45	3.25	1.19	-0.08	0.45	0.19	-0.03	-0.27	0.05
75	60	2.82	0.86	-0.45	0.40	0.20	-0.01	-0.22	0.05
75	90	1.24	-0.02	-1.33	0.26	0.20	0.01	-0.19	0.04
75	120	0.58	-0.66	-2.27	0.30	0.17	-0.02	-0.23	0.04
75	135	0.28	-0.85	-2.48	0.33	0.16	-0.03	-0.23	0.04
75	150	0.07	-1.01	-2.78	0.35	0.13	-0.05	-0.27	0.04
75	180	-0.03	-1.15	-2.95	0.37	0.14	-0.05	-0.26	0.04
90	0	3.68	1.32	0.00	0.46	0.20	-0.03	-0.27	0.05
90	30	3.57	1.30	0.02	0.44	0.20	-0.06	-0.32	0.06
90	45	3.32	1.21	-0.10	0.44	0.25	-0.02	-0.26	0.05
90	60	3.01	0.94	-0.39	0.40	0.22	0.00	-0.22	0.05
90	90	1.29	0.00	-1.31	0.28	0.20	0.00	-0.20	0.05
90	120	0.47	-0.62	-2.09	0.30	0.20	-0.01	-0.22	0.05
90	135	0.35	-0.80	-2.43	0.34	0.23	-0.03	-0.24	0.05
90	150	0.17	-0.97	-2.65	0.37	0.21	-0.01	-0.21	0.04
90	180	0.11	-1.13	-3.13	0.38	0.22	-0.01	-0.23	0.05

Model 4		C _{FN}				C _{My}			
β (deg.)	θ (deg.)	(+) Peak	Mean	(-) Peak	S.D.	(+) Peak	Mean	(-) Peak	S.D.
0	0	0.50	-0.17	-0.83	0.14	0.13	-0.02	-0.19	0.04
0	30	0.57	-0.25	-0.93	0.16	0.09	-0.06	-0.22	0.03
0	45	0.75	-0.07	-0.74	0.17	0.15	0.00	-0.16	0.03
0	60	0.78	-0.11	-0.89	0.17	0.16	0.01	-0.15	0.03
0	90	0.83	0.03	-0.67	0.16	0.16	0.01	-0.13	0.03
0	120	0.75	-0.05	-0.76	0.16	0.16	0.00	-0.15	0.03
0	135	0.79	-0.09	-0.83	0.16	0.17	-0.01	-0.18	0.03
0	150	0.64	-0.10	-0.73	0.16	0.15	-0.02	-0.18	0.04
0	180	0.62	-0.10	-0.74	0.16	0.14	-0.03	-0.18	0.04
15	0	1.41	0.33	-0.43	0.23	0.12	-0.05	-0.26	0.04
15	30	1.33	0.29	-0.47	0.22	0.11	-0.04	-0.23	0.04
15	45	1.17	0.23	-0.54	0.21	0.14	-0.03	-0.22	0.04
15	60	1.09	0.12	-0.64	0.19	0.13	-0.02	-0.18	0.04
15	90	0.71	-0.06	-0.86	0.17	0.15	0.00	-0.15	0.03
15	120	0.62	-0.26	-1.14	0.17	0.14	-0.02	-0.18	0.03
15	135	0.41	-0.36	-1.20	0.17	0.12	-0.04	-0.21	0.04
15	150	0.40	-0.40	-1.19	0.17	0.12	-0.06	-0.24	0.04
15	180	0.28	-0.40	-1.24	0.17	0.10	-0.08	-0.28	0.04
30	0	2.38	0.76	-0.27	0.36	0.07	-0.12	-0.40	0.06
30	30	1.99	0.58	-0.40	0.33	0.04	-0.13	-0.36	0.05
30	45	1.80	0.52	-0.37	0.28	0.13	-0.05	-0.26	0.04
30	60	1.44	0.27	-0.50	0.23	0.15	-0.01	-0.21	0.04
30	90	0.91	-0.07	-1.01	0.17	0.13	-0.02	-0.18	0.03
30	120	0.28	-0.59	-1.70	0.23	0.08	-0.06	-0.24	0.04
30	135	0.14	-0.68	-1.75	0.23	0.07	-0.08	-0.26	0.04
30	150	0.04	-0.76	-1.96	0.23	0.06	-0.10	-0.30	0.04
30	180	0.08	-0.83	-2.17	0.26	0.05	-0.12	-0.37	0.05
45	0	2.93	1.12	-0.11	0.42	0.10	-0.09	-0.37	0.05
45	30	2.92	1.00	-0.11	0.40	0.11	-0.07	-0.30	0.05
45	45	2.38	0.82	-0.19	0.35	0.14	-0.05	-0.26	0.04
45	60	1.93	0.52	-0.44	0.28	0.16	-0.03	-0.23	0.04
45	90	0.88	-0.01	-0.98	0.20	0.16	0.01	-0.16	0.04
45	120	0.34	-0.59	-1.76	0.25	0.11	-0.05	-0.24	0.04
45	135	0.10	-0.73	-2.24	0.26	0.11	-0.06	-0.25	0.04
45	150	0.15	-0.81	-2.03	0.26	0.10	-0.07	-0.27	0.04
45	180	-0.09	-1.04	-2.32	0.29	0.06	-0.12	-0.33	0.04

Model 4		C _{FN}			C _{My}				
β (deg.)	θ (deg.)	(+) Peak	Mean	(-) Peak	S.D.	(+) Peak	Mean	(-) Peak	S.D.
60	0	3.05	1.20	0.01	0.43	0.10	-0.08	-0.30	0.04
60	30	3.13	1.14	0.01	0.41	0.06	-0.10	-0.33	0.04
60	45	2.83	1.01	-0.18	0.40	0.09	-0.09	-0.27	0.04
60	60	2.51	0.70	-0.38	0.34	0.14	-0.02	-0.20	0.04
60	90	0.94	-0.06	-1.10	0.23	0.19	0.01	-0.15	0.04
60	120	0.27	-0.64	-2.07	0.27	0.12	-0.04	-0.21	0.04
60	135	0.13	-0.77	-2.08	0.27	0.11	-0.04	-0.20	0.04
60	150	0.02	-0.93	-2.35	0.29	0.09	-0.07	-0.26	0.04
60	180	-0.07	-1.05	-2.63	0.32	0.10	-0.09	-0.29	0.04
75	0	3.52	1.26	0.07	0.45	0.13	-0.05	-0.25	0.04
75	30	3.25	1.19	-0.11	0.43	0.14	-0.04	-0.26	0.04
75	45	3.13	1.06	-0.15	0.41	0.17	-0.02	-0.23	0.04
75	60	2.48	0.77	-0.41	0.36	0.17	-0.01	-0.22	0.04
75	90	1.15	-0.02	-1.24	0.26	0.19	0.00	-0.17	0.04
75	120	0.48	-0.61	-2.14	0.29	0.16	-0.01	-0.19	0.04
75	135	0.15	-0.80	-2.24	0.30	0.15	-0.03	-0.21	0.04
75	150	0.01	-0.96	-2.50	0.32	0.15	-0.03	-0.22	0.04
75	180	-0.10	-1.09	-3.00	0.35	0.15	-0.04	-0.24	0.04
90	0	3.47	1.35	0.07	0.43	0.16	-0.05	-0.27	0.04
90	30	3.22	1.24	0.00	0.41	0.16	-0.03	-0.23	0.04
90	45	3.18	1.13	-0.08	0.40	0.18	-0.01	-0.21	0.04
90	60	2.65	0.83	-0.34	0.37	0.20	0.00	-0.21	0.04
90	90	1.21	-0.02	-1.28	0.27	0.20	0.01	-0.17	0.04
90	120	0.37	-0.59	-2.03	0.29	0.15	-0.01	-0.17	0.04
90	135	0.32	-0.76	-2.29	0.30	0.16	-0.01	-0.17	0.04
90	150	0.14	-0.93	-2.68	0.34	0.17	-0.01	-0.18	0.04
90	180	0.06	-1.08	-2.82	0.37	0.17	0.00	-0.19	0.04

Model 5		C _{FN}				C _{My}			
β (deg.)	θ (deg.)	(+) Peak	Mean	(-) Peak	S.D.	(+) Peak	Mean	(-) Peak	S.D.
0	0	0.85	-0.07	-0.90	0.20	0.25	0.01	-0.23	0.05
0	30	0.82	-0.09	-1.10	0.20	0.23	0.01	-0.21	0.04
0	45	0.84	-0.09	-0.96	0.20	0.21	0.01	-0.21	0.04
0	60	0.86	-0.08	-0.95	0.20	0.19	0.00	-0.19	0.04
0	90	0.89	-0.03	-0.85	0.19	0.16	0.00	-0.17	0.04
0	120	0.98	-0.04	-0.97	0.20	0.19	0.00	-0.19	0.04
0	135	1.00	-0.02	-0.86	0.21	0.20	-0.01	-0.20	0.04
0	150	0.98	-0.01	-0.94	0.21	0.21	-0.01	-0.22	0.04
0	180	1.06	0.02	-0.87	0.20	0.22	-0.01	-0.24	0.05
15	0	1.71	0.39	-0.66	0.28	0.15	-0.09	-0.39	0.06
15	30	1.69	0.36	-0.60	0.27	0.13	-0.06	-0.33	0.05
15	45	1.56	0.29	-0.63	0.26	0.15	-0.04	-0.30	0.05
15	60	1.29	0.13	-0.89	0.23	0.14	-0.03	-0.25	0.04
15	90	0.89	-0.07	-0.95	0.19	0.17	0.00	-0.17	0.04
15	120	0.58	-0.30	-1.34	0.20	0.14	-0.03	-0.24	0.04
15	135	0.50	-0.41	-1.50	0.21	0.14	-0.07	-0.32	0.05
15	150	0.37	-0.48	-1.53	0.22	0.14	-0.09	-0.36	0.05
15	180	0.43	-0.43	-1.42	0.21	0.10	-0.12	-0.38	0.05
30	0	2.96	0.98	-0.42	0.43	0.11	-0.13	-0.52	0.07
30	30	1.43	0.44	-0.16	0.20	0.04	-0.14	-0.25	0.06
30	45	2.43	0.70	-0.38	0.35	0.15	-0.09	-0.37	0.06
30	60	1.73	0.44	-0.57	0.28	0.13	-0.05	-0.28	0.05
30	90	0.96	-0.05	-1.07	0.20	0.18	0.00	-0.17	0.04
30	120	0.39	-0.53	-1.80	0.24	0.12	-0.07	-0.31	0.05
30	135	0.32	-0.75	-2.00	0.27	0.11	-0.11	-0.38	0.05
30	150	0.13	-0.92	-2.34	0.29	0.08	-0.14	-0.44	0.06
30	180	0.19	-0.85	-2.13	0.27	0.06	-0.15	-0.46	0.06
45	0	3.15	1.21	-0.12	0.45	0.13	-0.09	-0.44	0.06
45	30	3.18	1.13	-0.20	0.46	0.10	-0.12	-0.43	0.06
45	45	2.78	0.92	-0.24	0.40	0.11	-0.11	-0.40	0.06
45	60	2.35	0.66	-0.42	0.33	0.19	-0.04	-0.29	0.05
45	90	1.16	-0.05	-1.17	0.21	0.19	0.02	-0.17	0.04
45	120	0.27	-0.71	-2.16	0.28	0.12	-0.08	-0.34	0.05
45	135	0.19	-0.90	-2.44	0.32	0.09	-0.12	-0.40	0.05
45	150	0.06	-0.97	-2.55	0.32	0.10	-0.11	-0.38	0.05
45	180	0.07	-1.01	-2.65	0.32	0.11	-0.11	-0.39	0.05
60	0	3.62	1.30	-0.09	0.49	0.19	-0.06	-0.42	0.06

Model 5		C _{FN}				C _{My}			
β (deg.)	θ (deg.)	(+) Peak	Mean	(-) Peak	S.D.	(+) Peak	Mean	(-) Peak	S.D.
60	30	3.61	1.29	-0.11	0.47	0.15	-0.09	-0.39	0.06
60	45	3.45	1.16	-0.15	0.46	0.18	-0.07	-0.38	0.06
60	60	2.84	0.85	-0.43	0.38	0.18	-0.05	-0.32	0.05
60	90	1.10	-0.02	-1.36	0.23	0.23	0.01	-0.20	0.05
60	120	0.35	-0.77	-2.64	0.31	0.15	-0.05	-0.30	0.05
60	135	0.27	-0.88	-2.51	0.31	0.15	-0.06	-0.31	0.05
60	150	0.05	-1.01	-3.00	0.35	0.13	-0.08	-0.35	0.05
60	180	-0.01	-1.10	-2.91	0.35	0.11	-0.09	-0.40	0.05
75	0	3.81	1.34	0.00	0.49	0.18	-0.06	-0.35	0.06
75	30	3.60	1.30	0.00	0.47	0.17	-0.08	-0.36	0.05
75	45	3.62	1.22	-0.13	0.46	0.14	-0.09	-0.38	0.05
75	60	2.86	0.90	-0.25	0.40	0.20	-0.04	-0.30	0.05
75	90	1.20	0.00	-1.23	0.25	0.24	0.02	-0.21	0.05
75	120	0.47	-0.72	-2.41	0.33	0.20	-0.04	-0.28	0.05
75	135	0.19	-0.88	-2.50	0.34	0.16	-0.04	-0.28	0.05
75	150	0.15	-1.06	-3.17	0.38	0.17	-0.04	-0.31	0.05
75	180	0.02	-1.12	-2.93	0.39	0.16	-0.07	-0.32	0.05
90	0	3.74	1.39	0.05	0.50	0.25	-0.02	-0.32	0.06
90	30	3.78	1.36	-0.01	0.47	0.26	-0.06	-0.36	0.06
90	45	3.48	1.26	-0.13	0.45	0.22	-0.06	-0.38	0.06
90	60	2.96	0.98	-0.30	0.41	0.22	0.00	-0.25	0.06
90	90	1.28	-0.01	-1.14	0.26	0.26	0.02	-0.21	0.05
90	120	0.43	-0.73	-2.56	0.34	0.23	0.00	-0.24	0.05
90	135	0.22	-0.86	-2.48	0.36	0.23	-0.03	-0.27	0.05
90	150	0.09	-1.05	-2.88	0.39	0.24	-0.04	-0.27	0.05
90	180	0.05	-1.09	-3.00	0.40	0.18	-0.04	-0.30	0.05

Model 6		C _{FN}				C _{My}			
β (deg.)	θ (deg.)	(+) Peak	Mean	(-) Peak	S.D.	(+) Peak	Mean	(-) Peak	S.D.
0	0	0.78	-0.07	-0.84	0.18	0.29	0.01	-0.26	0.06
0	30	0.89	-0.08	-0.91	0.19	0.22	-0.03	-0.27	0.05
0	45	0.85	-0.09	-0.95	0.20	0.21	-0.03	-0.29	0.05
0	60	0.98	-0.05	-0.86	0.19	0.21	0.00	-0.22	0.05
0	90	0.80	-0.08	-0.84	0.18	0.20	0.00	-0.22	0.05
0	120	0.88	-0.06	-0.86	0.18	0.20	0.01	-0.18	0.04
0	135	0.88	-0.11	-0.94	0.19	0.18	-0.03	-0.23	0.04
0	150	0.78	-0.11	-1.03	0.20	0.22	-0.03	-0.24	0.05
0	180	0.79	-0.08	-0.92	0.19	0.19	-0.04	-0.27	0.05
15	0	1.80	0.42	-0.52	0.27	0.19	-0.08	-0.42	0.07
15	30	1.65	0.38	-0.66	0.27	0.14	-0.09	-0.40	0.06
15	45	1.51	0.30	-0.66	0.25	0.16	-0.08	-0.36	0.06
15	60	1.30	0.21	-0.66	0.23	0.17	-0.03	-0.25	0.05
15	90	0.97	-0.03	-0.83	0.18	0.19	0.00	-0.21	0.04
15	120	0.59	-0.26	-1.23	0.19	0.18	-0.04	-0.23	0.04
15	135	0.47	-0.39	-1.35	0.20	0.16	-0.07	-0.29	0.05
15	150	0.40	-0.46	-1.52	0.21	0.14	-0.09	-0.37	0.06
15	180	0.43	-0.47	-1.57	0.21	0.10	-0.14	-0.46	0.06
30	0	2.47	0.83	-0.38	0.40	0.17	-0.12	-0.48	0.08
30	30	2.43	0.72	-0.45	0.36	0.14	-0.12	-0.46	0.07
30	45	2.02	0.57	-0.56	0.33	0.12	-0.12	-0.43	0.06
30	60	1.85	0.43	-0.54	0.28	0.16	-0.04	-0.28	0.05
30	90	0.93	-0.02	-0.85	0.19	0.20	0.01	-0.20	0.04
30	120	0.43	-0.52	-1.67	0.22	0.14	-0.06	-0.30	0.05
30	135	0.30	-0.69	-2.04	0.26	0.11	-0.11	-0.38	0.05
30	150	0.20	-0.80	-2.35	0.28	0.10	-0.13	-0.44	0.06
30	180	0.26	-0.82	-2.17	0.28	0.08	-0.17	-0.47	0.06
45	0	2.98	1.15	-0.14	0.43	0.13	-0.11	-0.43	0.06
45	30	3.02	1.10	-0.21	0.43	0.13	-0.14	-0.49	0.06
45	45	2.71	0.89	-0.39	0.40	0.12	-0.13	-0.42	0.06
45	60	2.25	0.57	-0.46	0.32	0.16	-0.07	-0.30	0.05
45	90	1.00	-0.10	-1.05	0.21	0.17	-0.02	-0.22	0.04
45	120	0.36	-0.71	-2.14	0.27	0.08	-0.10	-0.36	0.05
45	135	0.11	-0.90	-2.38	0.31	0.07	-0.14	-0.41	0.05
45	150	0.10	-0.99	-2.62	0.32	0.10	-0.14	-0.43	0.06
45	180	0.02	-1.15	-2.83	0.32	0.03	-0.19	-0.51	0.06
60	0	3.73	1.23	-0.10	0.47	0.21	-0.06	-0.37	0.06

Model 6		C_{FN}			C_{My}				
β (deg.)	θ (deg.)	(+) Peak	Mean	(-) Peak	S.D.	(+) Peak	Mean	(-) Peak	S.D.
60	30	3.49	1.24	-0.05	0.47	0.16	-0.09	-0.38	0.06
60	45	3.36	1.12	-0.20	0.44	0.18	-0.08	-0.37	0.06
60	60	2.61	0.77	-0.33	0.37	0.18	-0.05	-0.32	0.05
60	90	1.00	-0.04	-1.09	0.23	0.21	0.00	-0.20	0.04
60	120	0.39	-0.73	-2.14	0.30	0.14	-0.06	-0.32	0.05
60	135	0.15	-0.85	-2.58	0.31	0.12	-0.08	-0.35	0.05
60	150	0.08	-0.98	-2.66	0.34	0.12	-0.10	-0.38	0.05
60	180	0.11	-1.10	-3.04	0.36	0.13	-0.11	-0.39	0.06
75	0	3.58	1.37	0.05	0.48	0.23	-0.05	-0.33	0.06
75	30	3.48	1.32	0.01	0.46	0.18	-0.08	-0.37	0.06
75	45	3.29	1.19	-0.08	0.44	0.16	-0.08	-0.33	0.05
75	60	2.84	0.88	-0.28	0.38	0.20	-0.03	-0.29	0.05
75	90	1.21	-0.02	-1.19	0.24	0.23	0.01	-0.22	0.05
75	120	0.41	-0.70	-2.41	0.31	0.19	-0.03	-0.26	0.05
75	135	0.12	-0.84	-2.40	0.32	0.15	-0.07	-0.29	0.05
75	150	0.04	-1.04	-3.12	0.37	0.13	-0.08	-0.32	0.05
75	180	-0.01	-1.12	-2.94	0.38	0.12	-0.11	-0.37	0.05
90	0	3.59	1.41	0.09	0.49	0.26	-0.05	-0.32	0.06
90	30	3.59	1.40	0.16	0.47	0.13	-0.11	-0.42	0.06
90	45	3.26	1.25	0.08	0.42	0.15	-0.11	-0.38	0.06
90	60	2.96	0.98	-0.14	0.39	0.16	-0.07	-0.31	0.05
90	90	1.22	0.07	-1.05	0.24	0.17	-0.05	-0.28	0.05
90	120	0.51	-0.60	-2.20	0.32	0.18	-0.05	-0.28	0.05
90	135	0.29	-0.82	-2.75	0.34	0.17	-0.06	-0.28	0.05
90	150	0.17	-1.00	-2.99	0.39	0.17	-0.06	-0.31	0.05
90	180	0.10	-1.07	-2.92	0.39	0.18	-0.07	-0.36	0.06

Model 7		C _{FN}				C _{My}			
β (deg.)	θ (deg.)	(+) Peak	Mean	(-) Peak	S.D.	(+) Peak	Mean	(-) Peak	S.D.
0	0	0.69	-0.07	-0.85	0.16	0.29	0.03	-0.21	0.05
0	30	0.70	-0.07	-0.82	0.16	0.24	0.00	-0.22	0.04
0	45	0.79	-0.08	-0.89	0.17	0.21	-0.01	-0.21	0.04
0	60	0.71	-0.14	-0.83	0.16	0.17	-0.01	-0.21	0.04
0	90	0.75	-0.05	-0.72	0.15	0.20	0.00	-0.19	0.04
0	120	0.76	-0.04	-0.71	0.16	0.17	-0.01	-0.18	0.04
0	135	0.84	-0.09	-0.83	0.18	0.18	-0.02	-0.21	0.04
0	150	0.85	-0.07	-0.83	0.18	0.19	-0.03	-0.22	0.04
0	180	0.79	-0.05	-0.79	0.18	0.19	-0.03	-0.24	0.05
15	0	1.69	0.36	-0.47	0.26	0.14	-0.08	-0.39	0.06
15	30	1.53	0.35	-0.44	0.24	0.12	-0.09	-0.37	0.05
15	45	1.35	0.26	-0.55	0.23	0.12	-0.08	-0.31	0.05
15	60	1.11	0.12	-0.61	0.20	0.15	-0.04	-0.25	0.04
15	90	0.70	-0.05	-0.72	0.16	0.19	0.01	-0.18	0.04
15	120	0.36	-0.35	-1.20	0.17	0.13	-0.04	-0.25	0.04
15	135	0.32	-0.47	-1.41	0.18	0.13	-0.07	-0.27	0.04
15	150	0.27	-0.52	-1.51	0.20	0.11	-0.09	-0.34	0.05
15	180	0.30	-0.50	-1.42	0.19	0.08	-0.11	-0.37	0.05
30	0	2.68	0.90	-0.30	0.40	0.11	-0.14	-0.54	0.07
30	30	2.38	0.74	-0.32	0.35	0.09	-0.13	-0.42	0.06
30	45	1.89	0.58	-0.36	0.31	0.09	-0.11	-0.40	0.05
30	60	1.66	0.34	-0.50	0.26	0.13	-0.06	-0.28	0.04
30	90	0.78	-0.11	-0.84	0.16	0.16	-0.02	-0.18	0.04
30	120	0.24	-0.54	-1.71	0.20	0.12	-0.07	-0.32	0.04
30	135	0.14	-0.73	-1.85	0.24	0.08	-0.10	-0.36	0.05
30	150	0.09	-0.84	-2.30	0.26	0.08	-0.12	-0.41	0.05
30	180	-0.14	-1.01	-2.43	0.26	0.03	-0.18	-0.46	0.06
45	0	2.88	1.07	-0.15	0.44	0.14	-0.13	-0.42	0.06
45	30	3.06	1.01	-0.19	0.43	0.09	-0.15	-0.44	0.06
45	45	2.65	0.81	-0.27	0.38	0.08	-0.13	-0.42	0.05
45	60	2.02	0.47	-0.53	0.31	0.15	-0.08	-0.31	0.05
45	90	0.78	-0.12	-1.18	0.19	0.18	-0.03	-0.21	0.04
45	120	0.21	-0.70	-1.92	0.25	0.10	-0.10	-0.36	0.05
45	135	0.13	-0.89	-2.55	0.29	0.09	-0.12	-0.40	0.05
45	150	0.02	-0.97	-2.62	0.29	0.10	-0.13	-0.42	0.05
45	180	-0.16	-1.11	-2.44	0.30	0.03	-0.18	-0.47	0.05
60	0	3.31	1.23	-0.01	0.44	0.18	-0.07	-0.38	0.06

Model 7		C _{FN}				C _{My}			
β (deg.)	θ (deg.)	(+) Peak	Mean	(-) Peak	S.D.	(+) Peak	Mean	(-) Peak	S.D.
60	30	3.30	1.20	-0.07	0.44	0.17	-0.10	-0.38	0.06
60	45	2.91	1.03	-0.14	0.40	0.14	-0.09	-0.36	0.05
60	60	2.31	0.70	-0.34	0.34	0.19	-0.04	-0.30	0.05
60	90	0.95	-0.03	-1.15	0.20	0.20	-0.01	-0.20	0.04
60	120	0.31	-0.63	-1.94	0.27	0.14	-0.07	-0.33	0.05
60	135	0.20	-0.78	-2.21	0.28	0.12	-0.08	-0.33	0.05
60	150	0.14	-0.94	-2.35	0.32	0.11	-0.09	-0.32	0.05
60	180	0.03	-1.09	-2.78	0.34	0.07	-0.13	-0.38	0.05
75	0	3.63	1.31	-0.02	0.48	0.21	-0.03	-0.35	0.06
75	30	3.25	1.23	-0.12	0.44	0.18	-0.06	-0.32	0.06
75	45	3.20	1.09	-0.19	0.42	0.19	-0.05	-0.33	0.05
75	60	2.69	0.83	-0.33	0.37	0.19	-0.02	-0.28	0.05
75	90	1.19	-0.01	-1.16	0.22	0.22	0.00	-0.20	0.04
75	120	0.32	-0.65	-2.18	0.29	0.18	-0.03	-0.26	0.05
75	135	0.17	-0.84	-2.31	0.32	0.15	-0.07	-0.30	0.05
75	150	0.07	-1.01	-2.62	0.36	0.14	-0.08	-0.29	0.05
75	180	-0.12	-1.14	-3.00	0.37	0.14	-0.10	-0.35	0.05
90	0	3.73	1.37	0.12	0.46	0.24	-0.03	-0.33	0.06
90	30	3.36	1.30	0.03	0.44	0.20	-0.06	-0.34	0.06
90	45	3.12	1.19	0.02	0.41	0.20	-0.05	-0.30	0.06
90	60	2.64	0.85	-0.32	0.37	0.22	0.00	-0.23	0.05
90	90	1.24	0.00	-1.19	0.24	0.22	0.00	-0.21	0.05
90	120	0.45	-0.61	-2.05	0.30	0.23	-0.02	-0.29	0.05
90	135	0.25	-0.81	-2.63	0.33	0.23	-0.02	-0.25	0.05
90	150	0.07	-1.01	-3.05	0.38	0.25	-0.03	-0.28	0.05
90	180	0.00	-1.13	-3.01	0.40	0.26	-0.03	-0.33	0.06

APPENDIX B

B1. CALCULATION OF DESIGN LOADS AS PER ASCE 7-05

Design wind loads for a full scale ground mounted photovoltaic tracker (PVT) were obtained by idealizing the PVT system as a monoslope free roof. The net pressure coefficients defined in Figure 6-18A of ASCE 7-05 (Figure B1) were used. The wind directions $\gamma=0^\circ$ and $\gamma=180^\circ$ in ASCE 7-05, correspond to 180° and 0° wind directions of wind tunnel tests, respectively.

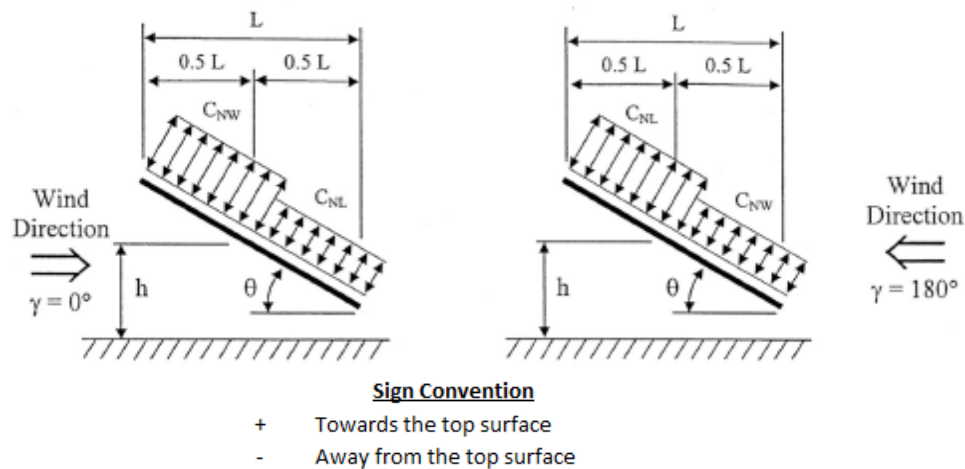


Figure B1 Net pressure coefficients for monoslope free roofs shown in Figure 6-18A of ASCE 7-05

PVT Prototype Dimensions

L =	16.00	ft	=	192	in
W =	16.00	ft	=	192	in
H =	11.00	ft	=	132	in

Calculation of velocity pressure as per Sec. 6.5.10 of ASCE 7-05

$$\begin{aligned}
 V_{3sec} &= 90 \text{ mph} = 40.23 \text{ m/s} \\
 K_z &= 0.85 \\
 K_{zt} &= 1 \\
 K_d &= 0.85 \\
 I &= 0.87 \\
 q_h &= 13.03413 \text{ psf} \\
 G &= 0.85
 \end{aligned}$$

From Sec. 6.5.15 of ASCE 7-05, the design wind load on PVT = $q_h G C_N A_{ref}$

Where, A_{ref} = prototype reference area of solid PVT = 16ft x 16ft = 256 ft²

The design wind loads calculated for four pitch angles of the prototype PVT model using the ASCE 7-05 standard are shown in Tables B1 through B4.

Table B1. Design Normal Force as per ASCE 7-05 for Pitch Angle = 0°

θ	Pressure (psf)	$\gamma = 0^\circ$				$\gamma = 180^\circ$			
		Clear		Obstructed		Clear		Obstructed	
		CNW	CNL	CNW	CNL	CNW	CNL	CNW	CNL
0	A	1.20	0.30	-0.50	-0.20	1.20	0.30	-0.50	-1.20
	B	-1.10	-0.10	-1.10	-0.60	-1.10	-0.10	-1.10	-0.60
Pressue (psf)	A	13.29	3.32	-5.54	-2.22	13.29	3.32	-5.54	-13.29
	B	-12.19	-1.11	-12.19	-6.65	-12.19	-1.11	-12.19	-6.65
Load Case A	F _N (lbs)	1701.74	425.43	-709.06	-283.62	1701.74	425.43	-709.06	-1701.74
	F _x (lbs)	0.00	0.00	0.00	0.00	0.00	0.00	0.00	0.00
	F _z (lbs)	-1701.74	-425.43	709.06	283.62	-1701.74	-425.43	709.06	1701.74
Load Case B	F _N (lbs)	-1559.92	-141.81	-1559.92	-850.87	-1559.92	-141.81	-1559.92	-850.87
	F _x (lbs)	0.00	0.00	0.00	0.00	0.00	0.00	0.00	0.00
	F _z (lbs)	1559.92	141.81	1559.92	850.87	1559.92	141.81	1559.92	850.87

Table B2. Design Normal Force as per ASCE 7-05 for Pitch Angle = 15°

θ	15	$\gamma = 0^\circ$				$\gamma = 180^\circ$			
		Clear		Obstructed		Clear		Obstructed	
		CNW	CNL	CNW	CNL	CNW	CNL	CNW	CNL
Pressure (psf)	A	-0.90	-1.30	-1.10	-1.50	1.30	1.60	0.40	-1.10
	B	-1.90	0.00	-2.10	-0.60	1.80	0.60	1.20	-0.30
Load Case A	F _N (lbs)	-1276.30	-1843.55	-1559.92	-2127.17	1843.55	2268.98	567.25	-1559.92
	F _x (lbs)	-330.33	-477.15	-403.74	-550.55	477.15	587.26	146.81	-403.74
	F _z (lbs)	1232.81	1780.73	1506.77	2054.69	-1780.73	-2191.67	-547.92	1506.77
Load Case B	F _N (lbs)	-2694.42	0.00	-2978.04	-850.87	2552.60	850.87	1701.74	-425.43
	F _x (lbs)	-697.37	0.00	-770.77	-220.22	660.66	220.22	440.44	-110.11
	F _z (lbs)	2602.61	0.00	2876.56	821.88	-2465.63	-821.88	-1643.75	410.94

Table B3. Design Normal Force as per ASCE 7-05 for Pitch Angle = 30°

θ	30	$\gamma = 0^\circ$				$\gamma = 180^\circ$			
		Clear		Obstructed		Clear		Obstructed	
		CNW	CNL	CNW	CNL	CNW	CNL	CNW	CNL
Pressure (psf)	A	-1.80	-1.80	-1.50	-1.80	2.10	2.10	0.60	-1.00
	B	-2.50	-0.50	-2.30	-1.10	2.60	1.00	1.60	0.10
Load Case A	F _N (lbs)	-2552.60	-2552.60	-2127.17	-2552.60	2978.04	2978.04	850.87	-1418.11
	F _x (lbs)	-1276.30	-1276.30	-1063.59	-1276.30	1489.02	1489.02	425.43	-709.06
	F _z (lbs)	2210.62	2210.62	1842.18	2210.62	-2579.06	-2579.06	-736.87	1228.12
Load Case B	F _N (lbs)	-3545.28	-709.06	-3261.66	-1559.92	3687.10	1418.11	2268.98	141.81
	F _x (lbs)	-1772.64	-354.53	-1630.83	-779.96	1843.55	709.06	1134.49	70.91
	F _z (lbs)	3070.31	614.06	2824.68	1350.93	-3193.12	-1228.12	-1965.00	-122.81

Table B4. Design Normal Force as per ASCE 7-05 for Pitch Angle = 45°

θ	45	$\gamma = 0^\circ$				$\gamma = 180^\circ$			
		Clear		Obstructed		Clear		Obstructed	
		CNW	CNL	CNW	CNL	CNW	CNL	CNW	CNL
A	-1.60	-1.80	-1.30	-1.80	2.20	2.50	0.80	-0.90	
B	-2.30	-0.70	-1.90	-1.20	2.60	1.40	2.10	0.40	
Pressure (psf)	A	-17.73	-19.94	-14.40	-19.94	24.37	27.70	8.86	-9.97
	B	-25.48	-7.76	-21.05	-13.29	28.81	15.51	23.27	4.43
Load Case A	F _N (lbs)	-2268.98	-2552.60	-1843.55	-2552.60	3119.85	3545.28	1134.49	-1276.30
	F _x (lbs)	-1604.41	-1804.96	-1303.58	-1804.96	2206.07	2506.89	802.21	-902.48
	F _z (lbs)	1604.41	1804.96	1303.58	1804.96	-2206.07	-2506.89	-802.21	902.48
Load Case B	F _N (lbs)	-3261.66	-992.68	-2694.42	-1701.74	3687.10	1985.36	2978.04	567.25
	F _x (lbs)	-2306.34	-701.93	-1905.24	-1203.31	2607.17	1403.86	2105.79	401.10
	F _z (lbs)	2306.34	701.93	1905.24	1203.31	-2607.17	-1403.86	-2105.79	-401.10

B2. CALCULATION OF DESIGN LOADS USING WIND TUNNEL DATA

V_{33} = Design wind speed at 33 ft elevation from ground as per ASCE 7-05 = 90 mph

\bar{V}_{33} = Hourly mean wind speed at 33 ft elevation from ground

$$= \frac{V_{33}}{1.53} = \frac{90}{1.53} = 58.82 \text{ mph}$$

\bar{V}_H = Hourly mean wind speed at pivot height of the PVT

$$= \bar{V}_{33} \left(\frac{H}{33} \right)^{\frac{1}{9.5}} = 58.82 \left(\frac{11}{33} \right)^{\frac{1}{9.5}} = 52.34 \text{ mph}$$

q = Design pressure corresponding to mean hourly wind speed at PVT pivot height

$$= (0.00256) \bar{V}_H^2 = 7.029 \text{ psf}$$

A_{ref} = prototype reference area of solid PVT = 16ft x 16ft = 256 ft²

F_N = Design normal force for a design wind speed $V_{33} = q A_{ref} C_{FN}$

The design normal forces obtained for wind direction 0° and 180° of the wind tunnel tests is shown in Table B5 and B6.

Table B5. Experimental Design Normal Forces for Wind Direction = 0°

P.A. (deg.)	Wind Tunnel Test								
	CF _N				F _N (lbs.)				
	(+) Peak	Mean	(-) Peak	S.D.	(+) Peak	Mean	(-) Peak	S.D.	
Wind Direction 0°	0	1.04	-0.02	-0.95	0.23	1867.00	-37.29	-1712.61	411.07
	15	1.90	0.46	-0.59	0.33	3422.79	833.73	-1062.82	585.32
	30	2.98	1.05	-0.33	0.47	5358.22	1883.21	-590.99	841.76
	45	3.60	1.38	-0.06	0.49	6475.59	2479.35	-100.74	878.30
	60	4.05	1.41	-0.03	0.52	7283.15	2540.38	-55.95	928.18
	75	4.18	1.49	-0.02	0.52	7519.26	2676.99	-33.76	944.13
	90	3.90	1.45	-0.05	0.50	7015.04	2612.76	-92.98	898.27

Table B6. Experimental Design Normal Forces for Wind Direction = 180°

P.A. (deg.)	Wind Tunnel Test								
	CF _N				F _N (lbs.)				
	(+) Peak	Mean	(-) Peak	S.D.	(+) Peak	Mean	(-) Peak	S.D.	
Wind Direction 180°	0	1.03	-0.03	-0.98	0.22	1860.94	-53.73	-1765.74	404.09
	15	0.45	-0.50	-1.71	0.23	817.66	-901.21	-3083.11	405.00
	30	0.27	-0.88	-2.26	0.30	489.29	-1587.31	-4064.79	537.51
	45	0.15	-1.02	-2.71	0.34	267.65	-1830.88	-4883.75	614.02
	60	-0.01	-1.26	-3.07	0.38	-25.77	-2259.17	-5530.66	681.88
	75	0.06	-1.23	-3.02	0.42	99.98	-2212.58	-5431.43	747.51
	90	0.19	-1.25	-3.54	0.47	333.33	-2247.14	-6374.67	846.69

To compare with the ASCE 7-05 results, the experimental design normal forces boxed in the red rectangle were used as ASCE 7-05 limits the pitch angle of the roof to 45°.